รายงานวิจัยฉบับสมบูรณ์

โครงการ อนุภาคนาโนที่มีสมบัติการกรองรังสียูวี จากอนุพันธ์ของโพลีไวนิลแอลกอฮอล์

โดย

รศ. ดร. ศุภศร วนิชเวชารุ่งเรือง

ภาควิชาเคมี คณะวิทยาศาสตร์ จุฬาลงกรณ์มหาวิทยาลัย

กรกฎาคม 2552

บทนำ

ในปัจจุบัน อนุภาคระดับนาโนได้รับความสนใจในการใช้เป็นตัวนำส่งยา (drug delivery system) ซึ่งรวมไปถึงการนำส่งสารออกฤทธิ์ในเครื่องสำอางด้วย การกักเก็บตัวยาหรือสารออกฤทธิ์ ในอนุภาคนาโนนั้น สามารถทำได้โดยไม่ต้องใช้ปฏิกิริยาเคมีใดๆกับสารออกฤทธิ์เหล่านั้น จึงเป็นวิธีที่สามารถคงฤทธิ์ของยาไว้ได้ดี การวิจัยเกี่ยวกับสารกรองรังสียูวีได้ก่อให้เกิดการยอมรับถึงประโยชน์ของสารกรองรังสียูวี อย่างไรก็ตาม ปัญหาเรื่องการดูดซึมของสารกรองรังสียูวีเข้าสู่ร่างกาย และปัญหาเรื่องความเสถียรของสารออกฤทธิ์สำหรับเครื่องสำอางก็ยังคงมีอยู่ ในงานวิจัยนี้ ผู้วิจัยต้องการสร้างอนุภาคนาโนที่ตัวอนุภาคเองมีสมบัติการกรองรังสียูวี ด้วยแนวความคิดที่ว่า ตัวนำส่งสารนี้น่าจะมีสมบัติในการปกป้องสารออกฤทธิ์จากแสงยูวีได้ด้วย ทั้งนี้เพื่อผลลัพธ์ทั้งในแง่การเพิ่มความเสถียรให้กับสารออกฤทธิ์ที่ถูกกักอยู่ในอนุภาคดังกล่าว และ การเพิ่มประโยชน์ของระบบนำส่งให้สามารถทำหน้าที่เป็นสารกรองรังสียูวีให้กับผิวด้วย เนื่องจากอนุภาคนาโนเกิดขึ้นจากโมเลกุลพอลิเมอร์ขนาดใหญ่ ดังนั้นเมื่อพอลิเมอร์ดังกล่าวถูกปรับโครงสร้างให้สามารถดูดกลืนแสงยูวีได้ สารกรองรังสียูวีที่อยู่ในรูปอนุภาคนาโนนี้ จึงน่าจะถูกดูดซึมเข้าสู่ร่างกายได้ช้าลง เมื่อเทียบกับสารกรองรังสียูวีโมเลกุลเล็กๆที่ใช้กันทั่วไปในเครื่องสำอาง ดังนั้น ระบบใหม่ที่ได้ จึงเป็นสารกรองรังสียูวีแบบใหม่ที่น่าจะสามารถช่วยแก้ปัญหาเรื่องการดูดซึมของสารกรองรังสียูวีเข้าสู่ร่างกายได้ โดยตัวมันเองยังสามารถทำหน้าที่เป็นตัวนำส่งสารออกฤทธิ์ที่มีประสิทธิภาพในการเพิ่มความเสถียรให้กับสารออกฤทธิ์ด้วย โดยโครงการวิจัยนี้จะเป็นงานวิจัยพื้นฐานของการสร้างระบบดังกล่าว

การทดลอง

การทดลองในโครงการวิจัยนี้ประกอบด้วย

1) **การหาโครโมฟอร์ที่สามารถดูดกลืนแสงยูวีสำหรับกราฟต์ลงบน พอลิไวนิล แอลกอฮอล์**

เนื่องจากโครโมฟอร์ดูดกลืนแสงยูวีบีที่มีความเสถียรในระดับยอมรับได้มีให้เลือกใช้อยู่แล้ว คือ 4-methoxycinnamoyl group โครโมฟอร์นี้เป็นส่วนโครโมฟอร์ที่อยู่ในสารกรองรังสียูวีบี ethylhexyl-4-methoxycinnamate ซึ่งมีการใช้อย่างแพร่หลาย อย่างไรก็ตาม โครโมฟอร์ที่สามารถดูดกลืนแสงยูวีเอ ที่มีความเสถียรยังไม่สามารถหาได้ ดังนั้นในขั้นแรกของโครงการวิจัย จึงเป็นการตรวจสอบความปลอดภัยของโครโมฟอร์ 2,4,5-trimethoxycinnamoyl group ซึ่งเป็นโครโมฟอร์ดูดกลืนแสงยูวีเอที่ได้รับการพัฒนาขึ้นมาในห้องปฏิบัติการของผู้วิจัย งานส่วนนี้มีรายละเอียดอยู่ใน*ภาคผนวก ก*

2) การหาวิธีตรวจสอบความเสถียรของโครโมฟอร์ที่ใช้

แม้ว่าโครโมฟอร์ดูดกลืนแสงยูวีบี 4-methoxycinnamoyl group จะมีความเสถียรและได้รับความนิยมอย่างแพร่หลาย แต่โครโมฟอร์ชนิดนนี้ก็มีการเปลี่ยนแปลงทางเคมีที่ทำให้ประสิทธิภาพการดูดกลืนแสงลดลง กล่าวคือ เมื่อได้รับแสงยูวีบี โครโมฟอร์ดังกล่าวจะเกิดการเปลี่ยนคอนฟิกุเรชัน จาก *trans* เป็น *cis* และสารในรูป *cis* มีความสามารถดูดกลืนแสงเพียงครึ่งหนึ่งของสารในรูป *trans* ดังนั้นเมื่อนำโครโมฟอร์นี้ไปติดลงบน พอลิไวนิลแอลกอฮอล์ จะทำให้พอลิเมอร์ที่ได้มีปัญหาดังกล่าวได้ อย่างไรก็ตาม การเกิด self-assembly เป็นอนุภาคนาโนที่แขวนตัวอยู่ในน้ำน่าจะทำให้หมู่ดังกล่าวถูกหันเข้าสู่ภายใน ทำให้มีความเสถียรขึ้นได้ เนื่องจากอยู่ในใจกลางอนุภาคที่มีสภาวะขั้วต่ำ (การเกิด photoisomerization ของ cinnamate จะลดลงเมื่ออยู่ในตัวกลางไร้ขั้ว) แต่ปัญหาหลักในการตรวจสอบการเปลี่ยน configuration ของโครโมฟอร์ที่ถูกกราฟต์ลงบนสายพอลิเมอร์ก็คือ การที่เมื่อมันอยู่ในรูปอนุภาคนาโนทำให้ไม่สามารถใช้การวัดค่าการดูดกลืนแสงของสารละลายได้ ดังนั้นงานหนึ่งของโครงการวิจัยนี้คือ การหาวิธีตรวจวัดการเปลี่ยน configuration ของโครโมฟอร์ในสภาวะที่ไม่เป็นสารละลาย ในที่นี้ได้ใช้วิธีทาง FT-IR มาทำการติดตามการเปลี่ยน configuration รายละเอียดของงานส่วนนี้อยู่ใน*ภาคผนวก ข*

3) การศึกษาการดูดซึมผ่านชั้นผิวหนัง

ดังที่กล่าวไว้ในบทนำว่า สิ่งหนึ่งที่โครงการนี้ต้องการแสดงให้เห็นก็คือ การเตรียมอนุภาคที่มีสมบัติดูดกลืนแสงยูวี โดยสารกรองรังสียูวีที่เป็นพอลิเมอร์ที่ได้ควรมีการดูดซึมผ่านชั้นผิวหนังน้อยกว่าสารกรองรังสียูวีขนากโมเลกุลเล็กๆทั่วไป ในที่นี้จึงได้หาวิธีการตรวจสอบการซึมผ่านชั้นผิวหนังขึ้นมาเพื่อใช้ตรวจอนุภาคที่จะสังเคราะห์ต่อไป รายละเอียดของงานส่วนนี้อยู่ใน*ภาคผนวก ค* โดยในส่วนการดูดซึมของอนุภาคหรือพอลิเมอร์ จะเป็นการนำวิธีที่ได้นี้ไปใช้ และมีรายงานอยู่ในส่วนที่เกี่ยวข้องกับพอลิเมอร์นั้นๆ

4) การสังเคราะห์ อนุพันธ์พอลิไวนิลแอลกอฮอล์ที่มีหมู่โครโมฟอร์ติดอยู่ และนำไปเตรียมเป็นอนุภาคนาโน

เมื่อทราบว่า 2,4,5-trimethoxycinnamoyl group มีความปลอดภัย (จากการทดลองในข้อหนึ่ง) จึงได้ทำการติดโครโมฟอร์ดังกล่าวลงบน พอลิไวนิลแอลกอฮอล์ อย่างไรก็ตามเพื่อให้การศึกษาการเกิด self-assembly มีความสมบูรณ์ จึงทำการเตรียมอนุพันธ์อื่นๆด้วยคือ poly(vinylalcohol-co-vinyl-cinnamate), poly(vinylalcohol-co-vinyl-4-methoxycinnamate), poly(vinylalcohol-co-vinyl-2,4-dimethoxycinnamate) และ poly(vinylalcohol-covinyl-

2,4,5-trimethoxycinnamate) รายละเอียดการสังเคราะห์ และการสร้างอนุภาคมีอยู่ใน*ภาคผนวก ง*

5) การสังเคราะห์ พอลิเมอร์ที่สามารถดูดกลืนแสงได้ จากโครโมฟอร์ที่ใช้ในข้อ 1 และ 2 แต่อยู่ในรูปของ oligoesters ของ poly(p-alkoxycinnamate) และ poly(pentaethylene glycol cinnamate)

หลังจากได้สังเคาะห์อนุพันธ์พอลิไวนิลแอลกอฮอล์ที่มีหมู่โครโมฟอร์ติดอยู่ (ข้อสาม) ทำให้เกิดความต้องการเปรียบเทียบว่าหากอนุภาคเตรียมจากพอลิเมอร์ที่มีโครโมฟอร์เหมือนกัน แต่ไม่อยู่ในลักษณะกราฟต์ แต่เป็นส่วนของ backbone เลยจะเป็นเช่นใด จึงได่ทำการสังเคราะห์ poly(*p*-ethoxy-cinnamate), poly(*p*-propoxycinnamate), poly(*p*-hexyloxycinnamate), poly(*p*-undecyloxycinnamate) และ poly(pentaethylene glycol cinnamate) ขึ้นมา และศึกษาการเกิด self-assembly ของอนุพันธ์ที่ได้ รายละเอียดการสังเคราะห์ และการสร้างอนุภาคมีอยู่ใน*ภาคผนวก จ*

สรุปและวิจารณ์ผลการทดลอง

โครงการนี้สามารถชี้ให้เห็นอย่างชัดเจนว่า 2,4,5-trimethoxycinnamoyl group และ 4-methoxy-cinnamoyl group เป็นโครโมฟอร์ที่ดูดกลืนรังสียูวีเอ และ บี ที่ปลอดภัยตามลำดับ เหมาะแก่การนำไปใช้กราฟต์ลงบนพอลิไวนิลแอลกอฮอล์ การตรวจสอบการเปลี่ยนคอนฟิกุเรชันของหมู่โครโมฟอร์ที่ไม่ได้อยู่ในรูปสารละลายสามารถทำโดยใช้วิธี attenuated total reflection Fourier transform infrared spectroscopy (ATR-FT-IR) และการตรวจสอบการซึมผ่านชั้นผิวหนังสามาถทำโดยใช้หนังลูกหนู *Mus musculus* Linn. กับ Franz diffusion cell

สามารถสังเคราะห์ poly(vinylalcohol-co-vinylcinnamate), poly(vinylalcohol-co-vinyl-4-methoxycinnamate), poly(vinylalcohol-co-vinyl-2,4-dimethoxycinnamate) และ poly(vinylalcohol-covinyl-2,4,5-trimethoxycinnamate) และชักนำให้เป็นอนุภาคนาโนที่มีสมบัติดูดกลืนแสงยูวีได้ อนุภาคเหล่านี้มีการซึมผ่านชั้นผิวหนังน้อยกว่าโครโมฟอร์ขนาดเล็กมาก และหมู่โครโมฟอร์ 4-methoxycinnamate และ 2,4,5-trimethoxycinnamate ที่ติดอยู่ยังมีความเสถียรต่อแสงดีมาก

นอกจากนี้ยังสามารถสังเคราะห์ poly(*p*-ethoxycinnamate), poly(*p*-propoxycinnamate), poly(*p*-hexyloxycinnamate), poly(*p*-undecyloxycinnamate) และ poly(pentaethylene glycol cinnamate) ขึ้นมาได้ และสามารถชักนำให้ poly(pentaethylene glycol cinnamate) เป็นอนุภาคนาโนที่มีสมบัติดูดกลืนแสงยูวีได้

รายละเอียดผลการทดลองและสรุปสามารถดูได้จาก*ภาคผนวก ก-จ*

Outputs:

1. Klinubol, P., Asawanonda, P. and Wanichwecharungruang, S.P. Transdermal penetration of UV filters. 2008 Skin Pharmacol. Physiol. 21: 23-29.
2. Monhaphol, T., Yibchok-anun, S., Banlunara, W., Wittayasuporn, M., Palaga, T., Asawanonda, P. and Wanichweacharungruang, S.P. Cytotoxicity, acute oral toxicity and skin irritation of 2-ethylhexyl-2,4,5-trimethoxycinnamate and di(2-ethylhexyl)-2,4,5-trimethoxybenzalmalonate. 2008 Drug and Chemical Toxicology, 31: 2.
3. Pangnakorn, P., Nonthabenjawan, R., Ekgasit, S., Thammacharoen, C. and Wanichwecharungruang, S.P. Monitoring 2-Ethylhexyl-4-Methoxycinnamate Photoisomerization on Skin using ATR FT-IR. 2007 Appl. Spectrosc. 61: 193-198.
4. Luadthong, C., Tachaprutinun A. and Wanichwecharungruang, S.P. Synthesis and characterization of Micro/nanoparticles of poly(vinylalcohol-co-vinylcinnamate) derivatives. Eur. Pol. J. 2008; 44: 1285-1295.
5. Sasiwilaskorn, S., Klinubol, P., Tachaprutinun A. and Wanichwecharungruang, S. P. Oligoesters based on poly(p-alkoxycinnamate) and poly(pentaethylene glycol cinnamate) as potential UV filters. J. Appl. Pol. Sci. 2008; 109: 3502-3510.

ภาคผนวก ก

Drug and Chemical Toxicology, 31:289–301, 2008
Copyright © Informa Healthcare USA, Inc.
ISSN: 0148-0545 print / 1525-6014 online
DOI: 10.1080/01480540701873392

informa
healthcare

Cytotoxicity, Acute Oral Toxicity, and Skin Irritation of 2-ethylhexyl-2,4,5-trimethoxycinnamate and di(2-ethylhexyl)-2,4,5-trimethoxybenzalmalonate

Thitinun Monhaphol,[1] Sirinthorn Yibchok-anun,[2] Wijit Banlunara,[3] Mayura Wittayasuporn,[4] Tanapat Palaga,[5] Pravit Asawanonda,[6] and Supason Wanichweacharungruang[1]

[1]Sensor Research Unit, Department of Chemistry, Faculty of Science, Chulalongkorn University, Bangkok, Thailand
[2]Department of Pharmacology, Faculty of Veterinary Science, Chulalongkorn University, Bangkok, Thailand
[3]Department of Pathology, Faculty of Veterinary Science, Chulalongkorn University, Bangkok, Thailand
[4]The Program in Biotechnology, Faculty of Science, Chulalongkorn University, Bangkok, Thailand
[5]Department of Microbiology, Faculty of Science, Chulalongkorn University, Bangkok, Thailand
[6]Division of Dermatology, Department of Medicine, King Chulalongkorn Memorial Hospital, Bangkok, Thailand

Safety of two new ultraviolet (UV) filters, 2-ethylhexyl-2,4,5-trimethoxycinnamate (E8) and 2-ethylhexyl-2,4,5-trimethoxybenzalmalonate (B8), has been evaluated through the human melanoma cytotoxicity test and seven-day acute oral toxicity studies in rats. At 2.5 mg/mL, both compounds gave similar cell viability to the control. LD_{50} values for E8 and B8 are more than 5000 and 1000 mg/kg body weight, respectively. No significant difference in body weight and hematological parameters among the 0, 5, 50, 500, and 5000 mg/Kg E8-treated animals could be detected. Pathological examination of rat tissues collected at the end of the study period revealed no significant difference between the control and all E8-administered rats. There was no significant difference in all clinical blood chemistry parameters (aspartate aminotransferase, creatinine,

Address correspondence to Supason Wanichweacharungruang, Department of Chemistry, Faculty of Science, Chulalongkorn University, Payatai, Bangkok 10330, Thailand; E-mail: psupason@chula.ac.th

blood urea nitrogen, and cholesterol), except alanine aminotransferase (ALT), between the control and the E8-treated animals. All ALT values were, however, in the normal range of SD rats. E8 showed negative results for the skin irritation study on human volunteers, using patch and photopatch tests. Excitation of respiratory signs of dyspnea in 10, 100, and 1000 mg/Kg B8-treated rats could be observed during 1–24 h. All groups were, however, normal during the second to the seventh day. Hematological parameters of the 0, 10, 100, and 1000 mg/Kg B8-treated animals showed no significant difference. Pathological examination revealed no significant difference between the control and all B8-administered rats. However, significant differences in some clinical blood chemistry parameters and body weights between the control and some B8-treated animals could be detected. All values, however, were in the normal ranges of the SD rats.

Keywords 2-ethylhexyl-2,4,5-trimethoxycinnamate, di(2-ethylhexyl)-2,4,5-trimethoxybenzalmalonate, Cytotoxicity, Acute oral toxicity, Skin irritation, Sunscreen.

INTRODUCTION

The use of sunscreens is a very practical way to counteract against various types of ultraviolet (UV)-induced skin damage, such as photoallergies, skin wrinkles, sunburn, and skin cancer (Poon et al., 2005; Kuchel et al., 2005, Vielhaber et al., 2006). Increasing evidence of the damaging effects of UVA on skin has resulted in the need for a safe, efficient UVA filter. At the moment, the choice of organic UVA filters is very limited. Benzophenones, although considered broad-spectrum filters, possess low absorption efficiency in the UVA region. In contrast, dibenzoylmethanes, although they have high-molar-absorption coefficients in the UVA region, are not photostable (Wahlberg et al., 1999). Many studies on the safety evaluations of many organic UV filters have been carried out. For example, a study has shown that 3-(4-methylbenzylidene)camphore (4-MBC) is weakly estrogenic in rats after oral administration at high doses, and the compound also processes a low affinity to the estrogen receptors (Schlumpf et al., 2004). Chukwuemeka S. and coworkers reported a safety evaluation of benzophenone-3, the major active ingredient in sunscreen and cosmetics, in an ointment base after dermal administration in male Sprague-Dawley rats (Okereke et al., 1995). It was found that body weight, organ-to-body weight ratios, and hematological and clinical chemistry parameters were not affected by a 100 mg/kg dose of the compound.

We have recently developed two broadband filters, 2-ethylhexyl-2,4,5-trimethoxycinnamate (E8) and di(2-ethylhexyl)-2,4,5-trimethoxybenzalmalonate (B8) (Figure 1; Monhaphol et al., 2007). The two compounds show excellent photostability, high absorption in both the UVB and UVA regions (12,000 $M^{-1}cm^{-1}$ at 290 nm and 14,000 $M^{-1}cm^{-1}$ at 350 nm), and good physicochemical properties for easy cosmetic formulations. Both compounds contain no reactive chemical functionality in their structure and are quite inert.

The present studies were conducted to determine the cytotoxicity, acute oral toxicity, and skin irritation of E8 and B8.

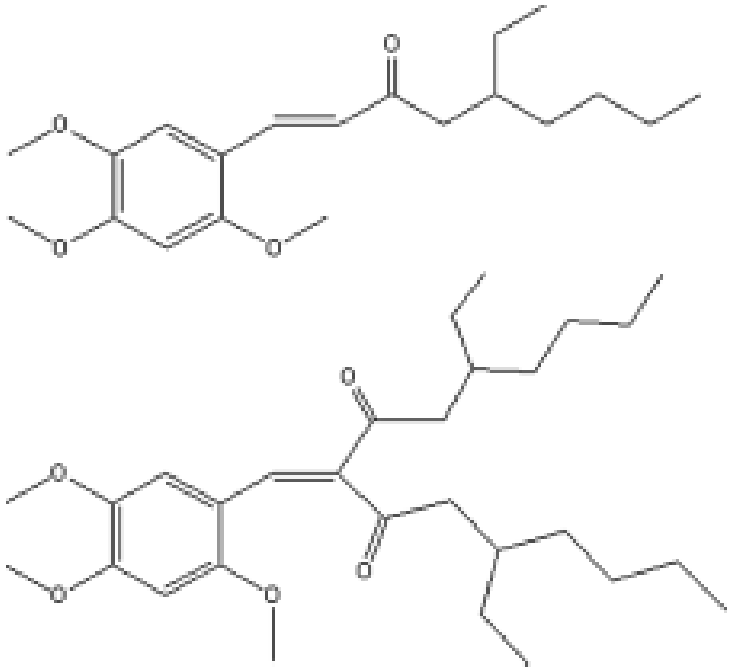

Figure 1: Chemical structure of 2-ethylhexyl-2,4,5-trimethoxycinnamate or E8 (top) and di(2-ethylhexyl)-2,4,5-trimethoxybenzalmalonate or B8 (bottom).

MATERIALS AND METHODS

Materials

The test materials, di(2-ethylhexyl)-2,4,5-trimethoxybenzalmalonate and 2-ethylhexyl-2,4,5-trimethoxycinnamate, were prepared as previously described (Monhaphol et al., 2007). Purity ≥ 99.0% was checked by both ^{1}H nuclear magnetic resonance (NMR) and high-performance liquid chromatography (HPLC) techniques.

RPMI 1640 media, fetal bovine serum (FBS), sodium pyruvate, 4H(2-hydroxyethyl)-1-piperazineethanesulfuric acid (HEPES) (free acid 1 M solution (238.3 g/L)), and Trypsin-ethylenediaminetetraacetic acid (EDTA) were obtained from HyClone (Thermo Fisher Scientific, Waltham, Massachusetts, USA). 3-(4,5-dimethyl-2-thaizolyl[2,5-diphenyl-2H-tetrazolium bromide]), or MTT, and gentamycin were obtained from Biobasic Inc. (Scarborough, Canada). Hematoxylin and eosin were purchased from Merck (Darmstadt, Germany). Mineral oil and polyoxyethylene (20) sorbitan monolaurate or polysorbate 20, were obtained from Sigma Chemical Co. (Steinheirg, Germany).

Cytotoxicity Tests

Sample Preparation

Dimethyl sulfoxide (DMSO) was used as a solvent to prepare the E8 and B8 stock solutions at the concentrations of 0.5 and 0.05 mg/μL. These stocks were then diluted with RPMI 1640 medium to give sample solutions at the concentrations of 0.05 and 0.005 mg/μL. These solutions were used for the assay and the final concentrations of the sample in the 96-well plates were 2.5 and 0.25 mg/mL. The final concentration of DMSO in the 96-well plates was 0.5% (v/v).

Cell Culture and Treatment

The human skin cancer cell line A375 (ATCC no. CRL-1619) derived from malignant melanoma was obtained from American Type Culture Collection (ATCC; Manassas, Virginia, USA). This cell line was maintained in RPMI 1640 complete medium supplemented with 10% FBS, 10 mM HEPES, 1 mM sodium pyruvate, and 1 mg/mL gentamycin, at 37°C under humidified a 5% CO_2 atmosphere. Cells were harvested with trypsin-EDTA and medium was changed every other day. For cytotoxicity tests, cells (1.0×10^6 cells/mL) were seeded in 96-well plates in 500 μL of culture and allowed to adhere for four to six hours. Five microliters of various concentrations of sample were added to each well and cells were incubated for 72 h.

Assessment of Cytotoxicity by MTT Assay

The human melanoma cell line A-375 cells were treated with samples as described above and 5 μL of MTT (5 mg/mL) was added to each well at four hours before harvesting. After 72 h of treatment, 100 μL of isopropanol in 0.04 N HCl were added to the wells to dissolve formazan crystals. Absorbances (Abs) were measured at 540 nm, using a microplate reader (BioTek Instruments, Winooski, Vemont, USA) (Diaz et al., 2006). Cell viability was calculated using the following formula:

$$\text{Cell viability (\%)} = (\text{Abs test cells}/\text{Abs control cells}) \times 100$$

Viability of cells left untreated was set at 100%. All experiments were carried out twice, at which time each of the experiments were performed in triplicate.

Acute Oral Toxicity Tests

Sample Preparation

E8 was diluted to the appropriated concentrations, using mineral oil, while the solid B8 was dispersed in polysorbate 20.

Acute Oral Exposure in Rats

All animal experimentation was performed under permission from the animal care and use commitee in the Faculty of Veterinary Science, Chulalongkorn University (IACUC).

Forty Sprague-Dawley (SD) rats (six weeks old) of both sexes (National Laboratory Animal Center [NLCA], Nakornpathom, Thailand) were kept in individual stainless steel cages for one week of acclimatization. The animals were maintained at 25 ± 2°C on a 12-h light/dark cycle and fed with a commercial pellet diet (082 diet;, NLCA, Thailand) and tap water bottles as provided *ad libitum*. In the oral acute-dose study, the animals were randomly divided into four groups (each group contained five males and five females) with a common ration of 1.0 as control, 50, 500, and 5000 mg/kg body weight for E8 and control, and 10, 100, and 1000 mg/kg body weight for B8. The test sample was fed by oral administration on the first day. Clinical signs of the animals were observed at 1, 4, and 24 h on the first day and every day for the next six days.

On the first day before the administration and on the seventh day for necropsy, blood was collected for hematology and clinical chemistry. The measured hematological parameters included white blood cell count (WBC), red blood cell count (RBC), % hemoglobin (%Hb), % hematocrit (%Hct), mean corpuscular volume (MCV), mean corpuscular hemoglobin volume (MCH), and mean corpuscular hemoglobin concentration (MCHC). Blood cells were manually counted on a hemocytometer (Life Science Co. Ltd., Bangkok, Thailand). The Hct was measured by microhematocrit centrifuge (Hettich Haematocrit, Tuttlingen, Germany), and the Hb was measured by the cyanomethemoglobin method. The clinical blood chemistry parameters monitored included blood urea nitrogen (BUN), creatinine, alanine aminotransferase (ALT, SGPT), aspartate aminotransferase (AST, SGOT), and cholesterol. The BUN value was determined by using the diacetyl monoxime (DAMO) method. SGPT and SGOT were measured by the Reitman–Frankel method. Creatinine was evaluated through the alkaline Pitrate–end-point reaction and cholesterol was determined by cholesterol oxidase, using the Chol-PAP method with the aid of a Spectronic 20 Genesys™ spectrophotometer (Spectronic Instruments, Rochester, New York, USA). The data were analyzed by a Student's *t*-test and analysis of variance (ANOVA) test ($p < 0.05$) using SAS version 8.0 computer software (SAS Institute Inc., Cary, North Carolina, USA).

The animals were sacrificed and their visceral organs were collected in 10% buffered formalin and subjected to histopathology evaluation. Liver, heart, lung, spleen, and kidney samples were histologically processed and stained with hematoxylin and eosin. Observation was carried out under a light microscope.

Skin Irritation Tests

The study protocol was approved by the Ethics Committee at the King Chulalongkorn Memorial Hospital. Informed consent was obtained from each participant.

The skin irritation test was performed using Finn chambers (Epitest Ltd., Tuusula, Finland). Photopatch testing was performed with 10 J/cm^2 of UVA irradiation, using a high-power targeted light source, DuaLight™ (TheraLight, Inc., Carlsbad, California, USA).

The test compounds (7.5% w/w) in white petrolatum were applied in duplicates on normal-appearing skin on the back of test subjects under occlusion with a Finn chamber. After 24 h, 10 J/cm^2 of UVA was irradiated to one set of test substances (the photopatch test). After an additional 24 h, both test areas were evaluated for signs of allergic contact dermatitis and irritation. The tests were performed on 43 female and 7 male volunteers. The age range of the volunteers was 17–63.

RESULTS AND DISCUSSION

Cytotoxicity of E8 and B8 on Human Skin Melanoma Cells

E8 and B8 were subjected to cytotoxicity assays, using human melanoma A-375 cells, as described above. The toxicity of these two compounds was assayed at the concentrations of 0.25 and 2.5 mg/mL. The test concentration of 2.5 mg/mL can be expressed as (1.8 mg/cm^2) (1.4 mg/cm). Since the recommended skin application dose of typical sunscreen formulation is 2 mg/cm^2 and assuming the maximum concentration of E8 or B8 in the formulation of 10% (W/V), normal coverage of the compounds on the skin during normal sunscreen application will be 0.2 mg/cm^2. Thus the test concentration much exceeded the possible maximum dose of the material. The results were obtained after 72 h, using the MTT method, which is the most commonly used colorimetric method for determining cell growth, via measuring metabolic activity in viable cells. Although the averages from six experimental values of the 0.25 mg/mL E8- and B8-treated samples seems to be significantly higher than the averages of the control and the 2.5 mg/mL samples, the Mann-Whitney U statistical analysis (six experimental values for each sample) rejected the significant difference at the probability of 0.05 or less. Mann-Whitney U statistical analysis also indicated no significant difference between the 2.5 mg/mL E8- and B8-treated samples and the control at the probability of 0.05 or less. Thus, it could be concluded that at the concentrations of 0.25 and 2.5 mg/mL, both E8 and B8 showed no significant difference in cell viability from the control (Table 1).

Table 1: Percent viability of the human skin cancer cells after being exposed to two doses of E8 and B8.

Samples	% cell viability (mean ± SD)
E8 at 0.25 mg/Ml	102.4±10.6
E8 at 2.5 mg/mL	79.4±17.0
B8 at 0.25 mg/mL	103.7±11.6
B8 at 2.5 mg/mL	87.4±11.2
0.5% DMSO (control)	88.9 ± 9.2

DMSO dimethyl sulfoxide.

Acute Oral Toxicity Tests of E8

There was neither death nor any signs of clinical change in rats administered with E8 at the dosages of 0, 50, 500, and 5,000 mg/kg body weight for the duration of 1, 4, and 24 h and two to seven days, suggesting that the lethal dose level (LD_{50}) for E8 exceeded 5000 mg/kg body weight.

During the seven days of acute toxicity study, there was no significant difference in body weight between the treated and control animals (Table 2).

Pathological examination of rat tissues (i.e., liver, kidneys, lung, heart, and spleen) collected at the end of the study period revealed no significant difference between the control and the three E8-administered groups. No significant pathological change in any tissues could be detected.

The hematological parameters were measured on the first day before the treatment and on the seventh day before necropsy. All hematological parameters were in the normal value range, and there was no significant difference among the four groups. Clinical chemistry evaluation showed that ALT, AST, creatinine, BUN, and cholesterol were all in the range of normal clinical chemistry values of the SD rats (Table 3). However, the serum ALT values were statistically reduced for all three E8-treated groups compared to the control group. The significant reduction of ALT value may indicate reduced hepatocellular damage and/or altered cell metabolism. More investigations should be carried out on this subject. In contrast, all animals including the treated and the control rats showed significantly increased creatinine values on the seventh day, compared to the values on the first day. However, all creatinine values were in the normal range. The increase was probably influenced by the growth rate, since the heavily muscled rats will normally produce more creatinine daily than the lightly muscled ones. The BUN values of the E8-treated and control animals were not different, thus indicating that renal function was not affected by E8.

Table 2 The body weights (mean ± SD) of the control and the rats administered with E8 at various doses.

	Body weights in grams (mean ± SD) of rats treated with various doses of E8							
	0 mg/Kg (Control)*		50 mg/kg*		500 mg/kg*		5000 mg/kg*	
Day	Male	Female	Male	Female	Male	Female	Male	Female
Day 0	238.0 ± 4.5	186.0 ± 5.5	222.0 ± 8.4	174.0 ± 5.5	226.0 ± 8.9	168.0 ± 4.5	232.0 ± 11.0	182.0 ± 8.4
Day 1	246.0 ± 6.2	195.6 ± 9.6	230.4 ± 11.6	184.0 ± 7.9	243.2 ± 6.4	182.2 ± 3.8	236.8 ± 8.4	186.8 ± 11.8
Day 2	260.0 ± 2.8	203.6 ± 7.5	250.8 ± 7.8	188.8 ± 6.7	253.2 ± 8.7	186.0 ± 2.8	240.8 ± 5.4	190.8 ± 12.7
Day 3	268.4 ± 8.4	206.8 ± 6.4	260.0 ± 10.8	194.0 ± 8.9	265.6 ± 6.8	189.2 ± 8.1	232.4 ± 14.8	194.4 ± 11.6
Day 4	269.2 ± 6.3	209.6 ± 7.9	257.2 ± 9.9	196.0 ± 6.5	262.8 ± 10.1	191.2 ± 5.8	255.6 ± 5.9	196.4 ± 11.5
Day 5	281.2 ± 4.4	214.0 ± 7.9	263.2 ± 10.6	202.4 ± 7.9	273.2 ± 8.9	196.0 ± 4.7	264.0 ± 6.5	202.0 ± 11.9
Day 6	292.8 ± 3.3	220.0 ± 10.3	275.6 ± 12.9	208.6 ± 9.3	284.8 ± 5.8	200.0 ± 7.2	277.6 ± 5.6	204.0 ± 13.1
Day 7	299.2 ± 2.3	223.2 ± 9.9	281.6 ± 9.7	210.8 ± 8.3	284.8 ± 10.3	202.4 ± 7.7	276.0 ± 6.0	208.4 ± 15.1

*No significant differences ($p < 0.05$) of weight among all groups

Table 3. The clinical chemistry parameters (mean ± SD) of the control rats and the rats administered with ES at various doses.

Parameters at days 0 and 7		Control		50 mg/kg		500 mg/kg		5000 mg/kg	
		M	F	M	F	M	F	M	F
ALT (IU/L)	Day 0	33.6 ± 5.9	27.2 ± 5.2	35.2 ± 3.4	30.4 ± 3.3	29.6 ± 1.7	26.0 ± 2.5	32.8 ± 4.2	30.4 ± 1.7
	Day 7	38.8 ± 8.3	28.4 ± 2.2	30.4 ± 3.6[a,b]	23.4 ± 6.5[a,b]	24.0 ± 4.0[a,b]	19.8 ± 4.3[a,b]	26.8 ± 5.4[a,b]	19.6 ± 5.5[a,b]
AST (IU/L)	Day 0	97.0 ± 20.1	81.0 ± 22.5	84 ± 18.3	100.6 ± 27.6	97.0 ± 25.8	98.2 ± 10.3	113.4 ± 18.3	86.7 ± 18.2
	Day 7	83.3 ± 33.9	82.1 ± 32.6	79.1 ± 11.4	63.7 ± 22.5	76.0 ± 27.9	77.8 ± 6.4	74.7 ± 12.9	75.2 ± 8.1
Creatinine (mg/dL)	Day 0	0.35 ± 0.05	0.3 ± 0.01	0.29 ± 0.01	0.31 ± 0.02	0.33 ± 0.04	0.33 ± 0.04	0.35 ± 0.05	0.35 ± 0.05
	Day 7	1.12 ± 0.46[a]	1.06 ± 0.52[a]	1.12 ± 0.33[a]	0.90 ± 0.39[a]	1.18 ± 0.47[a]	1.12 ± 0.4[a]	1.12 ± 0.4[a]	1.14 ± 0.3[a]
BUN (mg/dL)	Day 0	15.6 ± 2.7	15.6 ± 2.1	15.3 ± 2.2	16.7 ± 2.8	15.6 ± 1.0	16.1 ± 2.4	14.4 ± 1.4	16.2 ± 1.2
	Day 7	14.5 ± 1.5	14.4 ± 1.2	15.5 ± 0.9	14.4 ± 1.4	16.8 ± 1.2	14.0 ± 1.1	14.0 ± 0.9	13.0 ± 1.8
Cholesterol (mg/dL)	Day 0	124.4 ± 13.1	126.1±3.4	114.1 ± 21.3	113.1 ± 16.4	128.8 ± 40.2	139.4 ± 24.8	151.1 ± 41.2	152.6 ± 31.4
	Day 7	124.7 ± 45.3	123.0 ± 12.0	103.1 ± 8.2	124.4 ± 10.3	101.1 ± 12.8	134.3 ± 18.1	110.2 ± 7.6	129.1 ± 11.6

ALT, alanine aminotransferase; AST, aspartate aminotransferase; BUN, blood urea nitrogen.
[a]Significant differences ($p < 0.05$) in comparison to the day of treatment.
[b]Significant differences ($p < 0.05$) in comparison to the control group.

Acute Oral Toxicity Tests of B8

Similar to E8, there was also no deaths due to any administrated amounts of B8 for the duration of 1, 4, and 24 h and two to seven days after the treatment of B8 at the dosages of 0, 10, 100, and 1000 mg/kg body weight. It should be noted here that 1000 mg/kg body weight was the maximum administration amount of the solid B8 compound into the rats. This is because of a limited dispersibility of the compound in polysorbate 20. Clinical observations indicated excitation of respiratory signs of dypsnea in all three B8-treated groups during 1–24 h. Some animals in the 1000 mg/kg group showed congestion of the eye during the first four hours after administration. All groups were, however, normal during the second to seventh day, suggesting that the calculation for LD_{50} is out of the range of 1000 mg/kg body weight.

During the seven-day acute toxicity study, there was significant difference in body weight and the average daily gain of the highest dose (1000 mg/kg) group of male rats from other groups ($p < 0.05$) (Table 4). However, no significant difference in body weight and the average daily gain could be found among the female rats.

Pathological examination of rat tissues (i.e., liver, kidneys, lung, heart, and spleen) collected at the end of the study period revealed no significant differences between the control and the treated groups. No pathological change in the tissues could be histopathologically detected.

All hematological parameters were measured on the first day before the treatment and on the seventh day for necropsy. For all groups, the hematological parameters obtained on the seventh day were in the normal range and there was no significant difference among the four groups. All clinical chemistry parameters monitored were in the normal values of the SD rats (Table 5).

In all groups, including the control, serum ALT values were significantly increased. In the control, 10 and 100 mg/kg B8-treated groups, significant increases of cholesterol could be detected. This suggested that the dispersing medium, polysorbate 20, might affect protein and fat metabolism in the liver. Creatinine values were statistically increased in control rats and all B8 treated rats; however, all values were in the normal ranges. The increase in the creatinine values agreed with the increase in body weight of the rats.

Skin Irritation Test

The patch and photopatch tests were selected as irritation tests for E8 and B8. Since most organic UV filters possess some risk of skin irritation, the experiment was carried out not only with E8 and B8, but also with the popularly used UVB filter, 2-ethylhexyl-4-methoxycinnamate or E3. Pure white petrolatum was used as a control. On patch testing, only 1 volunteer among 50 showed a weakly positive reaction to E3 at the 48-h postapplication. However, no subjects showed any erythema to E8 and B8. Therefore, these results are reassuring in terms of E8 and B8 safety. The result agrees well with a previous study on the contact

Table 4 The body weights in grams (mean ± SD) of the control rats and the rats administered E8 at various doses.

	Body weights in grams (mean ± SD) of rats treated with various doses of E8							
	0 mg/kg (Control)		10 mg/kg		100 mg/kg		1000 mg/kg	
Day	Male	Female	Male	Female	Male	Female	Male*	Female
Day 0	208.0 ± 4.5	174.0 ± 16.7	202.0 ± 8.4	174.0 ± 5.5	218.0 ± 8.4	174.0 ± 5.5	216.0 ± 8.9	172.0 ± 8.4
Day 1	208.4 ± 4.8	178.0 ± 17.5	204.0 ± 7.1	165.6 ± 3.6	216.4 ± 9.0	165.6 ± 6.5	214.4 ± 10.1	166.8 ± 5.8
Day 2	215.6 ± 5.7	181.0 ± 15.2	220.0 ± 6.3	175.6 ± 3.6	229.6 ± 7.9	178.0 ± 6.2	227.6 ± 7.5	179.6 ± 5.5
Day 3	225.2 ± 5.2	189.2 ± 13.2	230.4 ± 6.5	185.2 ± 4.8	246.0 ± 5.5	188.0 ± 5.7	244.0 ± 6.5	186.0 ± 7.6
Day 4	232.4 ± 6.8	194.8 ± 14.6	229.6 ± 7.8	185.2 ± 2.3	243.2 ± 13.1	190.4 ± 6.7	244.4 ± 8.2	191.2 ± 7.9
Day 5	232.4 ± 5.5	194.8 ± 13.8	232.0 ± 7.3	189.2 ± 3.0	247.6 ± 9.9	189.6 ± 8.3	250.8 ± 9.7	192.8 ± 5.8
Day 6	248.4 ± 4.3	202.8 ± 14.0	248.0 ± 8.4	196.0 ± 2.0	263.2 ± 10.4	196.4 ± 5.7	266.8 ± 11.2	202.0 ± 5.1
Day 7	244.4 ± 4.6	203.2 ± 14.0	249.0 ± 7.7	200.4 ± 3.0	264.8 ± 13.5	199.2 ± 7.3	278.4 ± 16.3	202.4 ± 6.2

*Significant differences ($p < 0.05$) of the 1000 mg/kg group from the control group.

Table 5: Clinical chemistry values (mean ± SD) of the rats administered with B8 at various doses.

Parameters at days 0 and 7		Control		10 mg/kg		100 mg/kg		1000 mg/kg	
		M	F	M	F	M	F	M	F
ALT (IU/L)	Day 0	14.7 ± 8.5	12.6 ± 4.8	15.2 ± 6.4	19.4 ± 5.2	13.8 ± 9.4	13.7 ± 3.9	19.4 ± 5.2	17.9 ± 4.2
	Day 7	18.7 ± 3.4	25.68 ± 5.0[a]	24.9 ± 4.7	27.1 ± 12.3	20.2 ± 6.4	28.7 ± 8.1	26.8 ± 6.4	34.7 ± 7.4[a]
AST (IU/L)	Day 0	160.4 ± 39.4	177.7 ± 28.0	129.0 ± 66.7	157.4 ± 30.6	198.4 ± 73.5	141.9 ± 22.8	157.4 ± 25.7	170.7 ± 23.6
	Day 7	152.4 ± 28.5	156.4 ± 10.6	192.2 ± 22.4	175.6 ± 27.5	222.6 ± 28.2[b]	177.7 ± 28.0	205.0 ± 31.2	177.0 ± 21.5
Creatinine (mg/dL)	Day 0	0.20 ± 0	0.30 ± 0.04	0.22 ± 0.02	0.3 ± 0.15	0.22 ± 0.03	0.6 ± 0.5	0.2 ± 0.02	0.5 ± 0.12
	Day 7	0.53 ± 0.2[a]	0.32 ± 0.1	0.61 ± 0.1[a]	0.3 ± 0.1	0.51 ± 0.2	0.7 ± 0.1[b]	1.55 ± 2.5[b]	0.68 ± 0.1[b]
BUN (mg/dL)	Day 0	8.9 ± 3.0	12.1 ± 1.6	10.9 ± 2.2	9.3 ± 1.3	10.4 ± 1.1	11.8 ± 1.0	9.5 ± 1.3	12.4 ± 1.7
Cholesterol (mg/dL)	Day 7	10.94 ± 1.5	9.9 ± 1.3	12.3 ± 1.0	14.3 ± 1.9[a,b]	13.4 ± 1.9	11.7 ± 3.2	12.08 ± 1.9	12.4 ± 2.0
	Day 0	75.9 ± 12.0	100.9 ± 15.8	137.3 ± 50.9[b]	101.6 ± 29.4	119.3 ± 8.6	102.4 ± 41.8	92.5 ± 17.8	141.3 ± 21.3
	Day 7	152.3 ± 36.9[a]	172.1 ± 43.9[a]	163.7 ± 11.0[a]	204.5 ± 61.3[a]	167.9 ± 14.1[a]	189.3 ± 32.0[a]	159.5 ± 26.4[a]	155.0 ± 28.4[a]

ALT, alanine aminotransferase; AST, aspartate aminotransferase; BUN, blood urea nitrogen.
[a] Significant differences ($p < 0.05$) from the day of treatment.
[b] Significant differences ($p < 0.05$) from the control group.

sensitization of E3 by the patch and photopatch tests, which indicated that the incidence of allergic contact dermatitis to E3 was low (Ricci et al., 1997).

CONCLUSION

This study has evaluated the safety of the two new UV filters, E8 and B8. The results indicate that the two compounds are not very cytotoxic to human melanoma A-375 cells (in the screening system employed), are not very toxic following single oral doses in rats, and do not appear to affect human skin adversely. Thus, they are relatively safe when considered as a cosmetic ingredient.

ACKNOWLEDGMENTS

This work was supported by the Royal Golden Jubilee Ph.D. program, Thailand Research Fund, and the 90th Anniversary of Chulalongkorn University Fund (Ratchadphisaksomphot Endowment Fund). The authors also thank Mr. Preecha Moonsan, Ms. Walaya Jittaprasatsin, and Mr. Supradit Wangnaitham for their laboratory animal assistance.

REFERENCES

Kuchel, J. M., Barnetson, R. S., Halliday, G. M. (2005). Cyclobutane pyrimidine dimer formation is a molecular trigger for solar-simulated ultraviolet radiation-induced suppression of memory immunity in humans. *Photochem. Photobiol. Sci.* 4:577–582.

Monhaphol, T., Albinsson, B., Pattanaargson, S. W. (2007). 2-ethylhexyl-2,4,5-trimethoxycinnamate and di-(2-ethylhexyl)-2,4,5-trimethoxybenzalmalonate as novel UVA filters. *J. Pharm. Pharmacol.* 59:279–288.

Okereke, C. S., Barat, S. A., Abdel-Rahman, M. S. (1995). Safety evaluation of benzophenone-3 after dermal administration in rats. *Toxicol. Lett.* 80:61–67.

Poon, T. S., Barnetson, R. S., Halliday, G. M. (2005). Sunlight-induced immunosuppression in humans is initially because of UVB, then UVA, followed by interactive effects. *J. Invest. Dermatol.* 125:840–846.

Ricci, C., Vaccari, S., Cavalli, M., Vincenzi, C. (1997). Contact sensitization to sunscreens. *Am. J. Contact Dermat.* 8:165–166.

Schlumpf, M., Schmid, P., Durrer, S., Conscience, M., Maerkel, K., Henseler, M., Gruetter, M., Herzog, I., Reolon, S., Ceccatelli, R. (2004). Endocrine activity and developmental toxicity of cosmetic UV filters-an update. *Toxicology* 205:113–122.

Vielhaber, G., Grether, B. S., Koch, O., Johncock, W., Krutmann, J. (2006) Sunscreens with an absorption maximum of > or = 360 nm provide optimal protection against UVA1-induced expression of matrix metalloproteinase-1, interleukin-1, and interleukin-6 in human dermal fibroblasts. *Photochem. Photobiol. Sci.* 5:275–282.

Wahlberg, N. T., Stenhagen, N., Larko, G., Rosen, O., Wennberg, A., Wennerström, O. (1999). Changes in ultraviolet absorption of sunscreens after ultraviolet irradiation. *J. Invest. Dermatol.* 113:547–553.

ภาคผนวก ข

Monitoring 2-Ethylhexyl-4-Methoxycinnamate Photoisomerization on Skin Using Attenuated Total Reflection Fourier Transform Infrared Spectroscopy

P. PANGNAKORN, R. NONTHABENJAWAN, S. EKGASIT, C. THAMMACHAROEN, and S. PATTANAARGSON WANICHWECHARUNGRUANG*

Senior Research Unit, Department of Chemistry, Faculty of Science, Chulalongkorn University, Bangkok, Thailand

Photoisomerization and photodimerization of a widely used UVB filter, 2-ethylhexy-4-methoxycinnamate (EHMC) on a ZnSe surface and baby mouse (*Mus musculus* Linn.) skin were monitored using attenuated total reflection Fourier transform infrared spectroscopy (ATR-FT-IR). Differentiation between the *E*- and the *Z*-EHMC could be achieved by examining the infrared (IR) peak at 981 cm^{-1} (h peak), which corresponds to the CH rocking deformation vibration of Ph–CH=CH– detected only in the *E* configuration. By plotting the ratio of the peak area of the h peak and an internal standard peak (1060–998 cm^{-1}) against mole percentage of *Z*-isomer in the *E*-*Z* mixture, a linear calibration plot was obtained. Thus, a simple estimation of the mole percentage of each configuration in a sample was obtained. At the same UVB exposure, photostationary equilibrium of the *EZ* isomerization on the surface varied with the applied amounts of EHMC. Photoisomerizations on ZnSe and on baby mouse skin were comparable. Less than 10% of *E*-EHMC changed configuration when the mouse skins applied with 1.0–4.0 mg/cm^2 *E*-EHMC were exposed to sunlight for 60 min (UVB radiant exposure of ~0.30 J/cm^2). This corresponded to less than 5% loss in UV filtering efficiency. However, at a typical EHMC skin coverage (~0.2 mg/cm^2), 0.30 J/cm^2 UVB exposure induced ~30% photoisomerization resulting in 25% loss of UV filtering efficiency. No photodimerization was detected even at the extreme EHMC coverage of 4.0 mg/cm^2 after a UVB exposure of 0.90 J/cm^2.

Index Headings: 2-Ethylhexy-4-methoxycinnamate; EHMC; Photoisomerization; Sunscreen; Attenuated total reflection Fourier transform infrared spectroscopy; ATR-FT-IR.

INTRODUCTION

Many adverse health effects of long-term ultraviolet (UV) exposure including direct cellular damage and immunosuppression leading to photoaging, mutations, and carcinogenesis have been well established.[1–3] Sunscreens have been widely used as the primary means to minimize these possible damaging effects, as well as other photosensitivity and phototoxicity on human skin. Among many UVB screening compounds, 2-ethylhexyl4-methoxycinnamate (EHMC) is popularly used in various cosmetic formulations in sunscreen products. EHMC not only possesses a high molar absorption coefficient (ε), approximately 22 000–24 000 M^{-1} cm^{-1} (at 310 nm), but also shows only a few allergic reactions to human skin.[4–7]

Solution phase studies have demonstrated that the EHMC molecule underwent a photoisomerization from *E* (*trans*) to *Z* (*cis*) configuration, leading to a decrease in UV absorption efficiency due to the lower molar absorption coefficient of the *Z*-EHMC (12 000 M^{-1} cm^{-1}) compared to that of the *E*-EHMC (22 000–24 000 M^{-1} cm^{-1}).[8–12] Kinetic studies in solution also revealed influences from both a solvent's polarity and EHMC concentration on the photostationary equilibrium of the *E*/*Z* photoisomerization reaction.[8] Photodimerization of EHMC in solution was more favorable at higher concentrations. Steady state and laser flash photolysis study of EHMC in aqueous and organic solutions revealed a fairly high (~0.5–1) quantum yield of photoisomerization.[13] Photophysical characterization of various cinnamate derivatives have suggested a singlet or very short lived triplet excited state for EHMC, indicating that the compound is unlikely to be a photosensitizer.[14–16]

Since all EHMC photoisomerization reports have been done in solution, but the use of EHMC as sunscreen is on skin, it is interesting to monitor the photochemical change of this sunscreen when directly applied to skin. In this paper, we report the monitoring of *E* to *Z* and *Z* to *E* photoisomerization and dimerization of the compound on a ZnSe surface and on baby mouse (*Mus musculus* Linn.) skin using attenuated total reflection Fourier transform infrared (ATR-FT-IR) spectroscopy.

MATERIALS AND METHODS

Materials. 2-Ethylhexyl-*p*-methoxycinnamate (Escalol® 557, EHMC) was obtained from Merck Co. Ltd. (Bangkok, Thailand). The solvents used were reagent or analytical grades purchased from Labscan (Bangkok, Thailand). LiChrosorb C-18 was purchased from Merck KgaA (Darmstadt, Germany).

Baby Mouse Skin Preparation. The skin specimens comprised both the epidermis and dermis of baby mice (*Mus musculus*) aged 3 weeks and were purchased from National Laboratory Animal Center (Thailand). They were kept frozen at −20 °C. Prior to each experiment, the frozen skin was allowed to defrost at room temperature before being cut into 5.0 × 0.5 cm^2 pieces. The skin's thickness was 1.76 ± 0.172 mm (mean ± S.D.).

Ultraviolet Irradiation Source. For UVB irradiation, a Daavlin Psoriwand broadband UVB lamp, PW-UVB-220 (Daavlin, OH), was used. UV irradiance was measured by a UVB power meter, UVB-500c (National biological corporation, Twinsburg, OH).

Preparation of *Z*-EHMC and Dimerized Product. A solution of 7 mM *E*-EHMC in methanol was exposed to 10 J/cm^2 broadband UVB. The light-exposed solution containing *E*-EHMC, *Z*-EHMC, and some dimerized products was then evaporated under vacuum at 50 °C. Isolation of *Z*-EHMC and dimer was done under light-proof conditions by reverse phase (LiChrosorb C-18) chromatography with gradient elution starting from 70:30 (v/v) methanol:water to pure methanol. The isolated-*Z*-EHMC and the isolated-dimer were analyzed

Received 3 August 2006; accepted 28 November 2006.
* Author to whom correspondence should be sent. E-mail: psupason@chula.ac.th.

0003-7028/07/6102-0193$2.00/0

through the use of ^{1}H nuclear magnetic resonance (NMR).[8] All Z-EHMC and dimer fractions were separately pooled together and immediately evaporated under vacuum at 50 °C. Care was given to prevent any light exposure to the eluted fractions.

Attenuated Total Reflection Fourier Transform Infrared Spectroscopy. Infrared spectra were obtained using a Nicolet Magna-IR®750 FT-IR spectrometer equipped with a DTGS detector (Nicolet Instrument Corporation, WI). Spectra were acquired at a resolution of 4 cm^{-1} with 64 scans at the wavelength of 4000–650 cm^{-1}. The spectrometer was linked to a PC equipped with Nicolet's OMNIC software package Version 5.1 to allow the automated collection of IR spectra. Transmission mode was used for all measurements. All experiments were done at ambient temperature, 25 ± 2 °C. Experiments were done either in duplicate or triplicate. Two types of reflection systems were employed in the experiments, a single reflection system and a multiple reflection system. In the single reflection system, a variable angle reflection accessory (the Seagull™, Harrick Scientific, Ossining, NY) with a hemispherical ZnSe (zinc selenide) was used. In the multiple reflection system, a multiple attenuated total reflectance accessory (MATR) was mounted into the sample compartment of the FT-IR spectrometer. The internal reflection crystal (Spectra Tech, Noblesville, IN), which was made of ZnSe, was set at 45 degrees (the angle between the incidence beam and the detected IR beam).

Infrared Spectra of *E*-EHMC, Z-EHMC, and Dimerized Product. The standard IR spectra of *E*-EHMC, Z-EHMC, and dimerized product were acquired using the single reflection system. A sample was dropped onto the Seagull™ accessory and the spectrum was recorded and processed using OMNIC 5.1 software.

Calibration Standards. In this experiment, all IR spectra were acquired using the multiple reflection system. The 0.10 mL of freshly prepared solution containing appropriate amounts of *E*-EHMC and Z-EHMC was dropped and spread over the flat surface of ZnSe (surface area = 5.0 × 0.5 cm^2). Three experimental sets at the final (*E*+*Z*) EHMC coverages on surfaces of 1.33×10^{-7}, 3.44×10^{-6}, and 6.89×10^{-6} mol/cm^2 were all done in duplicate. After solvent (methanol) evaporation, IR spectra were then recorded and processed using OMNIC software.

E to Z Photoisomerization on ZnSe. Monitoring of the *E*- to Z-EHMC photoisomerization was done by recording IR spectra at various times of UV irradiation using the multiple reflection system. For the first spectrum, a specific amount of *E*-EHMC solution (in methanol) was dropped over the flat surface of a ZnSe crystal (surface area = 5.0 × 0.5 cm^2) using an analytical syringe and was spread evenly over the surface. The final coverages of EHMC on the ZnSe surface were 1.34×10^{-7}, 3.44×10^{-7}, 6.89×10^{-7}, 1.38×10^{-6}, 2.04×10^{-6}, 3.44×10^{-6}, 6.89×10^{-6}, and 1.38×10^{-5} mol/cm^2, which corresponded to 0.04, 0.10, 0.20, 0.40, 0.60, 1.0, 2.0, and 4.0 mg/cm^2. This spread solution was dried under ambient and light-proof conditions for at least 5 min and the first IR spectrum (irradiation time = 0 min) was then acquired.

Before acquiring the next spectra, the ATR accessories were opened and the irradiation unit (a Dauvlin Psorawand broadband UVB lamp: PW-UVB-220) was set up to irradiate UVB directly upon the EHMC-covered ZnSe crystal surface. The UVB irradiation and IR recording process was then started with the sample receiving 0.25 mW/cm^2 UVB irradiation for 1 min. Immediately after such UVB exposure, the ATR accessories were closed and an IR acquisition was carried out. These 1 min UVB exposure period and IR recording steps were repeated for a total of 10 cycles (total UV exposure time of 10 min). After 10 cycles, the steps were repeated again but the UV exposure time was now changed from 1 min to 5 min. These repetitions of 5 min UV exposure period and IR recording were carried out for 10 cycles (total UV exposure time of 10 × 5 = 50 min). As a result, the recordings of IR spectra during the 60 min UVB exposure period were carried out every 1 min for the first 10 min and every 5 min for the next 50 min light exposure. In summary, IR recordings of the sample were done immediately after the sample received UVB doses of 0, 15, 30, 45, 60, 75, 90, 105, 120, 135, 150, 225, 300, 375, 450, 525, 600, 675, 750, 825, and 900 mJ/cm^2. The background spectrum was then subtracted from each IR spectrum obtained. The background spectrum was obtained by acquiring the IR spectrum of the ZnSe crystal before the application of EHMC. All experiments were done in triplicate.

Z to *E* Photoisomerization on ZnSe. The Z-EHMC solution (in methanol) was spread over the surface of a ZnSe crystal and left to dry as previously described, yielding a ZnSe surface covered with 1.34×10^{-7} mol/cm^2 Z-EHMC. Similar UV exposures and IR spectral acquisitions, as carried out on the *E* to Z photoisomerization on ZnSe, were done to the sample. The experiment was done in triplicate.

E to Z Photoisomerization on Baby Mouse Skin. A specific amount of *E*-EHMC solution (in methanol) was dropped and spread evenly over the surface (stratum corneum side) of a skin specimen (surface area = 5.0 × 0.5 cm^2). The final applied amounts of EHMC on the skin were 6.89×10^{-7}, 3.44×10^{-6}, 6.89×10^{-6}, and 1.38×10^{-5} mol/cm^2, which corresponded to 0.2, 1.0, 2.0, and 4.0 mg/cm^2. The sample was then dried under ambient and light-proof conditions for at least 5 min. The skin surface (stratum corneum side) was then pressed against a flat ZnSe crystal (multiple reflection system) and an IR spectrum was acquired. To receive UVB radiation, the skin sample was taken out and quickly irradiated with UVB for an appropriate time. Then the skin was quickly pressed back against the ZnSe crystal and another IR acquisition was carried out. Similar UV exposure and IR acquisition cycles as described earlier were used, i.e., over 60 min UVB exposure, recordings of IR spectra were done every 1 min for the first 10 min UV exposure and every 5 min for the next 50 min UV exposure. The background spectrum was then subtracted from each IR spectrum obtained. The background spectrum was obtained by acquiring the IR spectrum of each skin sample before EHMC was applied.

The baby mouse skin applied with 6.89×10^{-6} mol/cm^2 EHMC was exposed to sunlight for 0 and 60 min and the ATR FT-IR spectra were recorded. EHMC was applied to the mouse skin as described above. The IR spectrum of the unexposed EHMC applied skin (0 min exposure) was recorded by fixing the skin piece on ATR accessories (multiple reflection system) in such a way that the stratum corneum side was pressed against the ZnSe crystal. After the first IR recording, the skin sample was taken out and immediately brought into the sunlight with the stratum corneum face up. After 60 min under the sunlight, the skin sample was immediately put back into the ATR accessories and an IR recording was carried out. UVB irradiance of the sunlight was recorded during the experiment

using a UVB power meter. All experiments were done at least in triplicate.

RESULTS AND DISCUSSION

Infrared Spectra of *E*-EHMC, *Z*-EHMC, and Dimerized Product. Two major differences between the IR spectra of *E*-EHMC and *Z*-EHMC are shown in Figs. 1a–1d. The first difference was the CH out-of-plane deformation of the Ph–CH=CH– moiety at 720–690 cm^{-1} present only in the *Z* configuration (Fig. 1b). The second major difference appeared at 981 cm^{-1}, which corresponded to the CH rocking deformation vibration of Ph–CH=CH– detected only in the *E* configuration (Fig. 1c). Since the CH out-of-plane deformation peak at 720–690 cm^{-1} was too close to the ZnSe cut-off, the CH rocking deformation vibration at 981 cm^{-1} was chosen for monitoring the configuration change of the EHMC molecule in this work.

The most obvious difference between the IR spectrum of the dimerized product and the IR spectra of both EHMC isomers was at 1635–1555 cm^{-1} (*C* peak), which corresponded to C=C stretching (from Ph–CH=CH–). The *E*-EHMC showed medium to strong absorption at 1635–1620 cm^{-1} and the *Z* configuration displayed a medium to strong peak at 1640–1630 cm^{-1} for this stretching. The IR spectrum of the dimer showed an obvious absorption at these wavenumbers (Fig. 1d).

Calibration Standards. Figure 2 (top panel) shows a series of IR spectra of *E*–*Z* mixtures at various *E*/*Z* mole ratios. It can be clearly seen that the 981 cm^{-1} peak intensity varies with the *E*/*Z* ratio. To investigate the potential of using this IR signal to estimate the *E*/*Z* mole ratio, *E*–*Z* mixtures (calibration standards) containing 0, 10, 25, 50, 75, 90, and 100 mole percentages of *Z*-isomer were prepared and their IR spectra were acquired. Three experimental sets were done in duplicate at the total (*E*+*Z*) EHMC coverages on the ZnSe surface of 1.33×10^{-7}, 3.44×10^{-6}, and 6.89×10^{-6} mol/cm^2. By

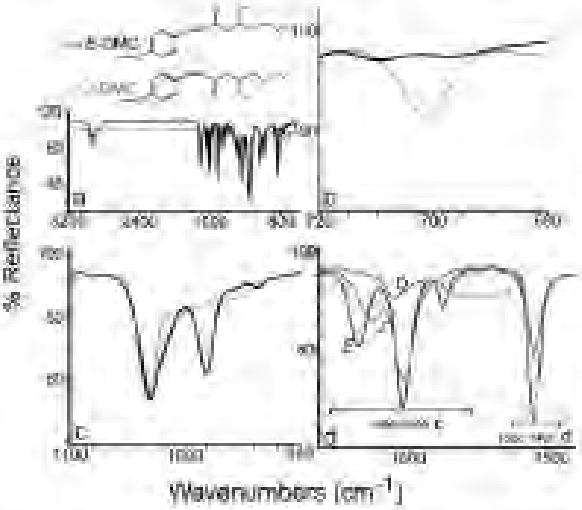

Fig. 1. ATR-FT-IR spectra on the ZnSe surface of (a) *E*-EHMC and *Z*-EHMC at 4000–700 cm^{-1}; (b) *E*-EHMC and *Z*-EHMC at 720–690 cm^{-1}; (c) *E*-EHMC and *Z*-EHMC at 1100–900 cm^{-1}; and (d) *E*-EHMC (E), *Z*-EHMC (Z), dimerized product (D), and 0.90 J/cm^2 UVB exposed *E*-EHMC (exposed E) at 1650–1450 cm^{-1}.

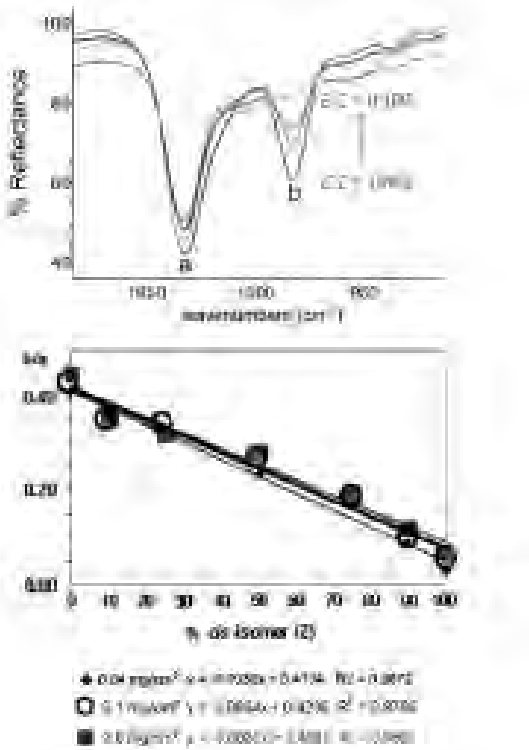

Fig. 2. Calibration experiments. (Top) Overlaid ATR-FT-IR transmittance spectra of the *E*-*Z* mixtures containing 0, 50, 75, and 100 mole percent of *Z*-EHMC. The total coverage of (*E*+*Z*) EHMC on the ZnSe surface was 1.34×10^{-7} mol/cm^2. (Bottom) plots of mole percentage of *Z*-EHMC in the *E*–*Z* mixture against the b/a ratio. The experiments were done at three total coverages of EHMC, 0.04, 0.1, and 2.0 mg/cm^2. Each point was an average of two experimental points. Linear correlations and R^2 values were obtained by the least square fits for each data set.

plotting the ratio of the peak area at 998–964 cm^{-1} (peak b indicating *E*-configuration) and 1060–998 cm^{-1} (internal standard peak, peak a), later referred to as the b/a ratio, against mole percentage of *Z*-isomer in the *E*–*Z* mixture, linear calibration plots were obtained (Fig. 2, bottom panel). Since good linearity was obtained at all three coverages, a simple estimation of a mole percentage of each configuration in an *E*–*Z* mixture could be done using the b/a ratio obtained from an IR spectrum.

By evaluating IR spectra, it was found that the ratio between the peak area at 1635–1555 cm^{-1} (from Ph–CH=CH– stretching, peak c) to the peak area at 1520–1495 cm^{-1} (peak d) was around 1.9–2.0 for both *E*- and *Z*-EHMC (see Fig. 1d). However, such c/d ratio for the dimer dropped significantly to less than 0.7. As a result, a c/d ratio of less than 1.9 can be used to indicate the presence of dimerized product in an irradiated EHMC sample. Since the presence of dimers will affect the *E*/*Z* ratio determination, looking for dimers in all IR spectra was done prior to the determination of the *E*/*Z* ratio.

EHMC Photoisomerization on the ZnSe Surface. Monitoring of the *E* to *Z* configuration change of EHMC on the ZnSe surface was done at various EHMC coverages. Analysis of an IR spectrum at each UV exposure gave the b/a ratio

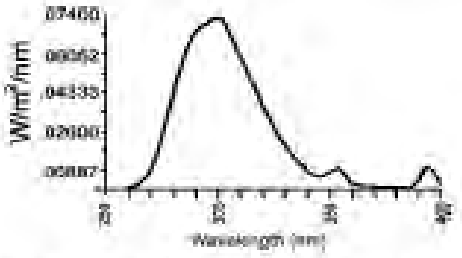

FIG. 3. Spectral radiance of the UVB lamp used in this experiment.

which, could be used to determine a mole percentage of each configuration using the standard curve obtained as described earlier.

E-EHMC on the ZnSe surface was irradiated with broadband UVB light (see Fig. 3 for spectral radiance of the lamp) and changes in the IR spectra, especially at the b peak (968–964 cm^{-1}), at various UV exposures were very obvious (Fig. 4). At the same exposure, changes were more pronounced at lower coverages of EHMC. A plot between %*Z*-EHMC (determined from the FT-IR spectra using the b/a ratio and the calibration curve described earlier) and the UVB radiant exposure indicates different degrees of isomerization for different coverages (Fig. 5a). No photodimerization could be detected even at the highest coverage of EHMC (1.38×10^{-5} mol/cm^2 or 4.0 mg/cm^2). This result agrees with the previous solution-phase study reported by Devabhaktuni and Ramamurthy, in which irradiation of cinnamate solutions in benzene (10^{-3}–10^{-4} M) resulted only in geometric isomerization.[10] In addition, the photostability study of EHMC solution in methanol (3.4×10^{-5} M) also showed only *cis*-isomer.[20]

At the same UVB exposure, isomerization was more pronounced at lower coverages of EHMC (Figs. 4 and 5a). At high coverages (6.29×10^{-6} and 1.38×10^{-5} mol/cm^2), no obvious spectral change at the b peak was observed after the irradiation, indicating no significant photoisomerization. This can be explained by the shielding effect of EHMC molecules, i.e., at a high coverage, the majority of EHMC molecules on the ZnSe surface should be shielded from UVB light by the

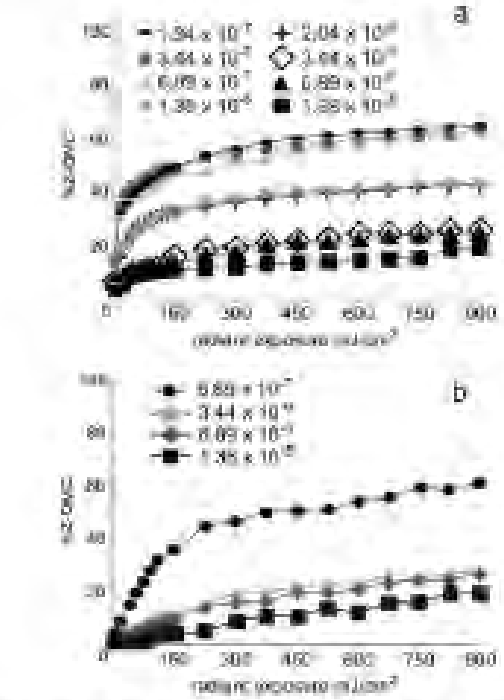

FIG. 5. Kinetics of *E*- to *Z*-EHMC photoisomerization on (a) ZnSe surface and (b) baby mouse skin. Each point was an average of three experimental data points. Standard deviation ranges of graph a and b were 2–6% and 2–11%, respectively.

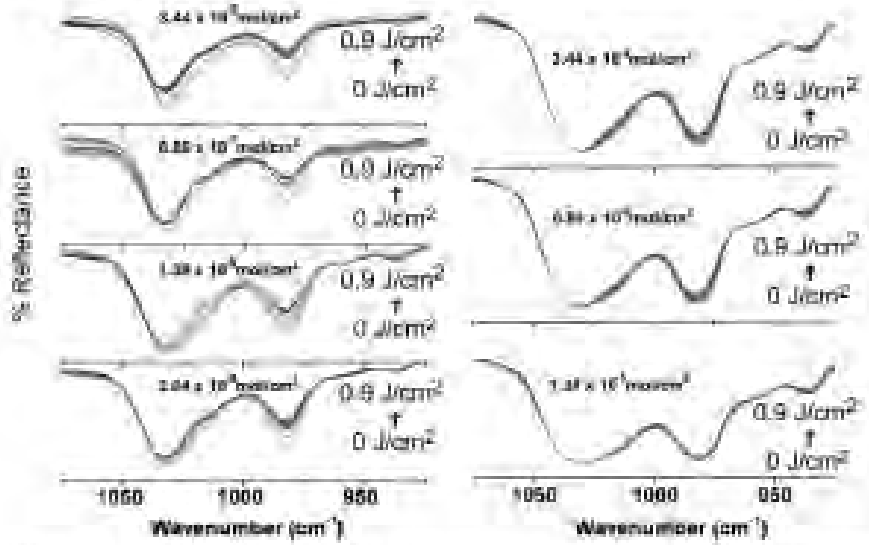

FIG. 4. Overlaid *E*-EHMC ATR-FT-IR spectra at various UVB exposures (0, 1.50, 3.01, 4.50, 6.01, 7.51, and 9.01 mJ/cm^2). At the same UVB exposure, different *E*-EHMC coverages (indicated in mol/cm^2) gave different degree of spectral changes at 1075–925 cm^{-1}.

UVB screening property of the EHMC molecules above them.

It should be noted here that the presence of any photodimerized products at every irradiation progress point was checked through the ratio of the peak area at 1655–1555 cm^{-1} (peak c) to peak area at 1520–1495 cm^{-1} (peak d) as described earlier. No dimerization was detected during the irradiation process. As shown in Fig. 3d, after 0.90 mJ/cm^2 irradiation onto a 4.0 mg/cm^2 EHMC covered ZnSe crystal, the IR spectrum still gave a c/d ratio of 2.0, thus indicating no dimerized product. Attempts at monitoring the EHMC photodimerization on surfaces at higher EHMC coverage failed due to over-saturated IR spectra. However, it should be noted here that the 4.0 mg/cm^2 EHMC coverage is already an extreme EHMC coverage considering that the normal use of EHMC on skin is around 0.1–0.2 mg/cm^2. Since photodimerization is expected to be more favorable at higher concentrations of EHMC, this result implies that photodimerization is very unlikely when EHMC is applied normally to the skin.

A study of the *Z*- to *E*-EHMC configuration change on the ZnSe surface was done at 1.34×10^{-7} mol/cm^2 (0.04 mg/cm^2) of EHMC coverage. The result indicated that Z-EHMC also underwent configuration change on the surface upon UVB irradiation.

It should be noted here that the uniformity of EHMC on the ZnSe surface may directly affect the degree of photoisomerization through some shielding effects among EHMC molecules. However, by using the multiple-reflection system, the IR signal obtained was already an average of many interactions of the IR light with EHMC molecules across the sampling surface. With the described experimental procedure, the spreading of EHMC was reproducible enough to give less than 5% standard deviation value for the b/a ratios obtained from different repetitions.

EHMC Photoisomerization on Baby Mouse Skin. By applying EHMC solution onto a baby mouse skin sample, allowing the solvent to evaporate, and pressing the stratum corneum side of the skin against the flat ZnSe crystal, the IR spectrum of the applied EHMC could be acquired. By taking the skin sample out of the ATR accessories and then repressing it against the ZnSe crystal to obtain another IR spectrum, reproducibility of the procedure could be checked. It was found that the b/a ratios among various repetitions are similar (Fig. 6a), thus confirming reproducibility of the method. In addition, a comparison among different skin pieces applied with the same coverage of EHMC was carried out. Results showed comparable c/d and b/a ratios among different skin pieces (Fig. 6b). The maximum standard deviation value obtained from different repetitions was 1%. It should also be noted here that the persistence of EHMC to the stratum corneum of the baby mouse skin was good enough to leave an insignificant amount of EHMC on the ZnSe crystal surface after each IR acquisition. In addition, for all EHMC coverages used in the experiment, EHMC peaks over-saturated the skin's background peaks; therefore, *E*–*Z* photoisomerization could be followed.

Analyzing the c/d ratios in all IR spectra indicated no dimerization of EHMC molecules on mouse skin. In other words, under these experimental conditions, all spectra showed a c/d ratio of at least 1.9. The *E* to *Z* configuration change of EHMC on baby mouse skin was estimated from ATR-FT-IR spectra using the b/a ratio as described previously. The ATR-FT-IR spectra of mouse skin applied with 0.2–4.0 mg/cm^2 *E*-EHMC revealed obvious photoisomerization of the compound after being exposed to broadband UVB light (lamp intensity of 0.25 mW/cm^2). Figure 5b shows the kinetics of *E*- to *Z*-EHMC photoisomerization on baby mouse skin. Similar to the results obtained from the experiment done on ZnSe, at the same UVB exposure, the photostationary equilibrium of EHMC on mouse skin varied with the amount of EHMC initially applied to the skin. The same shielding explanation as described in the ZnSe experiment could be applied. At similar coverages, the degrees of isomerization of EHMC on baby mouse skin and on ZnSe were comparable (see Figs. 5a and 5b). At 1.0–4.0 mg/cm^2, after receiving 0.90 J/cm^2 UVB, ~20–30 % of the *E*-EHMC had isomerized into the *Z* form, causing ~10–15% loss in UV filtering efficiency.

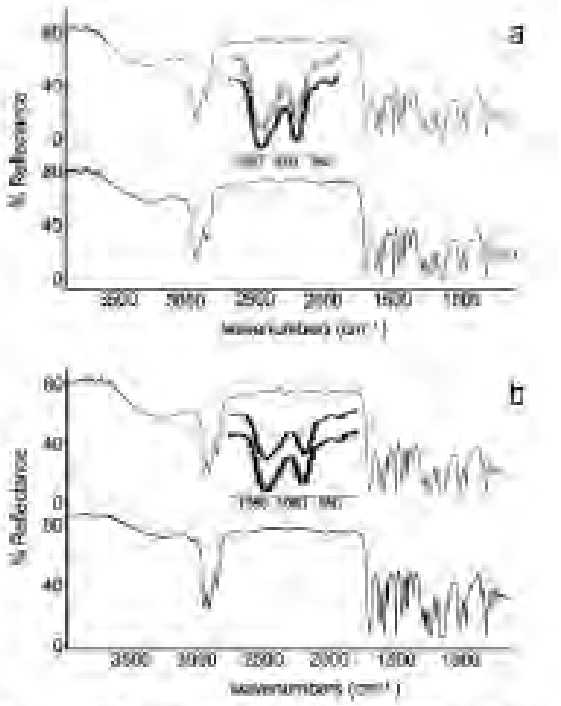

FIG. 6. ATR-FT-IR spectra of 5.44×10^{-8} mol/cm^2 *E*-EHMC on baby mouse skin: (a) spectra from two repetitions of the same skin piece, and (b) spectra from two different skin pieces.

An EHMC photoisomerization experiment using sunlight was carried out and the result was compared to the result obtained using an artificial UVB lamp. An ATR-FT-IR spectrum indicated that after one hour of sunlight exposure to the 6.89×10^{-6} mol/cm^2 or 2 mg/cm^2 EHMC covered baby mouse skin, approximately 10% Z-EHMC could be detected. Since the UVB irradiance from the sunlight during the experiment was about 0.085–0.092 mW/cm^2, one hour of sunlight exposure corresponded to a UVB dose of 0.32 J/cm^2. Figure 5b also indicated that 0.32 J/cm^2 UVB exposure to 6.89×10^{-6} mol/cm^2 EHMC covered baby mouse skin would cause ~10% photoisomerization from *E*- to *Z*-EHMC. This 10% isomerization corresponds to ~5% loss in UV filtering efficiency (using molar absorption coefficient values of 12 000 M^{-1} cm^{-1} for Z-EHMC and 24 000 M^{-1} cm^{-1} for *E*-EHMC). No dimerization could be detected during this sun

hour of sunlight exposure. Agreement between the results of the two UVB light sources thus validates the application of the results shown in Fig. 5b on an estimation of EHMC photoisomerization under sunlight exposure.

Since the recommended skin application dose of a typical sunscreen formulation is 2 mg/cm^2 and the allowed maximum concentration of EHMC in formulations is 7.5%, final coverage of EHMC on the skin during normal sunscreen application will be around 0.15 mg/cm^2. Information from Fig. 5b indicates that UVB radiant exposure of 0.30 J/cm^2 (~1 h sunlight exposure) will cause ~50% E to Z photoisomerization or ~25% loss of UV filtering efficiency.

Since the maximum penetration depth of evanescent waves in this ATR-FT-IR technique is ~1 μm from the sample surface, only EHMC molecules at the very top of the stratum corneum could be detected. The fact that a very good and reproducible ATR-FT-IR spectrum of EHMC could be obtained from the baby mouse skin applied with 0.2–4.0 mg/cm^2 EHMC even at 60 min post-application indicates that most of the EHMC molecules were still at the skin surface. A previous percutaneous absorption study of EHMC using human skin revealed that at 30 min post application, more than 70% of the applied EHMC could be recovered from the first tape stripping, thus indicating very little penetration of EHMC at 30 min post-application.[17] Other transdermal penetration studies of EHMC also indicated that at 60 min post-application, most of the applied materials were still at the surface of the stratum corneum, a reservoir for the applied substances.[18–19] Photoisomerization detected in this study, therefore, represented a chemical change of the bulk of the applied material at the surface of the stratum corneum.

CONCLUSION

It is known that in solution EHMC usually undergoes photoisomerization from E (*trans*) to Z (*cis*), leading to a decrease in UV absorption efficiency due to a lower molar absorption coefficient of the Z-EHMC (12 000 M^{-1} cm^{-1}) compared to that of the E-EHMC (22 000–24 000 M^{-1} cm^{-1}). Here we have demonstrated the use of ATR-FT-IR to monitor such photoisomerization on skin. This method is based on the differences among ATR-FT-IR spectra of E-EHMC, Z-EHMC, and the dimerized product. A linear relationship between the mole ratio of E-EHMC and the peak area at 981 cm^{-1} (from the Ph–CH=CH– rocking deformation vibration, present only in the E configuration) enables an easy estimation of the E/Z ratio in irradiated EHMC samples. An absence of C=C stretching (from Ph–CH=CH–) at 1655–1555 cm^{-1} in the dimerized product also provides a means to indicate the presence of any dimerized products in an irradiated EHMC sample.

Experiments on both a ZnSe surface and mouse skin clearly demonstrated that EHMC underwent E to Z and Z to E photoisomerization upon UVB exposure. When a small amount of EHMC was used on the skin, a significant loss of UV filtering efficiency will occur upon UVB exposure due to photoisomerization. However, at higher applied doses (≥1 mg/cm^2), there will be less photoisomerization. No dimerization could be detected even at 4.0 mg/cm^2, the highest EHMC coverage used in this work. From Fig. 5b, at 0.2 mg/cm^2 (a normal use of EHMC on skin), 25% loss of UV absorption efficiency from photoisomerization under 1 h sunlight exposure (0.32 J/cm^2 UVB exposure) could be estimated using molar absorption coefficient values of 12 000 M^{-1} cm^{-1} for Z-EHMC and 24 000 M^{-1} cm^{-1} for E-EHMC. Higher coverage of EHMC on the skin will not only increase an initial UV absorption efficiency but also help minimize the E to Z photoisomerization, thus retaining the UV absorption efficiency of the sunscreen film on the skin. This shielding effect should also be true for the combination of EHMC with other UVB filters in cosmetic formulations.

ACKNOWLEDGMENTS

This project is supported by the Thailand Research Fund.

1. C. R. Taylor, R. S. Stern, J. J. Leyden, and B. A. Gilchrest, J. Am. Acad. Dermatol. 22, 1 (1990).
2. C. R. Taylor and A. J. Sober, Annu. Rev. Med. 47, 181 (1996).
3. J. J. Finlay-Jones and P. H. Hart, Mut. Res. 422, 155 (1998).
4. K. Kimura and T. Katoh, Contact Dermatitis 32, 304 (1995).
5. S. Schauder and H. Ippen, Contact Dermatitis 37, 221 (1997).
6. C. Ricci, M. Pazzaglia, and A. Tosti, Contact Dermatitis 38, 343 (1998).
7. A. Darvay, I. R. White, R. J. G. Rycroft, A. B. Jones, J. L. Hawk, and J. P. McFadden, Br. J. Dermatol. 145, 597 (2001).
8. S. Pattanaargson, T. Munhapol, P. Hirunsupachot, and P. Luangthongaram, J. Photochem. Photobiol. A: Chem. 161, 269 (2004).
9. S. Pattanaargson and P. Limphong, Int. J. Cosmet. Sci. 23, 151 (2001).
10. S. Devanathan and V. Ramamurthy, J. Photochem. Photobiol. A 40, 67 (1987).
11. J. Meijer and M. Loden, J. Liquid Chromatogr. 18, 1821 (1995).
12. N. Tarras-Wahlberg, G. Stenhagen, O. Larko, A. Rosen, A. M. Wennberg, and O. Wennerstrom, J. Invest. Dermatol. 113, 548 (1999).
13. P. Morliere, O. Avice, T. S. E. Melo, L. Dubertret, M. Giraud, and R. Santus, Photochem. Photobiol. 36, 395 (1982).
14. Y. Shindo, J. Photochem. 26, 185 (1984).
15. T. Ishigami, K. Nakazato, M. Uehara, and T. Endo, Tetrahedron Lett. 10, 863 (1979).
16. F. D. Lewis, S. L. Quillen, and J. E. Elbert, J. Photochem. Photobiol., A: Chem. 47, 173 (1989).
17. V. Sarveiya, S. Risk, and H. A. E. Benson, J. Chromatogr., B 803, 225 (2004).
18. M. M. Jimenez, J. Pelletier, M. F. Bobin, and M. C. Martini, Int. J. Pharm. 272, 45 (2004).
19. G. Potard, C. Laugel, H. Schaefer, and J.-P. Marty, Skin Pharmacol. Appl. Skin Physiol. 13, 336 (2000).

ภาคผนวก ค

Original Paper

Skin Pharmacology and Physiology

Skin Pharmacol Physiol 2008;21:23–29
DOI: 10.1159/000106065

Received: March 15, 2007
Accepted after revision: July 3, 2007
Published online: October 4, 2007

Transdermal Penetration of UV Filters

P. Klinubol[b] P. Asawanonda[c] S.R. Wanichwecharungruang[a]

[a]Senior Research Unit, Department of Chemistry, Faculty of Science, [b]Program of Biotechnology, Faculty of Science, and [c]Division of Dermatology, Department of Medicine, Chulalongkorn University, Bangkok, Thailand

Key Words
UV filter · Transdermal penetration · Baby mouse skin · Human epidermis · Suction blister

Abstract
A penetration study of 2-ethylhexyl-4-methoxycinnamate (EHMC), 4-methyl benzylidenecamphor (MBC), butyl methoxydibenzoylmethane (BMBM), 2-ethylhexyl-2,4,5-trimethoxycinnamate (EHTMC) and di(2-ethylhexyl)-2,4,5-trimethoxybenzalmalonate (TMB) through baby mouse skin (*Mus musculus* Linn.) was carried out using a vertical Franz diffusion cell. At 4.4 mg/cm^2 coverage of UV filter on the skin, 2.98 ± 0.36, 1.15 ± 0.14 and 0.80 ± 0.28% of the applied EHMC, MBC and BMBM were detected in the receptor fluid at 24 h after application. Penetrations of UV filter in an ethanolic solution and lotion forms were comparable. EHTMC and TMB showed insignificant penetration across the baby mouse skins. Baby mouse skins kept at 4, –20 and –80°C gave similar EHMC penetration results. Penetrations of EHMC, BMBM, EHTMC and TMB across human epidermis were carried out upon 5 volunteers using the suction blister technique. The results also confirmed the significant penetrations of EHMC and BMBM and the insignificant penetrations of EHTMC and TMB.

Introduction

Ultraviolet (UV) filters or sunscreens are widely used to protect skin against UV radiation, thus minimizing various detrimental effects including sunburn, photoageing, immunosuppression and skin cancer. Ideal UV filters should possess a high extent of skin substantivity with the least transdermal penetration to the systemic circulation. However, several studies have demonstrated that certain UV filters can enter the body through topical application [1–11]. Among many organic UV filters, benzophenone-3 (oxybenzone), a broad-spectrum filter, can pass through the skin in significant amounts [1, 3, 5, 6, 8–12]. Both significant [1–5] and insignificant [6–9] transdermal penetration of 2-ethylhexyl-4-methoxycinnamate (EHMC), a widely used UVB filter, were reported. Effects of various additives and formulations [4, 12–15] together with micro- and nanocapsule encapsulations [2, 7, 16] on the EHMC transdermal penetration had also been investigated. In contrast to oxybenzone and EHMC, 4-(*tert*-butyl)-4′-methoxydibenzoylmethane (avobenzone, BMBM), a popular UVA filter, did not show significant transdermal penetration [12–15]. Absorption of 3-(4-methylbenzylidene) camphor (MBC), a UVB filter, was also reported [12]. MBC could be detected in the plasma and urine of healthy volunteers after topical application of a formulation containing the compound [3].

KARGER

© 2007 S. Karger AG, Basel
www.karger.com/spp

Accessible online at:
www.karger.com/spp

Dr. Supason Wanichwecharungruang
Faculty of Science, Chulalongkorn University
Pathumwan
Bangkok 10330 (Thailand)

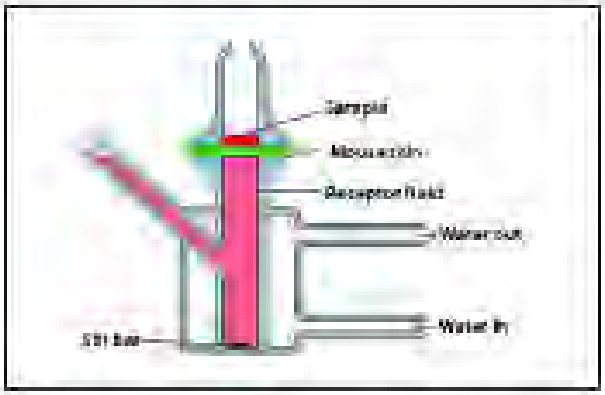

Fig. 1. Drawing of the Franz diffusion cell used in the experiment.

An evaluation of skin penetration of sunscreen has been carried out by several groups using different methodologies. The most popular technique is the diffusion cell method with the use of human skin [8–9, 13–15], pig skin [7, 17] and artificial membrane [2, 15]. Analyses of body fluids such as breast milk, plasma and urine have provided strong evidence for the systemic absorption of some organic UV filters [1, 3, 5, 10–11]. The tape stripping technique has been used to determine the accumulation of many UV filters in various skin layers [6, 16]. Quantitative analyses of the UV filters were mostly done by the HPLC method [2, 5–12, 14, 17]. Other analytical methods used include UV absorption spectroscopy [4, 16, 18, 19], gas chromatography/mass spectrometry [1] and radioactive labeling of the sunscreen [20].

In this paper we report the ex vivo transdermal penetration of some commercial UV filters and two newly developed UVA filters, 2-ethylhexyl-2,4,5-trimethoxycinnamate (EHTMC) and di(2-ethylhexyl)-2,4,5-trimethoxybenzalmalonate (TMB) [21], through the baby mouse skin (*Mus musculus* Linn.) using a vertical Franz diffusion cell. In addition, an in vivo transepidermal penetration study of some UV filters in human volunteers using the suction blister technique was also performed.

Materials and Methods

Chemicals

EHMC, BMBM, MBC and Eusolex UV pearl EHMC were kindly provided by Merck Thailand Co. Ltd. (Bangkok, Thailand). The two newly developed UV filters, TMB and EHTMC were prepared as described previously [21].

Preparation of Test Samples

Tested Solutions for the Diffusion Cell Experiment

A 100 mg/ml ethanolic solution of each UV filter was freshly prepared by dissolving 1.00 g of the UV filter into ethanol and adjusting the final volume to 10.0 ml.

Lotion Containing UV Filter

A body lotion was purchased from a local drug store. The lotion contains aqua, petrolatum, isopropyl palmitate, paraffinum liquidum, glyceryl stearate, ceteth-20, anhydrous lanolin, phenoxyethanol, methylparaben, hydroxyethylcellulose, carbomer, propylparaben and sodium hydroxide. One gram of the UV filter was first dissolved in 3.0 ml of ethanol. Then this solution was thoroughly mixed with the lotion to give a final volume of 10.0 ml. The concentration of the UV filter in the obtained lotion was 100 mg/ml.

Skin Specimens for Diffusion Cell Experiments

The skin specimens of 2-week-old baby mice (*Mus musculus* Linn.) were purchased from the National Laboratory Animal Center (Nakhonpathom, Thailand). The abdominal skin was removed by a surgical procedure. The skin comprised epidermis and dermis layers. They were kept at room temperature, –20 and –80°C and cut into approximately 2.0 × 2.5 cm^2 pieces prior to use. The full thickness of the baby mouse skin was approximately 1,700 ± 163.7 μm (mean ± SD). All skin pieces were brought to room temperature prior to use by leaving the skin at 25°C for 30 min.

Diffusion Cell Experiments

Ex vivo permeation studies were conducted with vertical Franz diffusion cells with a 13.0-ml capacity receptor compartment and a 2.27-cm^2 diffusion area. The abdominal skin of a 2-week-old baby mouse (*M. musculus* Linn.) was carefully mounted onto the receptor compartment of the diffusion cell with the stratum corneum facing in the direction of the donor compartment. When the donor compartment was fastened to the receptor compartment with a clamp, the skin acted as a seal between the two cell halves (fig. 1). The receptor medium consisted of isotonic phosphate-buffered saline, pH 7.4 (PBS), with 1% w/v Tween 20 to ensure the solubility of all UV filters [22, 23]. This medium was maintained at 37°C and constantly stirred with a magnetic bar. UV filters used in the experiments were freshly prepared into an ethanolic solution and lotion. UV filters used in the experiments included EHMC, BMBM, MBC, Eusolex UV pearl EHMC, EHTMC and TBM. The experiment was initiated by dropping 100 μl of the 100 mg/ml UV filter solution or lotion into the upper compartment of the diffusion cell, directly onto the mounted skin (UV filter final coverage = 4.4 mg/cm^2), then at 1, 2, 4 and 24 h, 2.0 ml of receptor fluid were withdrawn and replaced with a fresh receptor medium. Care was taken to avoid any air bubbles in the receptor fluid. Experiments were done at room temperature in 5 repetitions. Since the skins from different mice were different, penetration of each sunscreen sample was compared to the penetration of EHMC using skin from the same mouse to standardize the results.

The concentration of UV filters in the receptor fluid was determined by a UV absorption spectrophotometer. A calibration curve of each UV filter in receptor fluid was constructed by measuring the absorbance of the UV filter standard solution at its

Elsmbol/downloaded/
Wissenschaftsgruppe

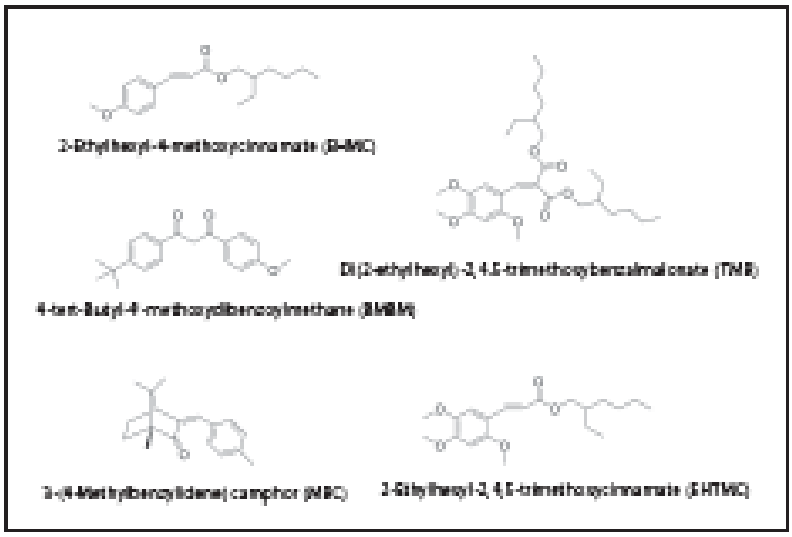

Fig. 2. Chemical structures of the 5 organic UV filters.

λ_{max}. The UV filter standard solution was prepared in the receptor fluid. Final concentrations were 0.0, 2.0, 4.0, 6.0, 8.0 and 10.0 mg/l. The graph between absorptions and concentrations of the UV filters was then constructed and used for the determination of UV filter in the receptor fluid obtained during the Franz diffusion cell experiments. To test for the possible contribution of lotion to the UV absorption spectrum, receptor fluid containing lotion at 100 µl/13 ml was compared to receptor fluid with no lotion. UV spectra of all samples were obtained with the aid of an HP 8453 UV/VIS spectrophotometer (Agilent Technologies, Calif., USA) using a quartz cell with 1 cm pathlength.

Suction Blister Experiments

The protocol was approved by the ethics committee of King Chulalongkorn Memorial Hospital/Chulalongkorn University. Informed consent was obtained from each participant.

The separation of viable epidermis from dermis was carried out by the suction blister method [24, 25]. Briefly, a suction pump was connected to one end of a plastic syringe through an intravenous tube, leaving the other end of the syringe free. The free end of the syringe was pressed against the volunteer's thigh skin, and negative pressure (200 mm Hg) was then applied. After 2–3 h of the negative pressure, the epidermis was separated from the underlying dermis forming the roof of the blisters and the resulting space (blister) was filled with interstitial fluid with the diameter at the blister's base of approximately 15 mm. Six spots of suction blister were induced on each volunteer. Twenty microliters of sample (2 mg UV filter) were dropped over the blister's roof. The sample was evenly spread over the blister roof giving approximately 0.6 mg/cm^2 sample coverage on the 3.5 cm^2 of epidermis. The suction blister fluid (SBF) was then collected after 5 h, using a fine needle.

The concentration of a UV filter in the SBF was determined by UV absorption spectrophotometry by diluting the withdrawn SBF (0.5 ml) with 2.5 ml of the isotonic PBS, prior to the measurement. The calibration curve of each compound was constructed for each individual using the individual's receptor fluid. Standard UV filter solutions for each volunteer were prepared using the SBF of each volunteer as solvent. Dilution of these standard solutions was carried out prior to UV absorption measurements, using 1 vol of the standard solution and 5 vol of the isotonic PBS, giving final concentrations of the sunscreen of 0.0, 1.0, 3.0 and 5.0 mg/l. The obtained absorbances at λ_{max} of the UV filters were plotted against concentrations, and linear regression analysis was carried out to obtain the best straight line. Experiments were carried out on 5 volunteers. Four UV filters, EHMC, BMBM, EHTMC and TMB, were tested on every volunteer.

Results and Discussion

Penetration of Various Sunscreens through Baby Mouse Skin Using the Franz Diffusion Cell Technique

Analysis of Sunscreen in Receptor Fluid by UV/Visible Spectrophotometry

The receptor fluid used in the receptor compartment of the diffusion cell consisted of isotonic PBS, pH 7.4, with 1% w/v Tween 20. This medium could solubilize all the tested UV filters at the concentration of at least 20–40 mg/13 ml. The amount of the UV filter in this fluid was then determined by UV absorption spectroscopy.

In this experiment 3 commercially available organic UV filters (EHMC, MBC and BMBM) and 2 newly developed organic UV filters (EHTMC and TMB) were used (see fig. 2 for their chemical structures). UV absorption spectra of these UV filters in the receptor fluid show

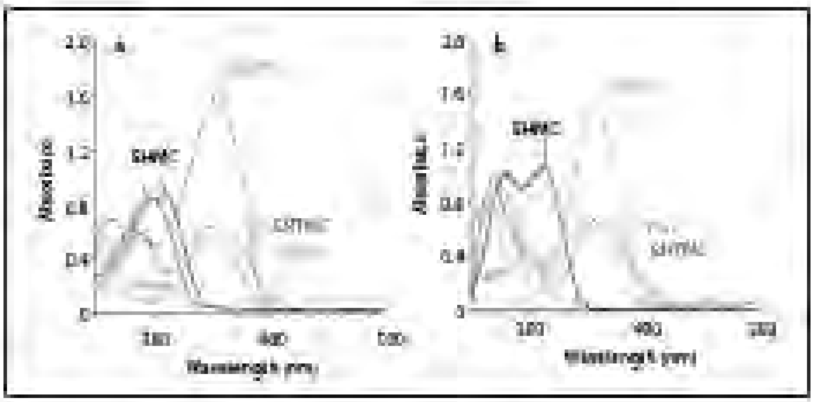

Fig. 5. UV absorption spectra of various UV filters in receptor fluid (a) and SBF (b).

characteristic peaks, i.e. maximum absorption at 310 nm for EHMC, 300 nm for MBC, 360 nm for BMBM, 365 nm for EHTMC and 360 nm for TMB (fig. 5a). Calibration curves of sunscreen solutions prepared in receptor fluid were constructed by plotting absorbances at the λ_{max} against concentrations (0, 2, 4, 6, 8 and 10 mg/l). Since all calibration plots were linear with the r^2 values of greater than 0.9706, quantitation of sunscreen in the receptor fluid withdrawn from the Franz diffusion cell could be carried out with UV absorption spectroscopy. It should be noted here that in the 260- to 400-nm regions, the UV absorption spectrum of the receptor fluid spiked with lotion and that of the receptor fluid with no lotion was quite similar, thus permitting the use of UV absorption spectroscopy to quantitate UV filters in the receptor fluid in the lotion experiment.

Since the concentration of UV filter in the receptor fluid could be very low due to very little penetration, the analytical method used to determine the amount of the UV filter in such fluid must be sensitive enough. In the experiment, 10 mg of the UV filter were applied. If only 0.1% of the applied UV filter get into the 13 ml of receptor fluid, the concentration of the UV filter in the receptor fluid will be 0.8 mg/l. In this work, the withdrawn receptor fluid was directly subjected to UV absorption measurement without any preconcentration step. This was possible because the method is sensitive enough to easily detect the tested UV filter at the concentration of 0.8 mg/l. Detection limits of this analytical method for EHMC, BMBM, MBC, TMB and EHTMC are all lower than 0.8 mg/l. This is because all of the tested UV filters possess high molar absorption coefficient values: 23,300, 34,700, 24,500, 15,700 and 34,200 M/cm for EHMC, BMBM, MBC, TMB and EHTMC, respectively.

Comparison of Permeability of Fresh Skin, –20°C Frozen Skin and –80°C Frozen Skin

A comparison of the permeability of fresh abdominal baby mouse skin, skin kept at –80°C and skin kept at –20°C was carried out by the monitoring of EHMC penetration using Franz diffusion cells. The Franz diffusion cell used had the diffusion area of 2.27 cm² with 13 ml receptor volume. Final coverage of EHMC on the skin was 4.4 mg/cm², and quantitation of EHMC in the receptor fluid was carried out at 0, 2, 4 and 24 h after application. Taking into account the differences between skins from different mice, skin from the same mouse was divided into two pieces. Penetration of EHMC through fresh mouse skin (skin kept at 4°C for 4 h) and –20°C frozen skin (skin kept at –20°C for 4 h) was done using skin from the same mouse. Penetration of EHMC through fresh mouse skin and –80°C frozen skin (skin kept at –80°C for 4 h) was also done using skin from the same mouse. Although previous studies done by Brain et al. [26] indicated that the permeation of diethanolamine was a little greater through the frozen skin than through the fresh skin, Mann-Whitney U statistical analyses of the EHMC penetration results indicated no significant differences among the three skins.

It should be noted here that EHMC was chosen because not only is it one of the most widely used UVB filters, but also many studies have demonstrated its transdermal penetration [1–5].

The Monitoring of Transdermal Penetration of Various Sunscreens through Baby Mouse Skin Using the Franz Diffusion Cell Method

In this experiment, the penetration of 5 UV filters, EHMC, MBC, BMBM, EHTMC and TMB, across baby mouse skin (including both epidermis and dermis) was

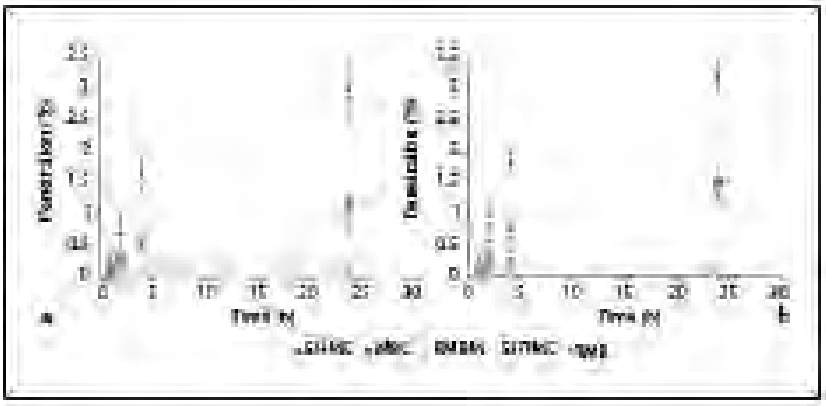

Fig. 4. Penetration of UV filters prepared as ethanolic solution (a) and lotion (b) through baby mouse skins using Franz diffusion cells with the skin contact area of 0.175 cm^2/ml and at the final coverage of UV filter on the baby mouse skin of 4.4 mg/cm^2. The results are shown as percentages of UV filters found in receptor fluid as relating to the amount of applied UV filter(s) at various postapplication times. The data are shown as average values of at least 5 experimental repetitions with the error bars representing their standard deviations.

monitored using the vertical Franz diffusion cell technique. At 4.4 mg/cm^2 coverage of UV filter on baby mouse skin with 0.175 cm^2 skin diffusion area per milliliter of receptor fluid, penetration through the skin into the receptor fluid was monitored at 0, 2, 4 and 24 h after application. Quantitative analysis of the UV filter in the receptor fluid was carried out by UV absorption spectrophotometry using a calibration curve. The skin used was the –20 °C frozen skin which had been allowed to defrost at room temperature. Experiments were carried out with sunscreens in both solution and lotion format. Since skins from different mice differed in thickness, the penetration result of each UV filter was always normalized to the EHMC penetration result obtained from skin of the same mouse.

Results from experiments done with UV filter solutions (fig. 4a) were quite similar to those obtained from experiments done using lotions containing UV filters (fig. 4b). After 24 h, a total of 2.98 ± 0.38% of EHMC, as relating to the total amount of applied EHMC, could be detected in the receptor fluid. The other 2 UV filters, MBC and BMBM, showed less penetration ability, i.e. 1.15 ± 0.14 and 0.80 ± 0.28% of the applied MBC and BMBM were detected in the receptor chamber 24 h after application. This result confirmed transdermal penetrations of EHMC, MBC and BMBM through baby mouse skin. However, the 2 newly developed UV filters, EHTMC and TMB, showed insignificant penetration 24 h after application.

The Eusolex UV pearl formulation, which is EHMC trapped within microbeads, gave no penetration at all. The result of Eusolex UV pearl was not directly compared with the other 5 UV filters because the amount of EHMC trapped within the microbeads could not be determined. As a result, the amount of EHMC (within the microbeads) applied to the skin could not be controlled to match the amount of other UV filters. The only implication from the experiment with Eusolex UV pearl is that trapping of EHMC within the microbeads may reduce the transdermal penetration of the material.

The Penetration of Various Sunscreens through Human Epidermis Using the Suction Blister Technique

Analysis of Sunscreen in SBF by UV/Visible Spectrophotometry

The UV absorption spectrum of the blister fluid diluted with PBS buffer shows the absorption maximum at 270 nm with no absorption at 305–500 nm. The absorption maxima of BMBM, EHTMC and TMB are well resolved from the absorption band of the blister fluid. Although the EHMC absorption is not well resolved from the blister fluid absorption, the maxima of the two were well separated from each other (fig. 3b). It is, therefore, possible to detect a presence of EHMC, BMBM, EHTMC or TMB in the blister fluid using UV absorption spectroscopy. Since blister fluids from different volunteers were different, the quantitation of UV filters in the blister fluid of each person was done using calibration curves constructed with UV filter standard solutions prepared in the volunteers' own blister fluid. At the concentration ranges of 0–5 mg/l, all calibration plots were linear with the minimal r^2 values from least-square analyses of 0.9852.

The previous explanation on the detection limit of the UV absorption spectroscopic method on the detection of sunscreen in the receptor fluid could also be applied to this suction blister experiment. Since the amount of UV filter applied to the blister's roof was 2 mg, this means that if 0.1% of the material was in the 0.9 ml SBF, the concentration of the UV filter in the SBF would be 2.2 mg/l.

Table 1. Penetration of UV filters across human epidermis

UV filters	Total amounts detected in the blister fluid 3 h after application, mg	Detected UV filters as relating to the amount applied, %
EHMC	0.0070 ± 0.0001	0.35
BMBM	0.0034 ± 0.0001	0.15
EHTMC	0	0
TMB	0	0

The total amount of the UV filter applied onto 3.5 cm^2 blister roof was 2 mg.

Diluting 0.5 ml of this SBF fluid with 2.5 ml of PBS should result in solution with UV filter concentration of 0.37 mg/l. Solution of EHMC, BMBM, TMB and EHTMC at this concentration could be detected easily using UV absorption spectroscopy.

The Monitoring of Transepidermal Penetration of Various Sunscreens Using the Suction Blister Technique

To monitor the penetration of UV filters through in vivo human epidermis, the tested UV filter was applied onto the epidermis at the blister roof to give a final coverage of 0.6 mg/cm^2. The separated epidermis has the surface area of 3.5 cm^2 with the SBF volume of approximately 0.9 ml. At 3 h after application time, all SBF volume was withdrawn and subjected to UV absorption spectroscopic analysis. Only EHMC and BMBM showed obvious transepidermal penetration at 3 h after application in all 5 volunteers (table 1). These transepidermal penetration results agree well with the mouse skin penetration results, i.e. EHMC showed an almost threefolds more effective penetration than BMBM while EHTMC and TMB showed insignificant penetration. In every volunteer, neither EHTMC nor TMB could be detected in the suction blister at 3 h after application time.

Both the human epidermis and baby mouse skin showed no penetration of EHTMC and TMB. Among the 5 UV filters, EHMC was the best penetrating compound through both the baby mouse skin and the human epidermis. Among the 3 commercially available UV filters used in this work, BMBM showed the least penetration ability. Both experiments indicated that penetration of EHMC almost tripled that of BMBM. This agrees with previous studies which indicated significant penetration of EHMC [1–5] but insignificant penetration of BMBM [12–15].

It can be seen clearly that the relative ease of penetration among the tested UV filters obtained from baby mouse skin and from human epidermis experiments was similar. This agreement indicates the possible prediction of the ease of UV filter penetration through human epidermis using baby mouse skin.

The fact that EHTMC penetrated skin poorly while EHMC showed substantial penetration indicated the role of methoxy substitution on the skin substantivity of the compound. Thus, methoxy substitution on the benzene ring of the cinnamate affects not only the absorption profile of the cinnamate [21], but also the skin permeability of the compound. It should be pointed out here that small increases in molecular weight of the tested compounds did not directly affect the skin penetration. This was obvious when comparing the penetration of EHMC (molecular weight of 290) to that of MBC (molecular weight of 254): EHMC penetration doubled that of MBC.

Conclusion

The ex vivo transdermal penetration study of 5 UV filter solutions across baby mouse skin using a vertical Franz diffusion cell indicated that at 4.4 mg/cm^2 coverage of EHMC, MBC and BMBM, 2.98 ± 0.38, 1.15 ± 0.14 and 0.80 ± 0.28% of the applied material could penetrate through the epidermis and dermis into the receptor fluid after 24 h following application. EHTMC and TMB showed insignificant penetration. Lotions containing similar UV filters gave comparable results. The in vivo transepidermal penetration study of 4 UV filters in 5 human volunteers using the suction blister technique also indicated obvious penetration of EHMC and BMBM but no penetration of EHTMC and TMB. Agreement between the baby mouse skin experiment and the human epidermis experiment indicated the possibility of using an ex vivo baby mouse skin experiment for the prediction of the transepidermal penetration of a material.

Acknowledgements

This work was supported by the Research Council of Thailand and the Thailand Research Fund.

References

1 Hany J, Nagel R: Detection of sunscreen agents in human breast-milk. Dtsch Lebensmittel Rundsch 1995;91:341–345.

2 Yener G, Incegul T, Yener N: Importance of using solid lipid microspheres as carriers for UV filters on the example octyl methoxycinnamate. Int J Pharm 2003;258:203–207.

3 Janjua NR, Mogensen B, Andersson AM, Petersen JH, Henriksen M, Skakkebaek NE, Wulf HC: Systemic absorption of the sunscreens benzophenone-3, octyl-methoxycinnamate, and 3-(4-methyl-benzylidene) camphor after whole-body topical application and reproductive hormone levels in humans. J Invest Dermatol 2004;123:57–61.

4 Calderilla-Fajardo SB, Cazares-Delgadillo J, Villalobos-Garcia R, Quintanar-Guerrero D, Ganem-Quintanar A, Robles R: Influence of sucrose esters on the in vivo percutaneous penetration of octyl methoxycinnamate formulated in nanocapsules, nanoemulsion, and emulsion. Drug Dev Ind Pharm 2006;32:107–113.

5 Sarveiya V, Risk S, Benson HA: Liquid chromatographic assay for common sunscreen agents: application to in vivo assessment of skin penetration and systemic absorption in human volunteers. J Chromatogr B Anal Technol Biomed Life Sci 2004;803:225–231.

6 Potard G, Laugel C, Schaefer H, Marty JP: The stripping technique: in vitro absorption and penetration of five UV filters on excised fresh human skin. Skin Pharmacol Appl Skin Physiol 2000;13:336–344.

7 Jimenez MM, Pelletier J, Bobin MF, Martini MC: Influence of encapsulation on the in vitro percutaneous absorption of octyl methoxycinnamate. Int J Pharm 2004;272:45–55.

8 Jiang R, Roberts MS, Collins DM, Benson HAE: Absorption of sunscreens across human skin: an evaluation of commercial products for children and adults. Br J Clin Pharmacol 1999;48:635–637.

9 Potard G, Laugel C, Baillet A, Schaefer H, Marty JP: Quantitative HPLC analysis of sunscreens and caffeine during in vitro percutaneous penetration studies. Int J Pharm 1999;189:249–260.

10 Hayden CGJ, Roberts MS, Benson HAE: Systemic absorption of sunscreen after topical application. Lancet 1997;350:863–864.

11 Gonzalez H, Farbrot A, Larko O, Wennberg AM: Percutaneous absorption of the sunscreen benzophenone-3 after repeated whole-body applications, with and without ultraviolet irradiation. Br J Dermatol 2006;154:337–340.

12 Hagedorn-Leweke U, Lippold BC: Absorption of sunscreens and other compounds through human skin in vivo: derivation of a method to predict maximum fluxes. Pharm Res 1995;12:1354–1360.

13 Chatelain E, Gabard B, Surber C: Skin penetration and sun protection factor of five UV filters: effect of the vehicle. Skin Pharmacol Appl Skin Physiol 2003;16:28–35.

14 Simeoni S, Scalia S, Benson HA: Influence of cyclodextrins on in vitro human skin absorption of the sunscreen, butyl-methoxydibenzoylmethane. Int J Pharm 2004;280:163–171.

15 Montenegro L, Paolino D, Puglisi G: Effects of silicone emulsifiers on in vitro skin permeation of sunscreens from cosmetic emulsions. J Cosmet Sci 2004;55:509–518.

16 Olvera-Martinez BI, Cazares-Delgadillo J, Calderilla-Fajardo SB, Villalobos-Garcia R, Ganem-Quintanar A, Quintanar-Guerrero D: Preparation of polymeric nanocapsules containing octyl methoxycinnamate by the emulsification-diffusion technique: penetration across the stratum corneum. J Pharm Sci 2005;94:1552–1559.

17 Gu X, Wang T, Collins DM, Kasichayanula S, Burczynski FJ: In vitro evaluation of concurrent use of commercially available insect repellent and sunscreen preparations. Br J Dermatol 2005;152:1263–1267.

18 Weigmann HJ, Jacobi U, Antoniou C, Tsikrikas GN, Wendel V, Rapp C, Gers-Barlag H, Sterry W, Lademann J: Determination of penetration profiles of topically applied substances by means of tape stripping and optical spectroscopy: UV filter substance in sunscreens. J Biomed Opt 2005;10:14009.

19 Fernandez C, Nielloud F, Fortune R, Vian L, Marti-Mestres G: Benzophenone-3: rapid prediction and evaluation using non-invasive methods of in vivo human penetration. J Pharm Biomed Anal 2002;28:57–63.

20 Gupta VK, Zatz L, Rerek M: Percutaneous absorption of sunscreens through micro-Yucatan pig skin in vitro. Pharm Res 1999;16:1602–1607.

21 Monhaphol T, Albinsson B, Wanichweacharungruang PS: 2-Ethylhexyl-2,4,5-trimethoxycinnamate and di-(2-ethylhexyl)-2,4,5-trimethoxybenzalmalonate as novel UVA filters. J Pharm Pharmacol 2007;59:279–288.

22 Simeoni S, Scalia S, Benson HAE: Influence of cyclodextrins on in vitro human skin absorption of the sunscreen, butyl-methoxydibenzoylmethane. Int J Pharm 2004;280:163–171.

23 Jiang R, Hayden CGJ, Prankerd RJ, Roberts MS, Benson HAE: High-performance liquid chromatographic assay for common sunscreening agents in cosmetic products, bovine serum albumin solution and human plasma. J Chromatogr B 1996;682:137–145.

24 Kiistala U, Mustakallio KK: In-vivo separation of epidermis by production of suction blisters. Lancet 1964;283:1444–1445.

25 Oikarinen A, Viinikka L, Ryttälä H, Kiistala U, Ylikorkala O: Prostacyclin, thromboxane and prostaglandin $F_{2\alpha}$ in suction blister fluid of human skin: effect of systemic aspirin and local glucocorticosteroid treatment. Life Sci 1981;29:391–396.

26 Brain KR, Walters KA, Green DM, Brain S, Loretz LJ, Sharma RK, Dressler WE: Percutaneous penetration of diethanolamine through human skin in vitro: application from cosmetic vehicles. Food Chem Toxicol 2005;43:681–690.

ภาคผนวก ง

Available online at www.sciencedirect.com
ScienceDirect
European Polymer Journal 44 (2008) 1385–1395
EUROPEAN POLYMER JOURNAL
www.elsevier.com/locate/europolj

Macromolecular Nanotechnology

Synthesis and characterization of micro/nanoparticles of poly(vinylalcohol-co-vinylcinnamate) derivatives

C. Luadthong, A. Tachaprutinun, S.P. Wanichwecharungruang *

Sensor Research Unit, Department of Chemistry, Faculty of Science, Chulalongkorn University, Bangkok 10330, Thailand

Received 27 November 2007; received in revised form 4 February 2008; accepted 12 February 2008
Available online 20 February 2008

Abstract

Various poly(vinylalcohol-co-vinylcinnamate) derivatives including poly(vinylalcohol-co-vinylcinnamate), poly(vinylalcohol-co-vinyl-4-methoxycinnamate), poly(vinylalcohol-co-vinyl-2,4-dimethoxycinnamate) and poly(vinylalcohol-co-vinyl-2,4,5-trimethoxycinnamate) were synthesized by grafting poly(vinylalcohol) with appropriate cinnamoyl groups. The self-assembly of grafted products into spherical micellar nanoparticles was performed, and particles were analyzed using dynamic light scattering, scanning electron microscopy, and transmission electron microscopy. ^{1}H NMR analysis of the well-dispersed micellar particle suspensions and polymer solutions indicated that the hydroxyl groups of the polymer were on the outer surface of the spheres, while the cinnamoyl moieties were buried inside the spheres forming crystalline structure. Polymer with a higher degree of cinnamoyl substitution gave smaller particles upon self-assembly. Variations in particle sizes obtained from PV(OH) grafted with cinnamoyl derivatives of different methoxy substitution on the benzene ring were observed. Molecular weight of the polymers did not significantly affect nanoparticle size and morphology. In addition, self-assembly of the poly(vinylalcohol-co-vinylcinnamate) derivatives into hollow reverse micellar microparticles of uniform size was also demonstrated. ^{1}H NMR spectrum of the reverse micellar micro-particle suspension indicated that the cinnamoyl moieties were not in a crystalline state.

Keywords: Poly(vinyl alcohol); Cinnamate; Nanoparticle; Vinylcinnamate

1. Introduction

Amphiphilic polymers have gained increasing interest as drug and cosmetic carriers because of their ability to entrap biologically active molecules [1].

Poly(vinylalcohol) (PV(OH)) is a hydrophilic polymer that is biocompatible, biodegradable, non-toxic, and non-carcinogenic. PV(OH) is a well-accepted pharmaceutically safe polymer for both humans and the environment [2] and has been used in various pharmaceutical, medical, cosmetic, food, and agricultural products. In the drug delivery area, PV(OH) is widely used as a stabilizer during the preparation of micro/nanoparticles in the emulsion solvent extraction/evaporation process [3–5].

* Corresponding author. Tel.: +66 2 2187604; fax: +66 2 2541309.
E-mail address: psupason@chula.ac.th (S.P. Wanichwecharungruang).

0014-3057/$ - see front matter © 2008 Elsevier Ltd. All rights reserved.
doi:10.1016/j.eurpolymj.2008.02.010

The preparation of PV(OH) into a drug carrier was first demonstrated in 1998 by Xue Shen Wu and coworkers. The group prepared PV(OH) nanoparticles by the freeze–thaw process and demonstrated the use of such particles in protein/peptide drug delivery [6]. Researchers in Italy have reported the uses of oleic acid grafted PV(OH), oleyl-amine grafted PV(OH) and PV(OH) substituted with triethyleneglycolmonotolylether for the preparation of polymeric micelles [7–9]. The group also demonstrated the use of PV(OH) as a starting material to prepare hydrogel [10,11] and carriers for various drug molecules [12–14]. In 2004, Kishida, A. and coworkers in Japan prepared PV(OH)-DNA nanoparticles from PV(OH) of different molecular weights, degrees of saponification, and concentrations using ultra high pressure technology [15]. PV(OH) grafted with poly(lactide-co-glycolide) was also synthesized, prepared into nanoparticles and used as paclitaxel carrier [16].

Although the structural modification of PV(OH) and further preparation into nanoparticles has been demonstrated, basic details on the relationship between particle morphology and polymer structure has not been much investigated. In this paper, amphiphilic polymers, poly(vinylalcohol-co-vinylcinnamate) derivatives, were prepared from PV(OH) by grafting various cinnamoyl derivatives onto PV(OH). The influences of the degree of substitution, cinnamoyl structure, molecular weight of PV(OH), polymer concentration and type of solvent used during dialysis on the morphology of obtained particles were fully investigated and discussed. In addition, ^{1}H NMR analyses of the particle suspension were carried out to obtain details of the polymer chain's orientation upon self-assembly.

2. Materials and methods

The ^{1}H and ^{13}C NMR analyses were performed using a Varian Mercury spectrometer, which operated at 400.00 MHz for ^{1}H and 100.00 MHz for ^{13}C nuclei (Varian Company, Palo Alto, CA, USA) in deuterated chloroform ($CDCl_3$) or deuterated dimethylsulfoxide (DMSO-d_6) with tetramethylsilane (TMS) as an internal reference. UV Absorption spectra were acquired with a UV 2500 UV–vis spectrophotometer (Shimadzu Corporation, Kyoto, Japan) using a quartz cell with 1 cm pathlength. FT-IR spectra were obtained using a Nicolet Fourier transform Infrared spectrophotometer Impact 410 (Nicolet Instruments Technologies, Inc., Madison, WI, USA). Thermogram of each sample was acquired at 0–380 °C under nitrogen with a scanning rate of 20 °C/min using by differential scanning calorimetry: DSC 204 (Netzsch Group, Selb, Germany). Transmission electron micrographs (TEM) and scanning electron micrographs (SEM) were obtained using JEM-2100 (Jeol, Ltd., Japan) and JEM-6400 (Jeol, Ltd., Japan), respectively. The particle size and zeta potential were acquired by Mastersizer S and Zetasizer nano-series (Malvern Instruments, Worcestershire, UK), respectively. The particle suspension was freeze-dried using Freeze-Dry/Shell Freeze System Model 7753501 (Labconco Corp., Kansas, MI, USA).

Poly(vinyl alcohol), Mw 124,000–186,000, 87–89% deacetylated (PV(OH) 155,000 or *P*); poly(vinyl alcohol), M_w 35,000–50,000, 87–89% deacetylated (PV(OH) 43,000 or *P'*); poly(vinyl alcohol), M_w 9000–10,000, 80% deacetylated (PV(OH) 10,000 or *P''*) was purchased from Aldrich Chemical Company (Steinheim, Germany).

Cinnamic acid (CA) was purchased from Fluka Chemical Company (Buchs, Switzerland). 4-Methoxycinnamic acid, 2,4-dimethoxybenzaldehyde and 2,4,5-trimethoxybenzaldehyde were purchased from Acros Organics (Geel, Belgium). All other chemicals were reagent grade and were used without additional purification, except thionyl chloride, which was freshly distilled prior to use.

2.1. Synthesis of 2,4-dimethoxy-trans-cinnamic acid and 2,4,5-trimethoxy-trans-cinnamic acid

2,4-Dimethoxycinnamic acid and 2,4,5-trimethoxycinnamic acid were synthesized using Knoevenagel-Doebner condensation between appropriated benzaldehyde and malonic acid, Scheme 1 [17].

2.1.1. 2,4-Dimethoxy-trans-cinnamic acid (2,4-DMC)

Light yellow solid, yield: 84%. T_m: 156–162 °C. FT-IR (KBr, cm^{-1}): 3465 (COO–H, stretching), 3001, 2933, and 2835 (H–C=C, stretching), 1673 (C=O, stretching) and 1598, 1463 and 755 (aromatic ring). ^{1}H NMR (400 MHz, $CDCl_3$, δ, ppm): 10.55 (s, 1H, COOH), 7.76 (d, $J = 16.4$ Hz, 1H, Ar–C*H*=), 7.59 (d, $J = 7.8$ Hz, 1H, Ar–*H*), 6.68 (s, 1H, Ar–*H*), 6.57 (d, $J = 7.8$ Hz, 1H, Ar*H*), 6.36 (d, $J = 16.4$ Hz, 1H, =C*H*–COOH) and 3.85, 3.90 (s, 2 × 3H, 2 × OCH_3). UV–vis (DMSO) λ_{max}, nm (ε, M^{-1} cm^{-1}): 289 (10,795) and 327 (13,108).

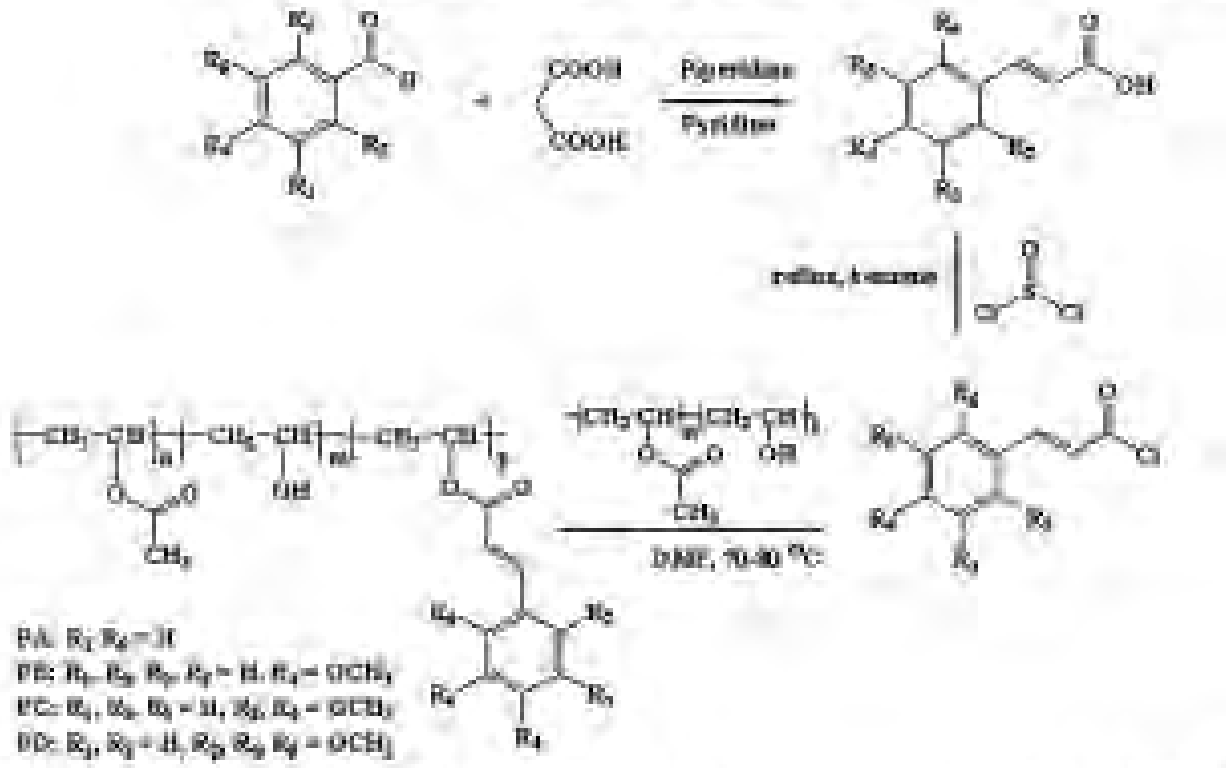

Scheme 1. Synthesis of trans-cinnamic acid of various methoxy substitutions and grafting of the obtained cinnamic acid onto PV(OH).

2.1.2. 2,4,5-Trimethoxy-trans-cinnamic acid (2,4,5-TMC)

Yellow solid, yield 89%, T_m 165–167 °C. FT-IR (KBr, cm^{-1}): 3483 (COO–H), 3000, 2935 and 2823 (H–C=C stretching), 1685 (C=O stretching) and 1600, 1463 and 755 (aromatic ring). ^{1}H NMR (400 MHz, $CDCl_3$, δ, ppm): 10.55 (s, 1H, COOH), 8.20 (d, J = 16.0 Hz, 1H, Ar–CH=), 6.73 and 7.49 (s, 2H, Ar–H), 6.61 (d, J = 15.5 Hz, 1H, =CH–COOH) and 4.17, 4.12 and 4.10 (s, 9H, 3 × OCH_3). UV–vis (DMSO): λ_{max}, nm (ε, M^{-1} cm^{-1}): 282 (12,000) and 350 (13,000).

2.2. Synthesis of poly(vinylalcohol-co-vinyl cinnamate) derivatives

The poly(vinylalcohol-co-vinyl cinnamate) derivatives were synthesized using a classical substitution reaction between *trans*-substituted cinnamoyl chloride and PV(OH) (Scheme 1). First, the *trans*-substituted cinnamoyl chloride was prepared by reacting *trans*-substituted cinnamic acid (see amount in Table 1) with excess thionyl chloride in a presence of pyridine (five drops) in 40 ml of dry benzene [18]. The mixture was refluxed overnight. Then, the solvent and excess thionyl chloride were removed by rotary evaporation under reduced pressure. Finally, benzene addition (5 ml) and evaporation were performed to remove the last traces of thionyl chloride. PV(OH) (1.19 g, 27 mmol monomeric units) were dissolved in 70 ml of heated anhydrous DMF. Then, pyridine (2.18 ml, 27 mmol) was added. The obtained clear solution was poured into a round bottom flask containing the freshly prepared *trans*-substituted cinnamoyl chloride. The mixture was stirred at 80–90 °C for 1–2 h. The substituted polymer was separated by precipitation with 1.0% w/v aq. Na_2CO_3. The precipitate was washed with distilled water and the obtained solid was dried under vacuum to constant weight.

2.2.1. Poly(vinylalcohol-co-vinyl 2,4,5-trimethoxy-trans-cinnamate) product PA1. White solid. DS: 0.04, T_g: 71.6 °C. FT-IR (KBr, cm^{-1}): 3377 (OH), 2939 (–C–H, stretching), 1710 (C=O, stretching), 1636, 1575 (C=C, stretching), 1434 (–CH_2–, bending) and 1262, 1186, 1095 (C–O, stretching). ^{1}H NMR (400 MHz, DMSO-d_6, δ, ppm): 7.71 (br, Ar–CH=), 7.63 (br, Ar–H), 7.39 (br, Ar–H), 6.62 (br, =CH–COOR), 4.66, 4.45

Table 1
Structure and physicochemical properties of the poly(vinylalcohol-co-vinylcinnamate) derivatives

Compounds	Amounts of *trans*-cinnamic acid derivative	Product characterization							Particle characteristics		
		n	m	P (DS)	λ_{max}	ε[b]	T_g[c] (°C)	T_m[d] (°C)	Average diameter (nm)[e]	Polydispersity Index (PDI)	Zeta-Potential (mV)
PVOH[a]	–	0.11	0.89	–	–	–	–	191.5	–	–	–
PA1	0.40g, 2.7 mmol	0.11	0.85	0.06	279	1164	71.6	142.1	364 ± 12	0.23	−22.7
PA2	4.00g, 27 mmol	0.11	0.75	0.14	282	2544	72.8	–	123 ± 2	0.12	−30.3
PA3	8.00g, 54 mmol	0.11	0.64	0.25	280	4814	73.1	–	177 ± 0.2	0.09	−32.9
PB1	0.48g, 2.7 mmol	0.11	0.88	0.01	311	131	63.8	163.8	–	–	–
PB2	1.44g, 8.1 mmol	0.11	0.8	0.09	311	2109	79.1	–	259 ± 7	0.22	−20.5
PB3	4.81g, 27 mmol	0.11	0.62	0.27	309	4242	79.6	–	151 ± 0.9	0.03	−29.2
PB4	9.62g, 54 mmol	0.11	0.45	0.44	310	10,072	82	–	162 ± 3	0.05	−29.1
PC	5.65g, 27 mmol	0.11	0.43	0.46	295, 328	6991, 8900	88	–	120 ± 1	0.07	−30.1
PD	6.49g, 27 mmol	0.11	0.36	0.53	292, 354	5232, 5079	106.7	–	124 ± 1	0.07	27.1
P'B3	4.81g, 27 mmol	0.1	0.62	0.28	310	6681	84.5	–	160 ± 3	0.06	−30.5
P"B4	4.81g, 27 mmol	0.2	0.34	0.46	310	8585	78.7	–	157 ± 1	0.06	−28.6

[a] M_w 124,000–186,000.
[b] Molar absorption coefficient values ($M^{-1}cm^{-1}$ per monomeric unit).
[c] Glass transition temperature.
[d] Melting temperature.
[e] Hydrodynamic diameters (nm) (Average size ± SD); P = PVOH 155,000; P' = PVOH 41,000; P" = PVOH 10,000; PA = poly(vinylalcohol-co-vinylcinnamate); PB = poly(vinylalcohol-co-vinyl-4-methoxycinnamate); PC = poly(vinylalcohol-co-vinyl-2,4-dimethoxycinnamate); PD = poly(vinylalcohol-co-vinyl-2,4,5-trimethoxycinnamate).

and 4.21 (s, –*OH*), 3.89 (br, –*CH*–OCOCH$_3$), 3.83 (br, –*CH*–OH), and 2.30–0.80 (br, –*CH*$_2$–CO and –CH–*CH*$_2$–CH– of PV(OH) backbone). UV–vis (DMSO) λ_{max}, nm (ε, M^{-1} cm^{-1}, monomeric unit^{-1}): 279 (1364).

PA2: Yellow solid. DS: 0.14. T_g: 72.8 °C. FT-IR (KBr, cm^{-1}): 3472 (OH), 3063, 3023 (=C–H, stretching), 2929 (–C–H, stretching), 1720 (C=O, stretching), 1636, 1575 (C=C, stretching), 1441 (–CH$_2$–, bending) and 1312, 1248, 1174 (C–O, stretching). ^{1}H NMR (400 MHz, DMSO-d_6, δ, ppm): 8.17 (br, Ar–*CH*=), 7.65 (br, Ar–*H*), 7.41 (br, Ar–*H*), 6.58 (br, =*CH*–COOR), 5.5–4.1 (br, –*OH*), 4.0–3.5 (br, –*CH*–OH and –*CH*–OCOCH$_3$) and 2.30–0.80 (br, –*CH*$_2$–CO and –CH–*CH*$_2$–CH– of PV(OH) backbone). UV–vis (DMSO) λ_{max}, nm (ε, M^{-1} cm^{-1}, monomeric unit^{-1}): 282 (2544).

PA3: Yellow solid. DS: 0.25. T_g: 73.1 °C. FT-IR (KBr, cm^{-1}): 3484 (OH), 3061, 3023 (=C–H, stretching), 2927 (–C–H, stretching), 1715 (C=O, stretching), 1633, 1575 (C=C, stretching), 1441 (–CH$_2$–, bending) and 1312, 1250, 1173 (C–O, stretching). ^{1}H NMR (400 MHz, DMSO-d_6, δ, ppm): 8.12 (br, Ar–*CH*=), 7.64 (br, Ar–*H*), 7.37 (br, Ar–*H*), 6.55 (br, =*CH*–COOR), 5.5–4.5 (br, –*OH*), 4.2–3.8 (br, –CH–OH and –*CH*–OCOCH$_3$) and 2.30–0.80 (br, –*CH*$_3$–CO and –CH–*CH*$_2$–CH– of PV(OH) backbone). UV–vis (DMSO) λ_{max}, nm (ε, M^{-1} cm^{-1}, monomeric unit^{-1}): 280 (4814).

2.2.2. *Poly(vinylalcohol-co-vinyl-4-methoxycinnamate) products*

PB1: White solid. DS: 0.01. T_g: 63.8 °C. FT-IR (KBr, cm^{-1}): 3330 (OH), 2940, 2915, 2850 (–C–H, stretching), 1712 (C=O, stretching), 1602, 1509 (C=C, stretching), 1428 (–CH$_2$–, bending) and 1327, 1248, 1169 (C–O, stretching). ^{1}H NMR (400 MHz, DMSO-d_6, δ, ppm): 8.21 (br, Ar–*CH*=), 7.60 (br, Ar–*H*), 6.97 (br, 2H, Ar–*H*), 6.45 (br, =*CH*–COOR), 4.66, 4.46 and 4.21 (br, –*OH*), 3.9–3.6 (br, –*CH*–OH, –*CH*–OCOCH$_3$ and OC*H*$_3$ from 4-methoxycinnamate) and 2.30–0.80 (br, C*H*$_3$–CO and –CH–*CH*$_2$–CH– of PV(OH) backbone). UV–vis (DMSO) λ_{max}, nm (ε, M^{-1} cm^{-1}, monomeric unit^{-1}): 311 (131).

PB2: White solid. DS: 0.09. T_g: 79.1 °C. FT-IR (KBr, cm^{-1}): 3362 (OH), 2939, 2841 (–C–H, stretching), 1724 (C=O, stretching), 1605, 1513 (C=C, stretching), 1429 (–CH$_2$–, bending) and 1256, 1173 (C–O, stretching). ^{1}H NMR (400 MHz, DMSO-d_6, δ, ppm): 7.59 (br, Ar–*H*), 6.90 (br, Ar–*H*), 6.41 (br, =*CH*–COOR), 4.68, 4.47 and 4.22 (br, –*OH*), 4.0–3.6 (br, –*CH*–OH and –*CH*–OCOCH$_3$), 3.79 (br, OC*H*$_3$) and 2.30–0.80 (br, C*H*$_3$–CO and –CH–*CH*$_2$–CH– of PV(OH) backbone). UV–vis (DMSO) λ_{max}, nm (ε, M^{-1} cm^{-1}, monomeric unit^{-1}): 311 (2109).

PB3: Light brown solid. DS: 0.27. T_g: 79.6 °C. FT-IR (KBr, cm^{-1}): 3485 (OH), 3072 (=C–H, stretching), 2931, 2835 (–C–H, stretching), 1710 (C=O, stretching), 1632, 1603 (C=C, stretching), 1426 (–CH$_2$–, bending) and 1253, 1169 (C–O, stretching). ^{1}H NMR (400 MHz, DMSO-d_6, δ, ppm): 8.15 (br, Ar–*CH*=), 7.56 (br, Ar–*H*), 6.90 (br, Ar–*H*), 6.39 (br, =*CH*–COOR), 5.5–4.4 (br, –*OH*), 4.3–3.9 (br, –*CH*–OH and –*CH*–OCOCH$_3$), 3.74 (br, OC*H*$_3$) and 2.30–1.00 (br, CH$_3$–CO and –CH–*CH*$_2$–CH– of PV(OH) backbone). UV–vis (DMSO) λ_{max}, nm (ε, M^{-1} cm^{-1}, monomeric unit^{-1}): 309 (4242).

PB4: Brown solid. DS: 0.44. T_g: 82.0 °C. FT-IR (KBr, cm^{-1}): 3493 (OH), 3069, 3026 (=C–H, stretching), 2934, 2839 (–C–H, stretching), 1709 (C=O, stretching), 1632, 1604 (C=C, stretching), 1427 (–CH$_2$–, bending) and 1252, 1166 (C–O, stretching). ^{1}H NMR (400 MHz, DMSO-d_6, δ, ppm): 8.14 (br, Ar–*CH*=), 7.48 (br, Ar–*H*), 6.82 (br, Ar–*H*), 6.29 (br, =*CH*–COOR), 5.6–4.5 (br, –*OH*), 4.4–3.9 (br, –*CH*–OH and –*CH*–OCOCH$_3$), 3.72 (br, OC*H*$_3$) and 2.30–0.80 (br, C*H*$_3$–CO and –CH–*CH*$_2$–CH– of PV(OH) backbone). UV–vis (DMSO) λ_{max}, nm (ε, M^{-1} cm^{-1}, monomeric unit^{-1}): 310 (10,072).

PB5: Brown solid. DS: 0.28. T_g: 84.5 °C. FT-IR (KBr, cm^{-1}): 3349 (OH), 3072, 3023 (=C–H, stretching), 2934, 2840 (–C–H, stretching), 1707 (C=O, stretching), 1632, 1604 (C=C, stretching), 1427 (–CH$_2$–, bending) and 1253, 1168 (C–O, stretching). ^{1}H NMR (400 MHz, DMSO-d_6, δ, ppm): 8.17 (br, Ar–*CH*=), 7.57 (br, Ar–*H*), 6.89 (br, Ar–*H*), 6.37 (br, =*CH*–COOR), 5.5–4.4 (br, –*OH*), 4.3–4.0 (br, –*CH*–OH and –*CH*–OCOCH$_3$), 3.75 (br, OC*H*$_3$) and 2.30–0.80 (br, C*H*$_3$–CO and –CH–*CH*$_2$–CH– of PV(OH) backbone). UV–vis (DMSO) λ_{max}, nm (ε, M^{-1} cm^{-1}, monomeric unit^{-1}): 310 (6681).

PB6: Brown solid. DS: 0.46. T_g: 78.7 °C. FT-IR (KBr, cm^{-1}): 3504 (OH), 3063, 3029 (=C–H, stretching), 2936, 2839 (–C–H, stretching), 1710 (C=O, stretching), 1632, 1604 (C=C, stretching), 1428 (–CH$_2$–, bending) and 1250, 1168 (C–O, stretching). ^{1}H NMR (400 MHz, DMSO-d_6, δ, ppm): 8.13 (br, Ar–*CH*=), 7.54 (br, Ar–*H*), 6.87 (br, Ar–*H*), 6.33 (br, =*CH*–COOR), 5.5–4.5 (br, –*OH*), 4.3–3.9 (br, of –*CH*–OH and –*CH*–OCOCH$_3$), 3.72 (br, OC*H*$_3$) and 2.30–0.80 (br, C*H*$_3$–CO and –CH

–CH_2–CH– of PV(OH) backbone). UV–vis (DMSO) λ_{max}, nm (ε, $M^{-1}cm^{-1}$, monomeric $unit^{-1}$): 310 (8585).

2.2.3. Poly(vinylalcohol-co-vinyl-2,4-dimethoxycinnamate) product

PC: Light yellow solid. DS: 0.46. T_g: 88 °C. FT-IR (KBr, cm^{-1}): 3467 (OH), 3072 (=C–H, stretching), 2940, 2839 (–C–H, stretching), 1706 (C=O, stretching), 1606 (C=C, stretching) and 1262, 1209, 1160 (C–O, stretching). ^{1}H NMR (400 MHz, DMSO-d_6, δ, ppm): 7.66 (br, Ar–C*H*=), 7.42, 6.42 (br, Ar–*H*), 6.29 (br, =C*H*–COOR), 5.5–4.6 (br, –*OH*), 4.5–3.9 (br, –C*H*–OH and –C*H*–OCOCH$_3$), 3.74 (br, OCH_3) and 2.30–1.00 (br, CH_3–CO and –CH–CH_2–CH– of PV(OH) backbone). UV–vis (DMSO) λ_{max}, nm (ε, $M^{-1}cm^{-1}$, monomeric $unit^{-1}$): 295 (6991) and 328 (8900).

2.2.4. Poly(vinylalcohol-co-vinyl-2,4,5-trimethoxycinnamate) product

PD: Light yellow solid. DS: 0.53. T_g: 106.7 °C. FT-IR (KBr, cm^{-1}): 3486 (OH), 3082 (=C–H, stretching), 2938, 2837 (–C–H, stretching), 1705 (C=O, stretching), 1611, 1575 (C=C, stretching) and 1256, 1211, 1163 (C–O, stretching). ^{1}H NMR (400 MHz, DMSO-d_6, δ, ppm): 7.71 (br, Ar–C*H*=), 7.05, 6.46 (br, Ar–*H*), 6.26 (br, =C*H*–COOR), 5.5–4.6 (br, –*OH*), 4.5–4.0 (br, –C*H*–OH and –C*H*–OCOCH$_3$), 3.76 (br, OCH_3) and 2.30–1.00 (br, CH_3–CO and –CH–CH_2–CH– of PV(OH) backbone). UV–vis (DMSO) λ_{max}, nm (ε, $M^{-1}cm^{-1}$, monomeric $unit^{-1}$): 292 (5232) and 354 (5679).

2.3. Preparation of the polymeric micro/nanoparticles

The formation of micro/nanoparticles was performed at room temperature using the dialysis method [19,20]. Twenty four milligrams of substituted PV(OH) were dissolved in 40 ml of DMF. The resulting solution was transferred into the CelluSep T4 dialysis tube (MWCO 12,000–14,000, 75 mm flatwidth, 17.9 mL/cm volume capacity, Membrane Filtration Products, Seguin, TX, USA). The distance between the two clipped ends of the dialysis tube was 4.5 cm (length of the flat tube) which accounted for approximately 75–80 mL volume. This left about 35–40 mL void volume inside the dialysis tube at the beginning of the dialysis process. The solution in the dialysis tube was dialyzed against 1000 mL deionized water (Milli-Q®). Eight changes of water were performed at 3, 8, 15, 20, 25, 35, 40 and 50 h. After dialysis, a volume of the obtained colloidal suspension inside the dialysis tube usually increased from its starting polymeric solution to approximately 70 mL. Water was added to the suspension to make the final volume of 80 mL. Then, the suspension of the resulting nanoparticles was subjected to SEM, TEM and dynamic light scattering analyses. Dry particles were obtained by freeze-drying the aqueous suspension.

2.4. Effects of concentration used during the particle formation in the self-assembly process

The obtained polymers were prepared into micellar particles at various concentrations during particle formation. Polymer solutions at concentrations of 0.006 0, 0.060, 0.60, 6.0 and 12.0 mg/mL were prepared in DMF and were dialyzed against deionized water (Milli-Q®). The obtained nanoparticulate suspensions were subjected to SEM analyses.

2.5. Effects of anti-solvent used in the self-assembly process

PB4 solution (0.60 mg/mL) was prepared in DMSO. The resulting solution was dialyzed against deionized water or hexane to induce self-assembling of the polymer into micellar particles or reverse micellar particles, respectively. Dialysis against water was performed as described above. Dialysis against hexane was performed using polyvinylidene difluoride (PVDF) dialysis tube (MWCO 250 kD, 24 mm flat width, Spectrum Laboratories Inc., USA), using the same procedure as described for the dialysis against water except that water was replaced with hexane. The obtained suspension was air-dried at room temperature.

2.6. X-Ray powder diffraction analysis

PB4 and PB3 nanoparticle suspensions were freeze-dried and subjected to X-ray powder diffraction (XRD) analysis. Solutions of PB4 and PB3 polymer in DMF were prepared and evaporated under reduced pressure to remove DMF. The obtained PB4 and PB3 solid in non-nanostructural state were also subjected to XRD analysis. XRD analysis was carried out with target: Cu, wavelength = 1.5406 Å, voltage/current: 40 kV/30 mA, on Bruker AXS, Model: D8 Advance (BRUKER AXS Inc., Madison,

WI, USA). The scanning from 20 to 5.0° to 90.0° was performed at 0.03°/1.2 s at room temperature.

3. Results and discussion

The *trans*-substituted cinnamic acids were successfully synthesized using the Knoevenagel-Doebner condensation between benzaldehyde and malonic acid. Grafting *trans*-substituted cinnamoyl moieties onto PV(OH) could be done successfully using a chemical esterification reaction that utilizes the hydroxyl functionality of PV(OH) and *trans*-substituted cinnamoyl chloride, which was prepared *in situ* from the synthesized *trans*-substituted cinnamic acid and thionyl chloride (Scheme 1).

^{1}H NMR spectrum of PV(OH) in DMSO displays the resonance of backbone methylene protons at 0.8–1.8 ppm and the methine protons attached to –OH and –OCOCH$_3$ at 3.83 and 3.88 ppm, respectively. The –CH$_3$ protons of the acetate group resonance at 1.94 ppm while the hydroxyl protons are separated into broads at 4.25, 4.49 and 4.68 ppm due to their hydrogen bonding with DMSO [21]. The ^{1}H spectra of the synthesized poly(vinylalcohol-*co*-cinnamate) derivatives in DMSO also displays resonance of the backbone methylene protons at 1.8 ppm, the methine protons attached to –OH or –OCOCH$_3$ or cinnamoyl group at 3.8 ppm, and additional Ar-C*H*=C*H* protons and aromatic protons from the cinnamoyl group at 6.2–8.4 ppm. The degree of substitution (*n*, *m* and *p*, see Table 1) was obtained from the integration of peaks at 6.2–8.4 ppm (–COC*H*=C*H*–Ar and Ar–*H*) against peaks at 0.8–2.3 ppm (–CH–C*H*$_2$–CH– and C*H*$_3$–CO– of PV(OH) backbone). It should be noted here that the ^{1}H NMR spectra obtained using the long delay times between pulses (25 S for 45° pulses) were similar to the spectra obtained using normal delay times (1 s for 45° pulses). By adjusting the amount of cinnamic acid derivatives used in the grafting reaction, products with various degrees of cinnamoyl substitution (DS) could be obtained (Table 1). UV absorption spectra of the grafted polymeric products correspond well with the λ_{max} of the grafted cinnamoyl chromophores [17]. Increases in the molar absorption coefficient (ε) of the grafted polymer also agrees with increases in the degree of cinnamoyl substitution (see details of the ε value of each product in the experimental section and Fig. 1). In addition, IR spectra of the products show obvious C=O stretching of the ester functionality at ~1710 cm^{-1}.

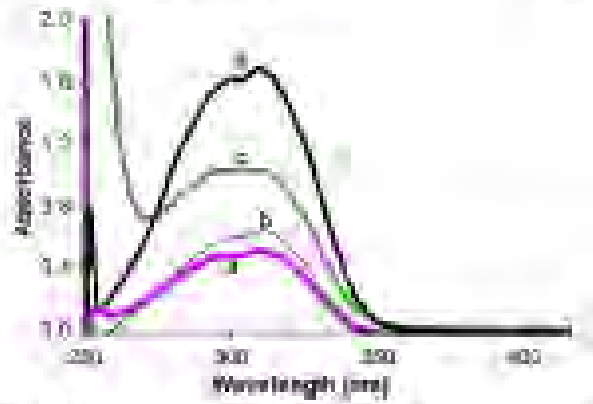

Fig. 1. UV absorption spectra of poly(vinylalcohol-*co*-cinnamate) solution in DMSO: 0.20 mg/mL of PB4 (a) and 0.020 mg/mL of PB2 (b), PB3 (c) and PB4 (d).

The obtained polymers could be induced into stable water dispersible micellar nanoparticles using the dialysis method with DMF as a solvent and water as an anti-solvent. It was speculated that when DMF was displaced by water, the hydrophobic groups (cinnamoyl moieties) were directed to the inside of the sphere, while the hydrophilic domains of the PV(OH) backbone (hydroxyl groups) arranged themselves at the outer surface of the sphere to provide maximal interaction with the hydrophilic water molecules leading to spontaneous particle formation. This resulted in an aqueous colloidal suspension of the polymeric particles. This speculation is confirmed by comparing ^{1}H NMR spectrum of the PB4 polymer solution in deuterated DMSO with spectra of PB4 nanoparticle suspension in D_2O and deuterated acetone (Fig. 2). The NMR spectrum of PB4 solution in DMSO clearly displays the resonance of cinnamoyl moieties (6.2–8.4 ppm) together with backbone methylene protons (1.8 ppm), backbone methine protons (3.8 ppm), and acetyl protons (2.4 ppm). The resonances of hydroxyl protons were very broad peaks at 4.6–5.5 ppm. However, no resonance from cinnamoyl moieties can be seen in the spectrum of nanoparticle suspension in both D_2O and acetone. This suggests that the cinnamoyl moieties buried inside of the spheres are in a crystalline state. Obvious resonances of hydroxyl protons in the spectrum of nanoparticle suspension in acetone could be observed at 3.92 and 3.93 ppm. No resonance of hydroxyl protons in the NMR spectrum of nanoparticle suspension in D_2O was caused by the rapid exchange of hydrogen atoms from hydroxyl groups on the outer surface of the spheres with

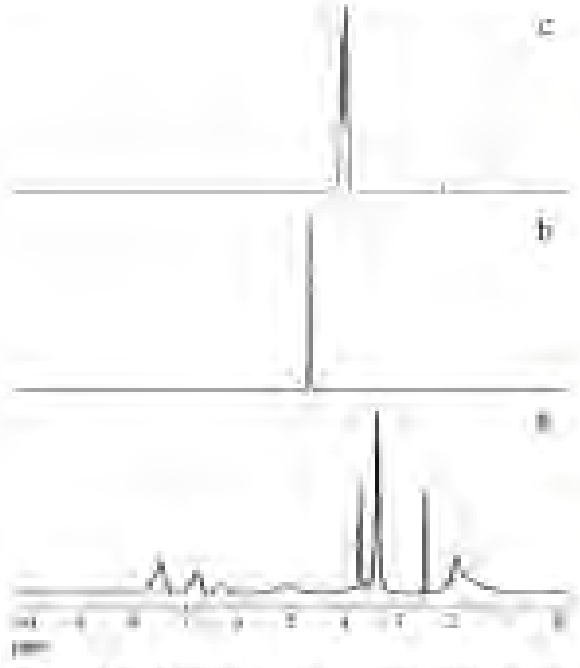

Fig. 2. ^{1}H NMR spectra of the poly(vinylalcohol-co-vinyl-6-carboxycinnamate) DS 0.44 (PB4) solution in DMSO-d_6 (a), PB4 nanoparticle suspension in D_2O (b) and PB4 nanoparticle suspension in deuterated acetone (c).

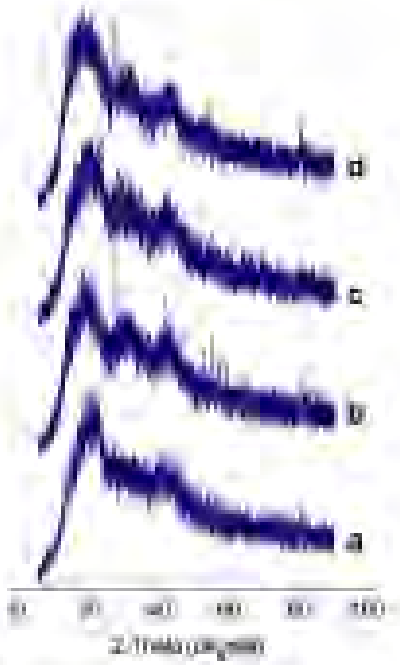

Fig. 4. XRD patterns of PB4 polymer in non-nanostructured solid state (a), PB4 nanoparticles (b), PB1 polymer in non-nanostructured solid state (c) PB1 nanoparticles (d).

deuterium atoms from D_2O. This, therefore, confirms that the hydroxyl groups are on the outer surface of the sphere.

XRD pattern of nanoparticles contains more peaks than that of their corresponding solid or non-nanostructured state (comparing Fig. 3a, b and Fig. 3c, d) thus confirming that nanoparticle formation has resulted in crystallinity at the particles' cores. XRD pattern of particles prepared from polymer with higher DS (PB4 particles) shows more peaks than that from polymer with a lower DS value (PB1 particles, comparing Fig. 3b–d) suggesting more crystallinity at the cores of particles prepared from polymer with more cinnamoyl substitution.

Under the conditions used, the non-derivatised PV(OH) could not self-assemble into particles via the dialysis method. This should be a result of insufficient hydrophobicity of the underivatised PV(OH). The grafted polymer with DS of only 0.01 (PB1) also did not self-assemble into stable particle, while all the prepared derivatives with DS ≥ 0.04 resulted in stable nanoparticles upon dialysis. In addition to zeta potential measurements, SEM and TEM analyses indicated that all the obtained nanoparticles were spherical with a smooth and negatively charged surface. The obtained particles showed an obvious relationship between particle size and the degree of cinnamoyl substitution on the PV(OH) polymeric backbone (Table 1). The particle size decreased with an increasing degree of cinnamoyl substitution. This result agrees with reports on other polymeric nanoparticle systems [22–24]. The size distribution of particles obtained from polymers with a higher DS is narrower than those from the lower DS (Fig. 4). It was speculated that more cinnamoyl moieties resulted in more hydrophobic interactions at the particle's core. The interaction among cinnamoyl groups is a driving force that pulls the polymer chain towards the center of the sphere resulting in smaller particles (see Fig. 5). This speculation agrees with the above discussion that the cinnamoyl moieties at the particle's core are in a crystalline state. Upon self-assembly, polymer with lower DS should have less hydrophobic interaction points which results in less compact nanostructure. This is because hydroxyl groups along the polymer chain will try to arrange themselves in order to have maximum interaction with water molecules (Fig. 5 right). In contrast, self-assembly of polymer chain with higher DS should yield more compact nanostructure (Fig. 5 left). If there is not

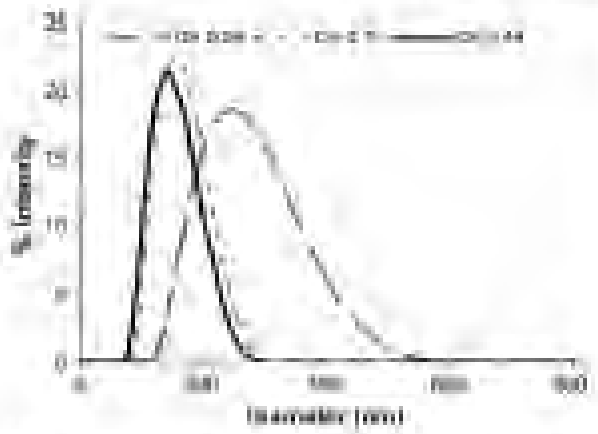

Fig. 4. Hydrodynamic size distribution of nanoparticles prepared from poly(vinylalcohol-co-vinyl-4-methoxycinnamate) containing various degrees of 4-methoxycinnamate substitution. Concentration of the polymeric solution during particle formation was 0.80 mg/mL.

enough cinnamoyl moieties, solvation of water molecules around the hydrophilic hydroxyl moieties along the chain can solubilize the polymer molecules. This explains why the DS of ≥0.04 is required for the formation of stable particles.

By comparing the size of spherical particles prepared from polymers grafted with different cinnamoyl derivatives (cinnamoyl, 4-methoxycinnamoyl, 2,4-dimethoxycinnamoyl and 2,4,5-trimethoxycinnamoyl) at similar DS, it can be concluded that the difference in methoxy substitution on the benzene ring of the cinnamoyl moieties significantly affects particle size. Poly(vinylalcohol-co-vinylcinnamate) seems to produce bigger particles than poly(vinylalcohol-co-vinyl-4-methoxycinnamate) (see PA3 and PB3 particles in Table 1). Poly(vinylalcohol-co-vinyl-4-methoxycinnamate) seems to produce bigger particles than poly(vinylalcohol-co-vinyl-2,4-dimethoxycinnamate) and poly(vinylalcohol-co-vinyl-2,4,5-trimethoxycinnamate) (see PB4, PC and PD particles in Table 1). Because DS also affects particle size, a comparison should be performed between derivatives with similar DS values. As mentioned earlier, the interactions among the grafted cinnamoyl derivative moieties inside the particles directly affects the size of the sphere, thus it is not surprising to observe significant differences in particle size obtained from PVi(OH) grafted with different cinnamoyl structures, which is likely a result of different crystallite structures at the particle's core.

Interestingly, particles obtained from poly(vinylalcohol-co-vinyl-4-methoxycinnamate) prepared from PVi(OH) of different molecular weights [M_w 155 kDa (PB3, PB4), M_w 43 kDa (PB2), M_w 10 kDa (PB1)] possessed similar spherical shape, size, and surface charge (comparing PB3 with PB3 and PB4 with PB4 in Table 1). It was speculated that the self-assembly of polymers into particles occurred slowly and was mainly governed by the balance between hydrophobic interaction inside the particles and the hydrophilic interaction on the outer surface of the particles. This resulted in particles with a narrow size distribution regardless of the polymer molecular weight. However, as has been frequently reported in the formation of polymeric nanoparticles, the particle size increased with increasing polymer concentration during particle formation (Fig. 6). Although self-assembly was mainly governed by the balance between hydrophobic interaction inside the particles and the hydrophilic interaction at the outer surface of the particles, an association among particles occurred, more frequently leading to bigger

Fig. 5. Schematic representation of a more compact assembling of a grafted polymeric chain with higher DS showing more hydrophobic interaction (two many grafted cinnamoyl moieties (left)) and a less compact assembling of a grafted polymer chain with lower DS showing less hydrophobic interaction resulted from a smaller number of the grafted cinnamoyl moieties (right).

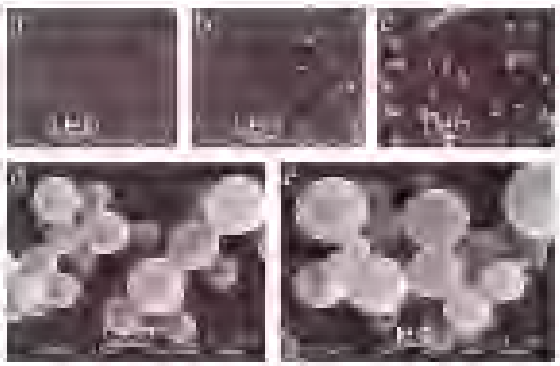

Fig. 6. Morphology of PB4 nanoparticles prepared at the polymer concentrations of 0.005 mg/mL (a), 0.040 mg/mL (b), 0.60 mg/mL (c), 1.0 mg/mL (d), 1.10 mg/mL (e).

particles at high concentrations during particle formation (Fig. 6d and e).

The effect of solvent on particle formation was examined using poly(vinyl-*co*-vinyl-4-methoxycinnamate) with a DS of 0.44 (PB4). Dialysis of PB4 solutions prepared in DMSO and DMF against water, gave particles of similar size (hydrodynamic diameters of 140–145 nm) and shape (observed by SEM and TEM). As mentioned earlier, the self-assembly of polymers into particles was mainly governed by the balance between hydrophobic interaction of cinnamoyl moieties inside the particles and the hydrophilic interaction between hydroxyl groups and water molecules on the outer surface of the particles, therefore changing from DMF to DMSO did not affect particle morphology.

PB4 solutions (0.60 mg/mL DMF) were dialyzed against deionized water (polar solvent) and hexane (non-polar solvent) to induce the self-assembly of PB4 into nanoparticles in micellar and reverse micellar fashions, respectively. Using hexane as an anti-solvent, uniform microparticles with diameter of >1 μm were obtained, while using water as an anti-solvent gave nanoparticles with diameter of ~142 nm (Fig. 7). Structures of the particles obtained using hexane as an anti-solvent were very homogeneous (Fig. 7b). It was speculated that these bigger sizes were neither a result of particles' association nor the result of fast particle formation in solvent with low viscosity (viscosity of hexane and water are 0.30 cP and 0.89 cP, respectively), but rather caused by the structure of the PB4 polymer itself. During the reverse micellar particle formation, hydroxyl groups should be directed inwards and cinnamoyl groups should be directed to the outer surface of the sphere. The small size of hydroxyl groups prevents them from filling up the particle core, and therefore, they only line the inner wall of the hollow particles. The hollowness of the micro-sphere was confirmed by the obvious indentation of particles (Fig. 7c). Since the reverse micellar PB4 nanoparticles did not disperse well in most organic solvents, including deuterated benzene, its ^{1}H NMR spectrum was of poor quality. Nevertheless, the resonance of protons from the benzene ring of cinnamoyl moieties (5.9–7.8 ppm) could be observed, which indicated that the cinnamoyl moieties of the reverse micellar particles were not in the crystalline state.

4. Conclusions

This study demonstrates that PV(OH) grafted with trans-substituted cinnamic acid are an interesting class of materials for micro/nanoparticle preparation. The self-assembly of poly(vinyl-alcohol-*co*-vinyl-cinnamate) derivatives into micellar nanoparticles could be performed by dialyzing the polymer against water. ^{1}H NMR spectrum implied that the hydroxyl groups of the polymer were on the outer surface of the spheres, while cinnamoyl moieties were buried inside the spheres forming crystalline structures. ^{1}H NMR indicated a rapid exchange of hydrogen atoms of the hydroxyl groups with the deuterium atoms from D_2O solvent. The crystalline structure of the cinnamoyl moieties was implied by a lack of resonance from protons of cinnamoyl moieties in the well-dispersed micellar particles. Polymers with a higher degree of cinnamoyl substitu-

Fig. 7. Morphology of particles prepared from PB4 solution (0.60 mg/mL in DMF) by dialyzing against water (micellar particles, a) and hexane (reverse micellar particles, b and c).

tion gave smaller particles upon self-assembly. Variations in particle sizes was observed amongs particles obtained from PV(OH) grafted with cinnamoyl derivatives of different methoxy substitution on the benzene ring. The molecular weight of the polymer did not significantly affect nanoparticle size and morphology. In addition, self-assembly of the poly(vinylalcohol-co-vinylcinnamate) derivatives into hollow reverse micellar microparticles of uniform size could be achieved by dialyzing the polymer solution against non-polar solvents such as hexane. In contrast to the micellar particles, cinnamoyl moieties of polymer could be observed with the ^{1}H NMR spectrum of reverse micellar micro-particle suspension. It should be stated here that this understanding of the relationship between particle's morphology and chemical structure of the polymer should help in fine-tuning the design of drug carrier systems.

Acknowledgements

This project is supported by the Thailand Research Fund (RMU4980003) and the Office of Commission for Higher Education-CU Graduate Thesis Grant.

References

[1] Jones MC, Leroux JC. Polymeric micelles – a new generation of colloidal drug carriers. Eur J Pharm Biopharm 1999;48:101.
[2] DeMerlis CC, Schoneker DR. Review of the oral toxicity of polyvinyl alcohol (PVA). Food Chem Toxicol 2003;41:319.
[3] Si-Shen F, Li M, Bing-Hung C, Daniel P. Polymeric nanospheres fabricated with natural emulsifiers for clinical administration of an anticancer drug paclitaxel (Taxol®). Mater Sci Eng C 2002;20:85.
[4] Seung CL, Jae TO, Myoung HJ, Soo BC. Quantitative analysis of polyvinyl alcohol on the surface of poly(D,L-lactide-co-glycolide) microparticles prepared by solvent evaporation method: effect of particle size and PVA concentration. J Control Release 1999;59:123.
[5] Fude C, Dongmei C, Anjin T, Mingshi Y, Kai S, Min Z, et al. Preparation and characterization of melittin-loaded poly(DL-lactic acid) or poly (DL-lactic-co-glycolic acid) microspheres made by the double emulsion method. J Control Release 2005;107:310.
[6] Li JK, Wang N, Wu XS. Poly(vinyl alcohol) nanoparticles prepared by freezing–thawing process for protein/peptide drug delivery. J Control Release 1998;56:117.
[7] Luppi B, Orienti I, Bigucci F, Cerchiara T, Zuccari G, Fazzi S, et al. Poly(vinylalcohol-co-vinyloleate) for the preparation of micelles enhancing retinyl palmitate transcutaneous permeation. Drug Deliv 2002;9:147.
[8] Zuccari G, Carosio R, Fini A, Montaldo PG, Orienti I. Modified polyvinylalcohol for encapsulation of all-trans-retinoic acid in polymeric micelles. J Control Release 2005;103:369.
[9] Orienti I, Bigucci F, Luppi B, Cerchiara T, Zuccari G, Giunchedi P, et al. Polyvinylalcohol substituted with triethyleneglycolmonoethylether as a new material for preparation of solid dispersions of hydrophobic drugs. Eur J Pharm Biopharm 2002;54:229.
[10] Orienti I, Trere R, Zecchi V. Hydrogels formed by cross-linked polyvinylalcohol as colon-specific drug delivery systems. Drug Dev Ind Pharm 2001;27:877.
[11] Orienti I, Trerè R, Luppi B, Bigucci F, Cerchiara T, Zuccari G, et al. Hydrogels formed by crosslinked poly(vinyl alcohol) as sustained drug delivery systems. Arch Pharm (Weinheim) 2002;335:89.
[12] Orienti I, Zuccari G, Bergamante V, Carosio R, Gotti R, Cilli M, et al. Fenretinide–polyvinylalcohol conjugates: new systems allowing fenretinide intravenous administration. Biomacromolecules 2007;8:3258.
[13] Cerchiara T, Luppi B, Bigucci F, Orienti I, Zecchi V. Substituted polyvinylalcohol as a drug carrier for beta-carotene. Eur J Pharm Biopharm 2003;56:401.
[14] Orienti I, Bigucci F, Gentilomi G, Zecchi V. Self-assembling poly(vinyl alcohol) derivatives, interactions with drugs and control of release. J Pharm Sci 2001;90:1435.
[15] Kimura T, Okuno A, Miyazaki K, Furuzono T, Ohya Y, Ouchi T, et al. Novel PVA-DNA nanoparticles prepared by ultra high pressure technology for gene delivery. Mater Sci Eng C 2004;24:797.
[16] Westedt U, Kalinowski M, Wittmar M, Merdan T, Unger F, Fuchs J, et al. Poly(vinyl alcohol)-graft-poly(lactide-co-glycolide) nanoparticles for local delivery of paclitaxel for restenosis treatment. J Control Release 2007;119:41.
[17] Monhaphol T, Albinsson B, Wanichwecharungruang SP. 2-Ethylhexyl-2,4,5-trimethoxy cinnamate and di-(2-ethylhexyl)-2,4,5-trimethoxybenzalmalonate as novel broadband UV filters. J Pharm Pharmacol 2007;59:279.
[18] Hartman RF, Rose SD. Kinetics and mechanism of the addition of nucleophiles to unsaturated thiol esters. J Org Chem 2006;71:6342.
[19] Lee JH, Jung SW, Kim IS, Jeong YH, Kim YH, Kim SH. Polymeric nanoparticle composed of fatty acids and poly(ethylene glycol) as a drug carrier. Int J Pharm 2003;251:23.
[20] Zhigang X, Chi-Hwa W. Self-assembled biodegradable nanoparticles developed by direct dialysis for the delivery of paclitaxel. Pharm Res 2005;22:2079.
[21] Moritani T, Kuruma I, Shibatani K, Fujiwara Y. Tacticity of poly(vinylalcohol) studied by nuclear magnetic resonance of hydroxyl protons. Macromolecules 1972;5:577.
[22] Minsu L, Yong WC, Jae HP, Hesson C, Seo YJ, Kwon C, et al. Size control of self-assembled nanoparticles by an emulsion/solvent evaporation method. Colloid Polym Sci 2006;284:506.
[23] Jae HJ, Hyung SK, Seung RY, Kinam P, Jong-Duk K. Biodegradable poly(asparagine) grafted with poly(caprolactone) and the effect of substitution on self-aggregation. Colloids Surf A: Physicochem Eng Aspects 2003;266:187.
[24] Yan YL, Xi GC, Cheng SL, Dong SC, Hyun JP, Chong ML. Effect of the molecular mass and degree of substitution of oleoylchitosan on the structure, rheological properties, and formation of nanoparticles. J Agric Food Chem 2007;55:4842.

ภาคผนวก จ

Oligoesters Based on Poly(*p*-alkoxycinnamate) and Poly(pentaethylene glycol cinnamate) as Potential UV Filters

S. Sasiwilaskorn,[1,2] P. Klinubol,[3] A. Tachaprutinun,[3] T. Udomsup,[3] S. P. Wanichwecharungruang[1,2]

[1]*Program of Petrochemistry and Polymer Science, Faculty of Science, Chulalongkorn University, Bangkok 10330, Thailand*
[2]*Science and Technology Division, Nong Khai Campus, Khon Kaen University, Nong Khai 43000, Thailand*
[3]*Sensor Research Unit, Department of Chemistry, Faculty of Science, Chulalongkorn University, Bangkok 10330, Thailand*

Received 16 September 2007; accepted 20 February 2008
DOI 10.1002/app.28335
Published online 2 June 2008 in Wiley InterScience (www.interscience.wiley.com).

ABSTRACT: Four solid UV-absorptive oligomers—poly(*p*-ethoxycinnamate) (P2), poly(*p*-propoxycinnamate) (P3), poly(*p*-hexyloxycinnamate) (P6), and poly(*p*-undecyloxycinnamate) (P11)—were condensation polymerized from *p*-(2-hydroxy-ethoxy) cinnamic acid, *p*-(3-hydroxy-propoxy) cinnamic acid, *p*-(6-hydroxy-hexyloxy) cinnamic acid, and *p*-(11-hydroxy-undecyloxy) cinnamic acid, respectively. The liquid UV-absorptive oligomer, poly(pentaethylene glycol cinnamate) (PPGC), was synthesized through the copolymerization between *p*-hydroxycinnamic acid and pentaethylene glycol dicrylate. Molecular weights of all five oligomers were in the range of 1600–8500. Absorption profiles of all synthesized polymers indicated UVB absorption characteristics. Upon UVB exposure, there to *cis* photoisomerization of all five oligomers was observed, leading to the decrease in their UVB absorption efficiency. No transdermal penetration across a baby mouse skin (*Mus musculus* Linn.) was detected for the five synthesized oligomers, while the penetration of the standard UVB filter, 2-ethylhexyl-*p*-methoxycinnamate, through the same skin could be clearly observed. In addition, PPGC, a yellowish water immiscible liquid, showed good solubility in various organic solvents and silicone fluids. PPGC and P3 could be induced into water dispersible nanoparticles using solvent displacement technique. © 2008 Wiley Periodicals, Inc. J Appl Polym Sci 109: 3502–3510, 2008

Key words: alkoxycinnamate; UV filter; poly(pentaethylene glycol cinnamate); nanoparticles

INTRODUCTION

Long-term exposure to UV radiation on normal human skin leads to direct cellular damage and immunosuppression, resulting in photoaging, mutations, and carcinogenesis.[1,2] UVB (280–315 nm) can interact directly with DNA bases and cause DNA lesions, particularly cyclobutane pyrimidine dimers (CPDs) and pyrimidine (6–4) pyrimidone photoproducts.[3,4] UVA Radiation produces not only the oxidative DNA damage through 8-oxo-7,8-dihydro-2′-deoxyguanosine,[5] but the radiation also induces CPDs formation probably via a triplet energy transfer photosensitization mechanism.[6] Therefore, sunscreen use has become widely practiced. Esters of *p*-methoxycinnamic acid are among the popular UVB screening compounds used in various cosmetic formulations. The most popularly-used derivative in this group is the 2-ethylhexyl *p*-methoxycinnamate (EHMC), which possesses a high molar absorption coefficient (ε), ~ 22,000–24,000 M^{-1} cm^{-1}, and shows only a few allergic reactions to human skin.[7,8] Nevertheless, transdermal permeation of the compound into the human body has been reported.[9,10] In fact, transdermal penetrations of many sunscreens have been demonstrated.[11,12] Transdermal absorption of the UV filter directly decreases the UV screening efficiency of the products. Attempts to increase the skin accumulation of UV absorbers include incorporations of the UV filters into delivery systems[13,14] and the alteration of existing formulations.[15] In addition, a few novel polymeric sunscreens have recently been reported. For example, grafting of the UV-absorptive cinnamoyl moieties onto polysaccharide backbone[16] and polysiloxane backbone[17] were carried out to obtain polysaccharide cinnamic acid derivatives and cinnamate-grafted silicone fluid with UV absorbing property, respectively. It should be stated here that, although there are many other investigations on cinnamate polymeric materials, most of them involve

Correspondence to: S. P. Wanichwecharungruang (pooyasom@chula.ac.th).
Contract grant sponsor: Thailand Research Fund, Office of Commission for Higher Education.

high molecular weight polymers used in optical and electrooptical applications.[18,19] In such applications, UV absorption property of the cinnamate moieties was not the main concern, their crosslinked liquid crystal and chiral photoisomerization properties were more important. In addition to cinnamate polymeric material, polymeric sunscreens based on other UV-absorptive functionalities were also reported.[20–22] Skin penetration of the polymeric UV filters could be avoided due to the presumed low diffusion of large polymers through skin over a limited period of time. In this study, we report the synthesis of UV-absorptive oligomers, poly(*p*-alkoxycinnamates) and poly (pentaethylene glycol cinnamate). The materials have similar UV-absorptive functionalities to EHMC. Their UV absorption properties and photostability were determined and their transdermal absorptions through baby mice skin were compared with EHMC.

EXPERIMENTAL

Solvents used in the synthesis and the spectroscopic works were of reagent or analytical grades purchased from Labscan (Bangkok, Thailand). *p*-Hydroxycinnamic acid, 2-bromoethanol, 3-bromo-1-propanol, 6-bromo-1-hexanol, 11-bromo-1-undecanol, 1-(3-dimethylaminopropyl)-3-ethylcarbodiimide hydrochloride (EDCI), and 1-hydroxy-benzotriazole (HOBt) were purchased from Acros (Geel, Belgium). Potassium carbonate, *p*-toluene sulfonic acid, Amberlyst-15, and pentaethylene glycol ditosylate were purchased from Fluka Chemical Company (Buchs, Switzerland). *N,N'*-dicyclohexylcarbodiimide (DCC) was purchased from Merck (Darmstad, Germany). Standard EHMC was a kind gift from Merck Thailand (Bangkok, Thailand).

The ^{1}H and ^{13}C NMR spectra were obtained in deuterated chloroform ($CDCl_3$) or deuterated dimethylsulfoxide (DMSO-d_6) with tetramethylsilane (TMS) as an internal reference using a Varian Mercury spectrometer that operated at 400.00 MHz for ^{1}H and 100.00 MHz for ^{13}C nuclei (Varian Company, Palo Alto, CA). The IR spectra were recorded on a Nicolet Fourier transform infrared spectrophotometer: Impact 410 (Nicolet Instrument Technologies, Madison, WI). Molecular weights were determined by gel permeation chromatography (GPC) using a Waters Styragel HR low molecular weight column and waters 600E multisolvent delivery system (Waters, MA). UV Spectra were obtained with the aid of an HP 8453 UV/VIS spectrophotometer (Agilent Technologies, CA) using a quartz cell with a 1-cm path length. The mass spectra of the synthesized monomers were recorded on a Micromass Quattro Micro API ESCi (Waters, MA) using negative electrospray ionization. The mass spectra of the oligomers were recorded on an Ultraflex MALDI-TOF mass spectrometer (Bruker Daltonics, Bremen, Germany). Melting points were determined with a Stuart Scientific Melting Point SMP 1 (Bibby Sterilin, Staffordshire, UK). Broadband UVB (280–320 nm) was generated by FS324T12/UVB/HO lamp (National Biological, Twinsburg, OH). UV irradiance was measured using UVB-500C power meters (National Biological, Twinsburg, OH). Thermogram of each sample was acquired at 0–380°C under nitrogen with a scanning rate of 20°C/min using a differential scanning calorimetry: DSC 204 (Netzsch Group, Selb, Germany). Scanning electron micrographs (SEM) were obtained using JEM-6400 (Jeol, Japan). A drop of the nanoparticle suspension (2 mg/mL) was placed on a glass slide and dried over night. After mounting the slide on aluminum pin, the sample was coated with a gold layer under vacuum at 10 kV for 90 s. Atomic force microscopy (AFM) image of a sample was acquired in a tapping mode using scanning probe microscope equipped with Nanoscope IV controller (Veeco Metrology Group, USA). The particle size distribution was analyzed by Mastersizer S nanoseries (Malvern Instruments, Worcestershire, UK).

Chemical synthesis (Scheme 1)

Synthesis of *p*-alkoxycinnamic acids

p-(2-hydroxy-ethoxy) cinnamic acid (M2) was prepared by refluxing a solution of *p*-hydroxycinnamic acid (0.01 mol) in acetonitrile (50 mL) with 2-bromoethanol in the presence of potassium carbonate (0.10 mol). The reaction was quenched by removing the heat and filtering out potassium carbonate. Then, saturated sodium bicarbonate (30 mL) was added to the filtrant and the mixture was extracted with dichloromethane (2 × 20 mL) to remove excess bromo alkyl alcohol. The aqueous layer was slowly poured into a beaker containing cold 40% hydrochloric acid (20 mL) and the white solid (*p*-(2-hydroxy

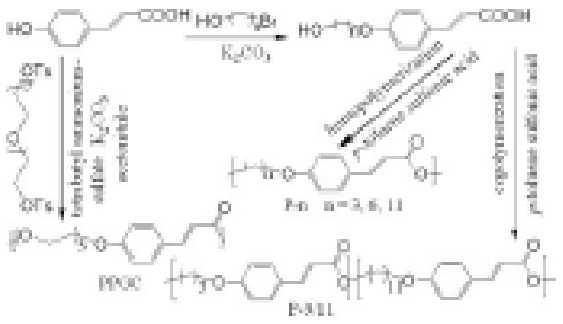

Scheme 1 Chemical synthesis of the monomers and the oligomers.

ethoxy) cinnamic acid) was separated by suction filtration, washed with cold water and dichloromethane.

p-(3-Hydroxy-propoxy) cinnamic acid (M3), *p*-(6-hydroxy-hexyloxy) cinnamic acid (M6) and *p*-(11-hydroxy-undecyloxy) cinnamic acid (M11) were prepared using a similar procedure. Corresponding bromo alkyl alcohol was used in place of 2-bromoethanol and hexane was used to extract 11-bromo-1-undecanol during the acid-base extraction procedure.

p-(2-Hydroxy-ethoxy) cinnamic acid (M2). White solid; yield: 73%. m.p.: 193.5–195.5°C. Retention factor or R_f: 0.31 (SiO_2, EtOAc/hexane, 70 : 30). ^{1}H NMR (400 MHz, $CDCl_3$, δ, ppm): 7.70 (d, J = 16.6 Hz, 1H, Ar—CH=), 7.50 (d, J = 8.6 Hz, 2H, Ar—H), 6.94 (d, J = 8.5 Hz, 2H, Ar—H), 6.32 (d, J = 15.3 Hz, 1H, = CH—COOH), 4.13 (t, 2H, $-CH_2-O-Ar$), 3.99 (t, 2H, $HO-CH_2$). ^{13}C NMR (100 MHz, DMSO-d_6, δ, ppm): 168.4 (—COOH), 144.3 (Ar—CH=), 160.9 (—O—Ar), 130.4 (2 × 1C), 127.2 (Ar—CH), 115.3 (2 × 1C) (aromatic carbons), 116.9 (=CH—COOH), 70.1 ($-CH_2-O-Ar$), 60.1 ($HO-CH_2-$). IR (KBr, cm^{-1}): 3387–2580, 1676, 1599, 1245. MS (*m/z*): calcd for $C_{11}H_{12}O_4$, 208; found, 207 $[M-H]^-$.

p-(3-Hydroxy-propoxy) cinnamic acid (M3). White solid; yield: 97%. m.p.: 152.0–154.0°C. R_f: 0.31 (SiO_2, EtOAc/hexane, 70 : 30). ^{1}H NMR (400 MHz, $CDCl_3$, δ, ppm): 7.71 (d, J = 16.6 Hz, 1H, Ar—CH=), 7.49 (d, J = 8.6 Hz, 2H, Ar—H), 6.92 (d, J = 8.6 Hz, 2H, Ar—H), 6.31 (d, J = 16.5 Hz, 1H, = CH—COOH), 4.16 (t, 2H, $-CH_2-O-Ar$), 3.88 (t, 2H, $HO-CH_2$). ^{13}C NMR (100 MHz,DMSO-d_6, δ, ppm): 168.3 (—COOH), 144.2 (Ar—CH=), 160.8 (—O—Ar), 130.4 (2 × 1C), 127.1 (Ar—CH), 115.2 (2 × 1C) (aromatic carbons), 116.8 (=CH—COOH), 65.2 ($-CH_2-O-Ar$), 57.6 ($HO-CH_2-$) and 32.4 ($-CH_2-$). IR (KBr, cm^{-1}): 3420–2362, 1676, 1603, and 1247. MS (*m/z*): calcd for $C_{12}H_{14}O_4$, 222; found, 221 $[M-H]^-$.

p-(6-Hydroxy-hexyloxy) cinnamic acid (M6). White solid; yield: 69%. m.p.: 162–165°C. R_f: 0.36 (SiO_2, EtOAc/hexane, 70 : 30). ^{1}H NMR (400 MHz, $CDCl_3$, δ, ppm): 7.70 (d, J = 15.5 Hz, 1H, Ar—CH=), 7.46 (d, J = 7.9 Hz, 2H, Ar—H), 6.90 (d, J = 7.8 Hz, 2H, Ar—H), 6.30 (d, J = 17.4 Hz, 1H,=CH—COOH), 3.99 (t, 2H, $-CH_2-O-Ar$), 3.66 (t, 2H, $HO-CH_2$). ^{13}C NMR (100 MHz, DMSO-d_6, δ, ppm): 168.0 (—COOH), 144.0 (Ar—CH=), 130.4 (2 × 1C), 160.8 (—O—Ar), 127.1 (Ar—CH), 115.2 (2 × 1C) (aromatic carbons), 116.8 (=CH—COOH), 68.0 ($-CH_2-O-Ar$), 61.1 ($HO-CH_2-$), 32.90, 29.08, and 25.82 (alkyl carbons). IR (KBr, cm^{-1}): 3250–2547, 1668, 1603, and 1247. MS (*m/z*): calcd for $C_{15}H_{20}O_4$, 264; found, 263 $[M-H]^-$.

p-(11-Hydroxy-undecyloxy) cinnamic acid (M11). White solid; Yield: 89%. m.p.: 128.0–130.0°C. R_f: 0.39 (SiO_2, EtOAc/hexane, 70 : 30). ^{1}H NMR (400 MHz, $CDCl_3$, δ, ppm): 7.71 (d, J = 15.8 Hz, 1H, Ar—CH=), 7.48 (d, J = 8.46 Hz, 2H, Ar—H), 6.90 (d, J = 8.56 Hz, 2H, Ar—H), 6.31 (d, J = 15.71 Hz, 1H,=CH—COOH), 3.99 (t, 2H, $-CH_2-O-Ar$), 3.64 (t, 2H, $HO-CH_2$). ^{13}C NMR (100 MHz, DMSO-d_6, δ, ppm): 168.3 (—COOH), 144.2 (Ar—CH=), 160.8 (—O—Ar), 130.3 (2 × 1C), 127.1 (Ar—CH), 115.2 (2 × 1C) (aromatic carbons), 116.8 (=CH—COOH), 68.0 ($-CH_2-O-Ar$), 61.2 ($HO-CH_2-$), 33.0, 29.4, and 26.0 (alkyl carbons). IR (KBr, cm^{-1}): 3396–2567, 1683, 1606, and 1280. MS (*m/z*): calcd for $C_{20}H_{30}O_4$, 334; found, 333 $[M-H]^-$.

Poly(*p*-propoxycinnamate) (P3), poly(*p*-hexyloxycinnamate) (P6), and poly(*p*-undecyloxycinnamate) (P11)

A monomer (0.50 g) and *p*-toluene sulfonic acid (0.10 g, 20% w/w) were refluxed in 30 mL toluene. The reaction mixture was quenched by cooling and filtering through No.1 Whatman filter paper. The filtrate was evaporated, dissolved in 25 mL dichloromethane, washed with saturated sodium bicarbonate solution (3 × 20 mL), dehydrated with anhydrous sodium sulfate and the solvent was removed by a rotary evaporator.

Low molecular weight poly (*p*-undecyloxycinnamate) (P11a)

To carry out polymerization of M11 at a more diluted concentration of the monomer, a similar polymerization reaction as described above was carried out for only 24 h. After 24 h, 250 mL of toluene was added into the reaction mixture and the mixture was refluxed for another 48 h. The reaction was then quenched by cooling and filtering. The filtrate was dried and then redissolved in 25 mL dichloromethane. The obtained solution was washed with saturated sodium bicarbonate solution (3 × 50 mL), dehydrated with anhydrous sodium sulfate and the solvent was removed by rotary evaporator.

Poly(p-propoxycinnamate) (P3). Pale brown solid; T_g: 50.7°C. Melting temperature or T_m: 154.2 °C. $\overline{M_n}$: 2000. ^{1}H NMR (400 MHz, $CDCl_3$, δ, ppm): 7.80–6.15 (br, Ar—H, Ar—CH=, =CH—COO—), 4.46–3.90 (br, $-CH_2-O-Ar$, $-COO-CH_2-$) and 2.48–1.86 (br, $-CH_2-$). IR (KBr, cm^{-1}): 3427, 2938, 1708, 1604, and 1251.

Poly(p-hexyloxycinnamate) (P6). Pale brown solid; $\overline{M_n}$: 3000. ^{1}H NMR (400 MHz, $CDCl_3$, δ, ppm): 7.69–6.10 (br, Ar—H, Ar—CH=,=CH—COO—), 4.24–3.29 (br, $-CH_2-O-Ar$, $-COO-CH_2-$) and 2.44–1.12 (br, $-CH_2-$). IR (KBr, cm^{-1}): 3403, 2939, 1709, 1605, and 1250.

Poly(p-undecyloxycinnamate) (P11). Pale brown solid; T_g: 53.4°C. $\overline{M_n}$: 5500. ^{1}H NMR (400 MHz, $CDCl_3$, δ, ppm): 7.67–6.25 (br, Ar—H, Ar—CH=, =CH—

COO—), 4.24–3.60 (br, $-CH_2-O-Ar$, $-COO-CH_2-$) and 1.83–1.15 (br, $-CH_2-$). IR (KBr, cm^{-1}): 3423, 2977, 1709, 1604, and 1252.

Poly(p-undecyloxycinnamate) (P11a). Pale yellow solid; T_g: 50.5°C. $\overline{M_n}$: 2500. ^1H NMR (400 MHz, $CDCl_3$, δ, ppm): 7.56 (d, J = 15.6 Hz, 1H, Ar—CH=), 7.38 (t, 2H, Ar—H), 6.80 (t, 2H, Ar—H), 6.23 (d, J = 16.3 Hz, 1H, =CH—COOH), 4.12, 3.86, and 3.56 (t, 2H, $-CH_2-O-Ar$ and $-COO-CH_2-$). IR (KBr, cm^{-1}): 3431, 2926, 1708, 1605, and 1257.

Poly(p-ethoxycinnamate) (P2). Monomer M2 (0.20 g, 1 × 10^{-3} mole) and *N,N*-dicyclohexylcarbodiimide, DCC (0.20 g, 1 × 10^{-3} mole) were refluxed in 15 mL acetone. After 24 h, the white solid (*N,N*-dicyclohexylurea, DCU) was removed by filtration. The filtrate was evaporated, dissolved in 30 mL dichloromethane and left for several days to precipitate out additional DCU. The solution was then filtered and washed with water (2 × 25 mL), dehydrated with anhydrous sodium sulfate and the solvent was removed by rotary evaporation.

Poly(p-ethoxy cinnamate) (P2). Orange solid; ^1H NMR (400 MHz, $CDCl_3$, δ, ppm): 7.89–6.40 (br, Ar—H, Ar—CH=, =CH—COO—), 4.13, 4.00, and 3.78 (br, $-O-CH_2-$, $-CH_2-O-Ar$ and $-COO-CH_2-$). IR (KBr, cm^{-1}): 3000–3302, 2932, 1704, 1647, and 1211–1130.

Poly(p-propoxycinnamate)-co-(p-undecyloxycinnamate) (P3/11)

M3 (0.25 g), M11 (0.09 g), and *p*-toluene sulfonic acid (0.10 g, 20% w/w) were refluxed in 30 mL toluene. During the 72 h of the reflux, two batches of 0.08 g M11 were added to the reaction mixture at hours 12 and 24 of the reaction. The reaction was quenched by removal from the heat and filtering through No.1 Whatman paper. The filtrate was evaporated, dissolved in 30 mL dichloromethane, washed with saturated sodium bicarbonate solution (3 × 25 mL), dehydrated with anhydrous sodium sulfate, and dried by rotary evaporation, to obtain P3/11. The insoluble part from the reaction mixture was washed with water prior to IR analysis.

Poly(p-propoxycinnamate)-co-(p-undecyloxycinnamate) (P3/11). Pale brown solid; $\overline{M_n}$: 2000. ^1H NMR (400 MHz, $CDCl_3$, δ, ppm): 7.75–6.09 (br, Ar—H, Ar—CH=, =CH—COO—), 4.40–3.44(br, $-CH_2-O-Ar$, $-COO-CH_2-$) and 2.17–1.10 (br, $-CH_2-$). IR (KBr, cm^{-1}): 3409, 2927, 1688, 1605, and 1252.

Poly(penta ethylene glycol cinnamate)

In the 50-mL two-neck round bottom flask, *p*-hydroxycinnamic acid (0.16 g, 1 × 10^{-3} mole) was dissolved in 10 mL of acetonitrile and potassium carbonate (1.38 g, 1 × 10^{-2} mole), after which tetrabutyl ammonium sulfate (0.04 g, 20% w/w) and pentaethylene glycol ditosylate (1.09 g, 2 × 10^{-3} mole) were added. The mixture was refluxed and the reaction was quenched by cooling to room temperature. The solvent was then removed and the product was dissolved in 25 mL ethyl acetate, washed with water (3 × 20 mL), dehydrated with anhydrous sodium sulfate and dried by rotary evaporation.

Poly(pentaethylene glycol cinnamate) (PPGC). Yellowish oil; T_m: 202.1°C. $\overline{M_n}$: 3000. ^1H NMR (400 MHz, $CDCl_3$, δ, ppm): 7.62 (d, J = 16.1 Hz, 1H, Ar—CH=), 7.43 (d, J = 8.16 Hz, 2H, Ar—H), 6.88 (d, J = 7.8 Hz, 2H, Ar—H), 6.31 (d, J = 15.5 Hz, 1H, =CH—COOH), 4.32 (br, $-COO-CH_2-CH_2-O$), 4.25 (br, $-CH_2-CH_2-O-$), 4.12 (br, $-CH_2-CH_2-O-Ar$), 3.86–3.54 (br, $-CH_2-O-Ar$). ^{13}C NMR (100 MHz, $CDCl_3$, δ, ppm): 167.2 (—COO—), 144.7 (Ar—CH=), 160.6 (—O—Ar), 129.7 (2 × 1C), 127.2 (Ar—CH), 114.9 (2 × 1C) (aromatic carbons), 115.3 (=CH—COO) and 72.7–61.6 (—O—CH_2—). IR (Nujol, cm^{-1}): 2955, 2856, 1707, 1603, and 1258.

UV absorption and photostability test

Solution containing the exact amount of the test material was freshly prepared and UV absorption spectrum was then acquired. The molar absorption coefficient of each compound was obtained from the slope of the graph between molar concentrations and absorbances (at maximum absorption wavelength).

The photostability tests were performed in dichloromethane and methanol. The freshly prepared test solutions were divided into two parts. One part was kept in a light-proof condition at room temperature (dark sample) while the other part (irradiated sample) was irradiated with 0.30 mW/cm^2 UVB at the same temperature for 5, 10, 15, 20, 25, 30, 40, 50, and 60 min, which correspond to UVB exposures of 0.15, 0.30, 0.45, 0.60, 0.75, 0.90, 1.2, 1.5, and 1.8 J, respectively. Next, the UV absorption profile of each sample was acquired using a UV/VIS spectrometer. The absorbances of the irradiated samples at various irradiant times were reported as relative percentages to the absorbance of the dark sample.

Transdermal penetration

Transdermal penetration of P3, P6, P11, PPGC, and EHMC across the abdominal skin of a two-week-old baby mouse (*Mus musculus Linn.*) was carried out as described previously using a Franz diffusion cell with a 13.0 mL capacity receptor compartment and 2.27 cm^2 diffusion area.[20] In short, the experiment was initiated by dropping 200 μL of the 0.17 mol of cinnamate unit/L sample solution into the upper

compartment of the diffusion cell, directly onto the mounted skin (UV filter final coverage = 1.5×10^{-5} mol of the cinnamate unit/cm^2). Then, at 1, 2, 4, and 24 h, 3.4 mL of receptor fluid was withdrawn and replaced with a fresh receptor medium. Experiments were performed at room temperature in five repetitions. Since the skins from different mice were different, the penetration of each sunscreen sample was compared to the penetration of EHMC using the skin from the same mouse. Analysis of the withdrawn fluid were done using UV absorption spectroscopy. A sample solution was prepared by dissolving the tested material in DMSO to give the final concentration of 0.17 mol of cinnamate unit/L.

Nanoparticulate formation

PPCC was induced into nanoparticulates using solvent displacement technique (dialysis method). Twenty milligrams of PPCC were dissolved in 5 mL of DMF/DMSO (3 : 2) and this solution was dialyzed against deionized water (Milli-Q®). After dialysis, a colloidal suspension of nanoparticles in water was obtained in the dialysis bag. Final volume of the suspension was adjusted to 10 mL with water to obtain the suspension at 2 mg/mL. Similar procedure was carried out with P3, P6, and P11.

RESULTS AND DISCUSSION

Successful preparation of *p*-alkoxycinnamic acid could be achieved from a substitution reaction between *p*-hydroxycinnamic acid and bromo alkyl alcohol using potassium carbonate to generate nucleophiles from *p*-hydroxycinnamic acid (pK_a of the phenolic proton ≥ 10 (Scheme 1)). Excess bromo alkyl alcohol was used to maximize the yield of this S_N1 reaction (Table I). After completing the reaction, excess bromo alkyl alcohol could be recovered from the reaction mixture by solvent extraction.

All four *p*-alkoxycinnamic acids, *p*-(2-hydroxy ethoxy) cinnamic acid (M2), *p*-(3-hydroxy-propoxy) cinnamic acid (M3), *p*-(6-hydroxy-hexyloxy) cinnamic acid (M6), and *p*-(11-hydroxy-undecyloxy) cinnamic acid (M11) showed a similar UVB absorption of ~26,000M^{-1} cm^{-1} (λ_{max} of 310 nm) in methanol. Similar UV absorption spectra among the four monomers corresponded well to the same UV-absorptive functionality among the four monomers.

Three monomers, M3, M6, and M11 were successfully condensation polymerized by an esterification reaction using *p*-toluene sulfonic acid as a catalyst (Scheme 1). ^{1}H NMR and IR spectra, together with molecular weight information from GPC, indicated that esterifications had been taking place for M3, M6, and M11 yielding poly(*p*-propoxy cinnamate) (P3), poly(*p*-hexyloxy) cinnamate) (P6) and poly(*p*-undecyloxy cinnamate) (P11), respectively. Both insoluble products (solid product precipitated out from the reaction medium) and soluble oligomeric products (soluble in the reaction medium) of P3, P6, and P11 were obtained in the reaction mixtures. In all three cases, both soluble and insoluble products gave similar IR spectra, indicating that the insoluble products possessed similar functionalities to the soluble products. It was observed that polymerization at higher monomer concentration yielded more insoluble solid product. The phase separation of the larger insoluble oligomers from the reaction mixture resulted in a dilution of the remaining soluble oligomers in the reaction mixture. It was speculated that such dilution might favor cyclization of the soluble oligomeric molecules. The soluble oligomers, therefore, stopped increasing their sizes. The small cyclized product was found by mass spectrometry. MALDI-TOF MS spectra gave m/z = 612 and 816 for P3, m/z = 738 and 984 for P6 and m/z = 632 and 948 for P11. It should be noted here that the lack of peak at higher m/z in the mass spectra is probably a result of undesorbable nature of the bigger species. Esterification was also verified by the differences in the positions of $-OCH_2-$ resonances between the monomers' and oligomers' ^{1}H NMR spectra [see details in the ^{1}H NMR information in the experimental section and Fig. 1(a,b)]. The lack of broad absorption band around 2300–3600 cm^{-1} (—COOH) in the FTIR spectra of P3, P6, and P11 together with the shift of carbonyl stretching from ~1670 cm^{-1} in the IR spectra of monomers to ~1710 cm^{-1} in the spectra of the oligomers also confirmed the complete condensations (Fig. 2). GPC analysis of the final soluble products gave $\overline{M_n}$ values for P3, P6, and P11 of ~1600, 3500, and 5500, respectively. It can

TABLE I
Reaction Conditions for the Synthesis of the Monomers

Monomer	n	Mole equivalent of bromo alkyl alcohol	Reaction time (h)	% yield
p-(2-hydroxy-ethoxy) cinnamic acid (M2)	2	10	36	75
p-(3-hydroxy-propoxy) cinnamic acid (M3)	3	5	27	97
p-(6-hydroxy-hexyloxy) cinnamic acid (M6)	6	3	40	69
p-(11-hydroxy-undecyloxy) cinnamic acid (M11)	11	3	40	89

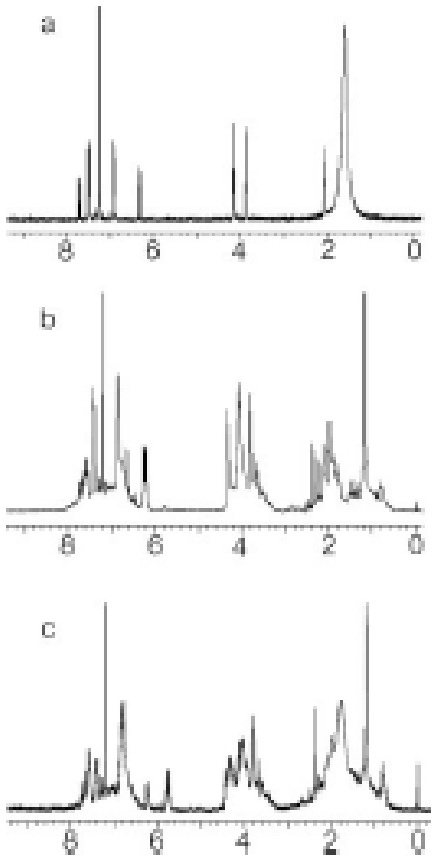

Figure 1 ^{1}H NMR spectra of (a) p-(3-hydroxy-propoxy) cinnamic acid (M3), (b) poly(p-propoxycinnamate) (P3), and (c) P3 after being exposed to 1.80 J of UVB.

be seen from the growth curves of P3 and P6 that the maximum $\overline{M_n}$ values for the two oligomers to stay soluble in the reaction medium, are probably 2500 and 4000, respectively, (Fig. 3). The decrease in the $\overline{M_n}$ value of the soluble P6 after the oligomers' size reached 4500 was probably caused by precipitation of those oligomers with $\overline{M_n}$ values over 4000. This situation can also be seen in P3. However, in the case of P11, a smooth growth curve was observed. This can be explained by the fact that P11 possesses a better solubility in the reaction medium than P3 and P6.

Since P3, P6, and P11 were polymerized at a similar molar concentration of the monomers, it can be concluded that the hydrocarbon chain length in the oligomeric structure directly affects the solubility of the compound. We speculated that the polymerization reaction carried out at a more diluted monomer concentration should yield more soluble oligomeric product with a smaller $\overline{M_n}$ value, and significantly less insoluble product. The experiment showed that polymerization under lower concentration of M11 gave P11a ($\overline{M_n}$ 2500) with no solid precipitate.

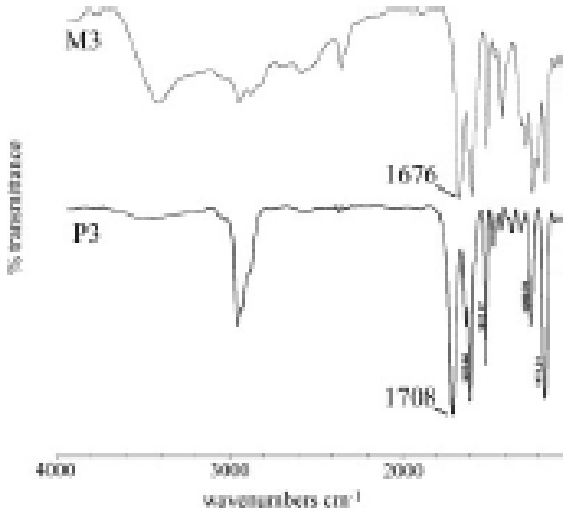

Figure 2 FTIR spectra of M3 (top) and P3 (bottom). M3 spectrum shows stretching of the carbonyl from carboxylic acid functionality at 1676 cm^{-1}, while P3 spectrum shows stretching from ester carbonyl at 1708 cm^{-1}.

It should be noted here that polymerization of M2 using either p-toluene sulfonic acid, Amberlyst-15 (cationic ion-exchange resin) or 1-(3-dimethylaminopropyl)-3-ethylcarbodiimide hydrochloride (EDCI) plus 1-hydroxy-benzotriazole (HOBt) failed. Only the use of *N,N*-dicyclohexylcarbodiimide (DCC) as coupling agent gave poly(p-(2-ethoxy)cinnamate), P2. ^{1}H NMR analysis indicated a little contamination of *N,N'*-dicyclohexylurea (DCU).

Copolymerization of M3 and M11 was successfully carried out using p-toluene sulfonic acid (Scheme 1). Since it was previously observed that M11 could be polymerized more easily than M3, the copolymerization was performed by starting with

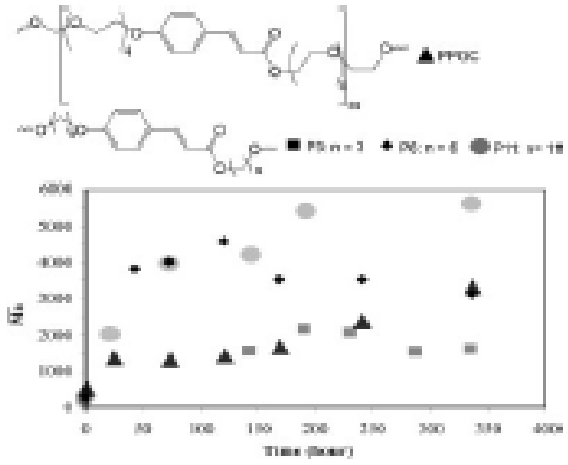

Figure 3 $\overline{M_n}$ of the soluble oligomers in the reaction mixture at various reaction times.

TABLE II
Solubility of P3, P6, P11, P11a, P3/11, and PPGC

Solvent	P3 ($\overline{Mn}$ = 2000)	P6 ($\overline{Mn}$ = 3000)	P11 ($\overline{Mn}$ = 5500)	P11a ($\overline{Mn}$ = 2500)	P3/11 ($\overline{Mn}$ = 2000)	PPGC ($\overline{Mn}$ = 3000)
Water	−−	−−	−−	−−	−−	−−
Acetonitrile	+−[a]	+−[a]	+−[a]	+−[a]	+−	++
Ethanol	+−[a]	+−[a]	+−[a]	+−[a]	+−[a]	+−[a]
Methanol	+−[a]	+−[a]	+−[a]	+−[a]	+−[a]	+−[a]
Acetone	++[a]	++[a]	++[a]	++[a]	++	+−
Ethyl acetate	++	++[a]	++[a]	++[a]	++	+−
Tetrahydrofuran	++	++	++	++	++	++
Chloroform	++	++	++	++	++	++
Dichloromethane	++	++	++	++	++	++
Diethyl ether	+−	++	++	++	++	−−
Toluene	++	++	++	++	++	−−
Hexane	−−	−−	−−	−−	−−	−−
DC200[b]	−−	−−	−−	−−	−−	++
DC556[c]	−−	−−	−−	−−	−−	++

−− less than 2 mg/mL; +− = 2–10 mg/mL; ++ more than 20 mg/mL.
[a] After heated.
[b] Linear polydimethylsiloxane polymers.
[c] Phenyl trimethicone.

more M3 than M11. Additional amounts of M11 were added at later times during the reaction. At the conclusion of the polymerization, the moles of the two monomers were equal. The resulting poly(*p*-propoxy cinnamate)-co-(*p*-undecyloxy cinnamate) or **P3/11** ($\overline{M_n}$ 2000) shows a better solubility than **P3** ($\overline{M_n}$ 1600) and **P11** ($\overline{M_n}$ 5500) (see Table II), i.e., **P3/11** is soluble in acetone at 25°C, while both **P3** and **P11** are soluble in hot acetone (reflux). This is likely a result of a random alternation between the *p*-propoxy cinnamoyl and the *p*-undecyloxy cinnamoyl units, which results in less stacking among cinnamoyl moieties.

Copolymerization between one mole equivalent of *p*-hydroxycinnamic acid and two mole equivalents of pentaethylene glycol ditosylate in acetonitrile using potassium carbonate as a catalyst and tetrabutylammonium sulfate as a phase transferring agent, yielded poly(penta ethylene glycol cinnamate) or PPGC (Scheme I) as a liquid product. Partitioning between ethyl acetate and water removed the polyethylene glycol from the product. It can be clearly seen that polymerization occurred steadily and the chain growth continued, even after reaction times of 2 weeks (Fig. 3). This steady growth was a result of an excellent solubility of the growing polymer chains. The outstanding characteristic of PPGC is that it is a light-yellow-oily liquid, miscible with silicone fluids used in the cosmetic industry (see Table II).

P2, **P3**, **P6**, **P11**, **P3/11**, and PPGC showed similar UVB absorption characteristics (Fig. 4). This is expected because all five oligomers contain similar chromophore (cinnamate moiety). It should be noted here that the molar absorption coefficients of all oligomers were calculated per mole of the cinnamate unit. This should permit the direct comparison in UVB absorption efficiency of cinnamate moieties of different compounds.

Photostability study of the commonly used UVB filter 2-ethylhexyl-*p*-methoxycinnamate (EHMC), **P3**, **P6**, **P11**, **P3/11**, and PPGC in dichloromethane indicated comparable photostability among the five oligomers and EHMC (Fig. 5). NMR analysis indicated *trans* to *cis* photoisomerization of the cinnamate moieties in all five oligomers and also in EHMC (decrease of resonance at 6.2 ppm (d, J = 16.0 Hz, 1H, *trans* CH=CH—COO) and appearance of resonance at 5.8 ppm (d, J = 8.0 Hz, 1H, *cis* CH=CH—COO), see Figure 1(b,c). The isomerization into the *cis* configuration, which possesses less molar absorption coefficient than that of the *trans*,[20,24] lowers the absorption efficiency of the oligomer. It should be noted here, however, that there was no other degradation product found during the photostability test. This indicated that all the oligomers could still act as UV absorbers during their UV exposures but with lower UV absorption efficiency.

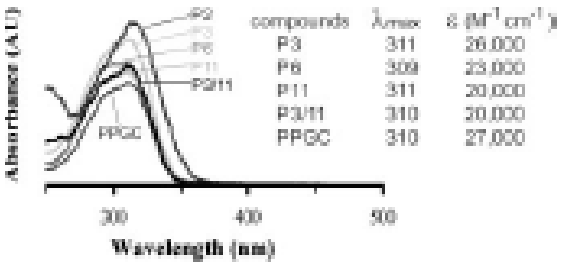

Figure 4 UV Absorption characteristics of the synthesized oligomers. The molar absorption coefficients (ε) were obtained from the slopes of the graphs between concentrations of the oligomers and the absorbances. The concentrations of the oligomers used were based on the molar concentrations of cinnamoyl monomeric units. Molar absorption coefficients are expressed based on molar concentration of cinnamoyl monomeric units.

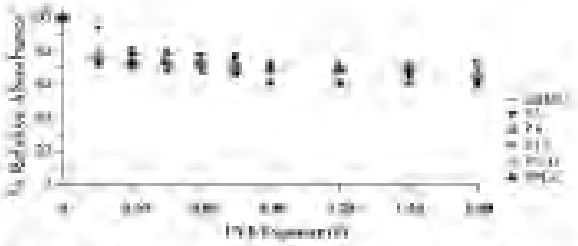

Figure 5 Photostability of each synthesized oligomer comparing with EHMC. The photostability was expressed as % relative absorbance of the material after being exposed to various UVB doses, as compared to the absorbance of the unexposed material.

P3, P6, P11, P3/11, and PPGC showed no transdermal penetration across baby mouse skin, while EHMC showed obvious penetration (Fig. 6). In the experiment, coverages of the materials on the skin were reported as cinnamate unit $\mu g/cm^2$. The experiments were carried out at similar cinnamate unit/cm^2 for all oligomers and EHMC; therefore, coverages of the chromophoric units (cinnamate units) on the skin were similar among different samples. The transdermal penetration of EHMC agrees well with previous study.[28] The nonpenetrating nature of the oligomers is likely a result of the bulky oligomeric structure of the materials. This nonpenetrating nature of the compounds should prolong the UV-absorption efficacy of the compound when being applied onto the skin. The water insolubility and liquid nature of PPGC also encourage further study for application of the compound in cosmetics.

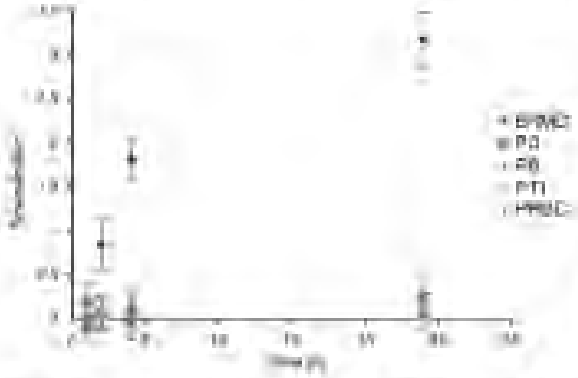

Figure 6 Penetration of the synthesized oligomers and EHMC through baby mouse skins using Franz diffusion cells with the skin contact area of 0.126 cm^2/mL, and at the final coverage of UV filter on the baby mouse skin of 4.4 mg/cm^2. The results are shown as percentage of UV filters found in receptor fluid as relating to the amount of applied UV filters, at various post-application times. The data are shown as average values of at least three experimental repetitions. Maximum standard deviation was 0.9%. [Color figure can be viewed in the online issue, which is available at www.interscience.wiley.com.]

Since PPGC is amphiphilic, there was a possibility that the compound could be formed into micelles. Self-assembly of the PPGC at the concentration of 0.4% (w/v) using solvent displacement (dialysis) technique, gave aqueous colloidal suspensions with mean hydrodynamic diameters of micelles from dynamic light scattering of ~164 nm (dispersity index, DPI, = 0.142) [Fig. 7(a)]. Scanning electron micrograph (SEM) at 20,000× magnification of PPGC-micelles revealed semispherical shape [Fig. 7(b)]. It should be noted here that it was very difficult to get the SEM picture of PPGC particles since most particles either melted or burst during the gold deposition process and during the impact of the high energy-electrons. One of the two particles shown in Figure 7(b), was in the middle of such burst. In fact, many of such bursts were observed during the SEM acquisition for the PPGC particles. Atomic force micrograph (AFM) of the PPGC particles also indicated soft semispherical particles [Fig. 7(c)]. At room temperature, PPGC colloidal suspension was stable and showed no precipitation even after being kept for 6 months. A self-assembly of amphiphilic polymer, although, is quite common,[29–35] the self-assembled amphiphilic PPGC-nanoparticles reported here is unique as the PPGC is UV-absorptive material by itself. In other words, organic UV absorptive nanoparticles were synthesized in this work. Further studies on the use of such particles as cosmetic active carrier, for an additional benefit on UV protection of the encapsulated materials, are currently being carried out in our laboratory.

P3, P6, and P11 which contain no hydrophilic PEG moieties, were also subjected to dialysis process to

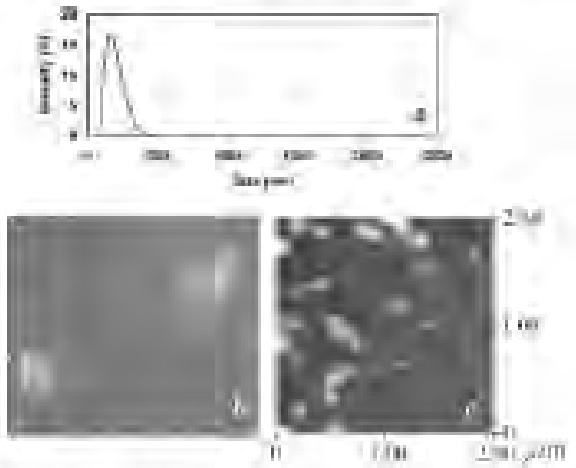

Figure 7 Size distribution of PPGC aqueous suspension prepared at 0.4% (w/v) of PPGC (top) and SEM of PPGC particles obtained at 20,000× magnification (bottom). [Color figure can be viewed in the online issue, which is available at www.interscience.wiley.com.]

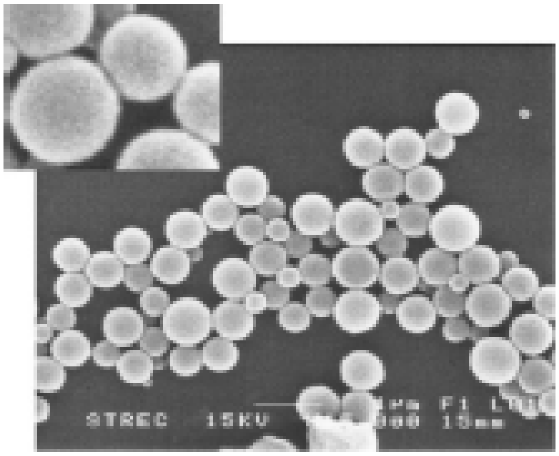

Figure 8 Scanning Electron Micrograph (SEM) of P3 particles.

induce self-assembly into particles. Only **P3** yielded colloidal suspension of spherical particles (Fig. 8). The **P3** colloidal suspension agglomerated and precipitated quickly. Association among **P3** particles could be observed clearly (see inset of Fig. 8). The fact that the **P3** particles did not disperse well in water while the PPGC particles could form stable colloidal suspension in water, indicates an importance of a big hydrophilic segment (PEG moiety) in PPGC structure. Since **P6** and **P11** were even more hydrophobic than **P3**, it was not surprised to observe that both oligomers did not give colloidal suspension after dialysis.

CONCLUSIONS

Three solid UV-absorptive oligomers—poly(*p*-propoxycinnamate) (**P3**, $\overline{M}_n$ 2000), poly(*p*-hexyloxycinnamate) (**P6**, $\overline{M}_n$ 3000), and poly(*p*-undecyloxycinnamate) (**P11**, $\overline{M}_n$ 5500 and **P11a**, $\overline{M}_n$ 2500)—were successfully condensation polymerized from *p*-(3-hydroxy-propoxy) cinnamic acid, *p*-(6-hydroxy-hexyloxy) cinnamic acid and *p*-(11-hydroxy-undecyloxy) cinnamic acid, respectively. Copolymerization between *p*-(3-hydroxy-propoxy) cinnamic acid and *p*-(11-hydroxy-undecyloxy) cinnamic acid yielded poly (*p*-propoxycinnamate)-co-(*p*-undecyloxycinnamate) (**P3/11**, $\overline{M}_n$ 2000). The liquid UV-absorptive oligomer, poly(pentaethylene glycol cinnamate) (PPGC, $\overline{M}_n$ 3000), was synthesized through the copolymerization between *p*-hydroxycinnamic acid and pentaethylene glycol ditosylate. Absorption profiles of all synthesized polymers indicated UVB absorption characteristics. Upon UVB exposure, all synthesized oligomers and the standard UVB filter, 2-ethylhexyl-*p*-methoxycinnamate (EHMC), underwent *trans* to *cis* photoisomerization at the cinnamoyl moieties which resulted in the decrease in UVB absorption efficiency of the materials. However, no transdermal penetration across a baby mouse skin (*Mus musculus* Linn.) was detected for all the synthesized oligomers, while the penetration of EHMC through the same skin was clearly observed. In addition, poly(pentaethylene glycol cinnamate), a yellowish water immiscible liquid, showed good solubility in various organic solvents and silicone fluids. Using solvent displacement technique, the amphiphilic PPGC oligomer could be induced into nanoparticles with the hydrodynamic size of ~164 nm (DPI = 0.142). These particles formed stable colloidal suspension in water.

References

1. Gallagher, R. P.; Lee, T. K. Prog Biophys Mol Biol 2006, 92, 119.
2. Daya-Grosjean, L.; Dumaz, N.; Sarasin, A. J Photochem Photobiol B 1995, 28, 115.
3. Taylor, J. S.; Lu, H. F.; Kotyk, J. J Photochem Photobiol 1990, 51, 161.
4. Ziegler, A.; Leffell, D. J.; Kunala, S.; Sharma, H. W.; Gailani, M.; Simon, J. A.; Halperin, A. J.; Baden, H. P.; Shapiro, P. E.; Bale, A. E. Proc Nat Acad Sci USA 1993, 90, 4216.
5. Kielbassa, C.; Roza, L.; Epe, B. Carcinogenesis 1997, 18, 811.
6. Courdavault, S.; Baudouin, C.; Charveron, M.; Canguilhem, B.; Favier, A.; Cadet, J.; Douki, T. DNA Repair 2005, 4, 836.
7. Kimura, K.; Katoh, T. Contact Dermat 1995, 32, 304.
8. Schauder, S.; Ippen, H. Contact Dermat 1997, 37, 221.
9. Hany, J.; Nagel, R. Deutsche Lebensmittel-Rundschau 1995, 91, 341.
10. Janjua, N. R.; Mogensen, B.; Andersson, A. M.; Petersen, J. H.; Henriksen, M.; Skakkebaek, N. E.; Wulf, H. C. J Invest Dermatol 2004, 123, 57.
11. Jiang, R.; Roberts, M. S.; Collins, D. M.; Benson, H. A. E. Brit J Clin Pharmaco 1999, 48, 635.
12. Hayden, C. G. J.; Roberts, M. S.; Benson, H. A. E. Lancet 1997, 350, 863.
13. Sener, G.; Incegul, T.; Yener, N. Int J Pharm 2003, 258, 203.
14. Calderilla-Fajardo, S. B.; Cazares-Delgadillo, J.; Villalobos-Garcia, R.; Quintanar-Guerrero, D.; Ganem-Quintanar, A.; Robles, R. Drug Dev Ind Pharm 2006, 32, 107.
15. Chatelain, E.; Gabard, B.; Surber, C. Skin Pharmacol Appl Skin Physiol 2003, 16, 28.
16. Kamiya, H.; Kita, K.; Fujikura, Y. Jpn. Pat. 7,173,027 (1995).
17. Pattanaargson, S.; Hongchinnagorn, N.; Hirunsupachot, P.; Sritanaanant, Y. Photochem Photobiol 2004, 80, 322.
18. Vaughan-Spickers, J.; Greenfield, S.; Hassall I. V. E.; Dunn, C. J.; Harding, R.; Jenkins, T.; May, A. L. U.S. Pat. 26,660 (2004).
19. Harding, R.; Hassall I. V. E.; Maren, S. A.; Brown, D. U.S. Pat. 7,294,369 (2007)
20. Richard, H.; Leduc, M. U.S. Pat. 6,090,880 (2000).
21. Leduc, M.; Richard, H.; Lagrange, A. U.S. Pat. 6,376,679B2 (2002).
22. Langer, M. E.; Khorshahi, F. U.S. Pat. 5,250,652 (1993).
23. Pattanaargson, S.; Limphong, P. Int J Cosmet Sci 2001, 23, 153.
24. Pattanaargson, S.; Munhapol, T.; Hirunsupachot, P.; Luangthongaram, P. J Photochem Photobiol 2004, 161, 269.
25. Klinubol, P.; Asawanonda, P.; Wanichwecharungruang, S. P. Skin Pharmacol Physiol 2008, 21, 23.
26. Letchford, K.; Burt, H. Eur J Pharm Biopharm 2007, 65, 259.
27. Chen, C.; Yu, C. H.; Cheng, Y. C.; Yu, P. H. F.; Cheung, M. K. Eur Polym Mater 2006, 42, 2211.
28. Kim, S. Y.; Shin, I. G.; Lee, Y. M. J Control Release 1998, 56, 197.